DETERMINATION AND ANALYSIS OF TURBIDITY OVER HAMILTON, ONTARIO

by

Bruce McArthur

A Thesis

Submitted to the Department of Geography

in Partial Fulfilment of the Requirements

for the Degree

Bachelor of Science

McMaster University

April, 1976

BACHELOR OF SCIENCE (1976)
(Geography)

McMaster University
Hamilton, Ontario

TITLE: Determination and Analysis of Turbidity over Hamilton, Ontario

AUTHOR: Lorne John Bruce McArthur

SUPERVISOR: Professor J.A. Davies

NUMBER OF PAGES: viii, 124

ABSTRACT:

Turbidity over Hamilton is determined using direct beam radiation in two manners for the summer period of 1975. These turbidities are then studies with respect to local regional and continental synoptic air masses.

The results of the study show a high correlation between the actinometric and residual methods of determining direct beam radiation. This allows turbidity to be easily evaluated at radiation measurement sites.

The most significant influence on the amount of particulate matter over Hamilton is the continental scale synoptic patterns.

ACKNOWLEDGEMENTS

This project was supported through research funds made available through Dr. J.A. Davies. I would like to extend special thanks to Dr. Davies for the time and effort he put in to produce this work in the form it is at present. I would also like to thank William Bailey and Alan Sawchuk for the time they spent in answering queries and giving suggestions on the material and form of the thesis. Final thanks goes to all those who helped me endure the high temperatures of the summer through their continual encouragement.

TABLE OF CONTENTS

LIST OF MAPS

LIST OF FIGURES

LIST OF TABLES

CHAPTER 1

INTRODUCTION

The determination of atmospheric turbidity using actinometric measurements is not new. As early as the 1930's, Soviet investigators (Mamontova and Khromov, 1933; Poliakova, Sivkov and Ternovskaya, 1935) were determining the difference in turbidities of air masses depending on their origins. Beside the pioneering work however, little interest has been given to the determination of turbidity until recently. Valko (1963) analysed turbidity measurements over Locarno Monti in Switzerland and found results supporting the early Soviet work. Unsworth and Monteith (1972) did a similar study in Britain after developing a new turbidity index. Others, such as Joseph and Manes (1971) have done considerable work in analysing past actinometric records and turbidities for Jerusalem to find long term trends; daily turbidity variation being of secondary interest.

In North America, virtually no work in this area has been carried out. Heidel (1972) applied the Linke turbidity factor to determine turbidities over Tuscon, Arizona. Flowers, McCormick and Kurfis (1969) have used photometers to determine approximate turbidity measures over selected sites throughout the U.S.A.

Unsworth and Monteith (1972) have produced definite evidence indicating that local sources of aerosols are not the major sources of high turbidities. The work producing these results and similar results however, has been carried out in relatively non-industrialized areas; local sources

being small. This study aims to determine whether similar measurements in an industrialized environment will verify the results of Unsworth and Monteith (1972) by showing that turbidity is more highly related to synoptic conditions than local sources of pollution.

A secondary purpose of this study is to determine the accuracy of a residual method in determining direct beam radiation when compared with actinometric methods. The usefulness of the procedure will be discussed in relation to the accuracy of determining direct beam radiation.

CHAPTER 2

THEORETICAL BACKGROUND

A method employed in determining the amount of particulate matter in the atmosphere is the turbidity factor. This is a comparison of the amount of radiant energy removed from a beam of light through scattering or absorption by particulate matter as it traverses the atmosphere, with the energy loss of a beam of light which traverses a similar atmosphere without particulate matter (Williamson, 1973). Since it is impossible to duplicate an atmosphere without particulate matter in nature, a model atmosphere must be determined.

The major attenuating components of direct beam radiation which must be included in a model atmosphere are molecular scattering and absorption and scattering by water vapour. These coefficients can be accurately evaluated if the amount of precipitable water and the optical air mass at a given time can be determined for the real atmosphere. The expressions for these quantities are derived accordingly.

Once the direct solar beam radiation incident at the earth's surface has been determined for the model atmosphere, several methods can be used to evaluate turbidity. Although many authors (Kondratyev, 1969; Ångstrom, 1964) developed turbidity factors, only two use integrated radiation measurements of the solar spectrum. These are the Linke Turbidity Factor, T (Linke, 1922), and the Unsworth and Monteith (1972) attenuation coefficient, τ_a. The Linke T has been further refined by Hoyt (1975) and Sivkov (1968), amongst others. Both of these

empirical formulations will be developed fully and compared as to their applicability in Hamilton. For simplicity, these variations will be referred to as the "Hoyt T" and the "Sivkov T" throughout the paper. The Unsworth and Monteith τ_a will also be developed and compared to the Linke Turbidity Factor in a following chapter.

Direct Beam Solar Radiation Model

As previously stated, direct beam solar radiation through a clean, dust-free atmosphere is a product of the atmospheric transmissions due to water vapour absorption ϕ_{wa}, water vapour scattering ϕ_{ws}, and Rayleigh scattering ϕ_{RS} (Houghton, 1954). The first two depend on the amount of precipitable water in the atmosphere w, and the air mass m, whereas ϕ_{RS} depends only on air mass. Houghton neglected the effects of ozone absorption and the changing sun - earth distance.

Unsworth and Monteith (1972) however, found the addition of ozone to be significant, while Sellers (1965), Kondratyev (1969) and others have shown the need to incorporate the radius vector. The latter correction was achieved by applying $\left(\frac{\bar{d}}{d}\right)^{2*}$ to the solar constant. Values were linearily interpolated from Table 169 of the Smithsonian Meteorological Tables (1963).

A constant reduction of 3% of the solar constant was applied as an estimate of ozone absorption (Davies, person. comm.). This is in agreement with the determinations of Sivkov (1968) where a bulk correction of 2.5% was established with a maximum derivation from the mean value of the solar constant in the sub-ozone layer of 0.5%.

---

* $\frac{\bar{d}}{d}$ is defined as the radius vector, and $\bar{d}$ is the average earth - sun distance.

Hought n assumed that scattering occurred after absorption. (Sivkov 1968) indicates that these attenuations occur after absorption in the ozone layer is complete.

The direct beam radiation on a surface perpendicular to the solar beam is given by

$$S = 0.97\, S_o \left(\frac{\bar{d}}{d}\right)^2 \phi_{wa}\, \phi_{ws}\, \phi_{RS} \qquad (1)$$

where S = *modelled direct beam radiation*

S_o = *solar constant.*

Calculation of Parameters

The value of the solar constant is taken as 1353 Wm^2 from the recent spectral work of Thekaekara (1972).

Optical air mass was determined by the method of Kasten (1966) which is more accurate than the commonly-used determination, sec z, because it allows for refraction effects. It is defined

$$m = 1/[\cos z + 0.15[(90 - z) + 3.88]^{-1.253}] \qquad (2)$$

where z = *zenith angle defined by*

$\cos z = \sin \phi \sin \sigma + \cos \phi \cos \sigma \cos h$

in which ϕ = *latitude*

δ = *solar declination*

h = *hour angle as defined by*

$h = 15|12 - LAT|$

where LAT = *local apparent time.*

Precipitable water was evaluated from the 1200 GMT radiosone ascent. It is defined

$$P = {}^{1}/_{g} \int_{p_u}^{p_o} q \, d \, p \qquad (3)$$

where g = *gravitational acceleration*

q = *specific humidity*

p_o = *pressure at the surface*

p_u = *the pressure measurement immediately preceding the pressure at which the dew point depression becomes unmeasureable*

where specific humidity is determined by the equation

$$q = 0.622e/(p - 0.378e) \qquad (4)$$

in which p = *pressure*

e = *water vapour pressure*

$= \alpha \exp(\beta T_d/(T_d + \gamma))$

where α = *0.6 1073 kPa*

β = *21.875 for water*

237.30 for ice

γ = *265.50 for water*

237.30 for ice

T_d = *dew point temperature*

($T_d < 0.0°C$ are with respect to ice) (Dilley, 1968).

The atmospheric column was divided by standard pressure levels: surface ($\simeq$ *100.0kPa)85.0, 70.0, 50.0, 40.0, 30.0 kPa.* For each layer i, a mean specific humidity $(\overline{q_i})$, a pressure thickness (Δp_i), and a mean pressure $(\overline{p_i})$ were determined. From these, the corrected optical depth for the layers was calculated (DW_i)

$$DW_i = (\overline{q_i}\ \overline{p_i}\ \Delta p_i)/9.81 \qquad (5)$$

Precipitable water for the i^{th} layer is then

$$P_i = DW_i/\overline{p_i} \tag{6}$$

The total preciptable water is determined by

$$P = \sum_{o=1}^{n} P_i \tag{7}$$

The scattering coefficients used in the direct beam model were determined using numerical approximations to the curves presented by Houghton (Figure 1). Water vapour absorption, however, was evaluated from McDonald's reassessment of the Smithsonian data (McDonald, 1960):

$$\phi w_a = 1. - 0.077\ (Wm)^{.3} \tag{8}$$

$$\phi w_s = 1.0059 - 0.0224545\ (Wm) \tag{9}$$

$$\phi_{RS} = 0.9716084 - 0.0826204\ (m) + 0.0093269\ (m)^2 - 0.000946\ (m)^3 + 0.0000437\ (m)^4 \tag{10}$$

Theoretical Development of the Linke T

Turbidity is the attenuation of the solar beam by particulate matter. It is therefore important to understand the physical development of the turbidity factor before applying it. Another method to describe the effects of the attenuating parameters of the atmosphere is by the atmospheric optical thickness. This can be defined for a given wavelength λ as:

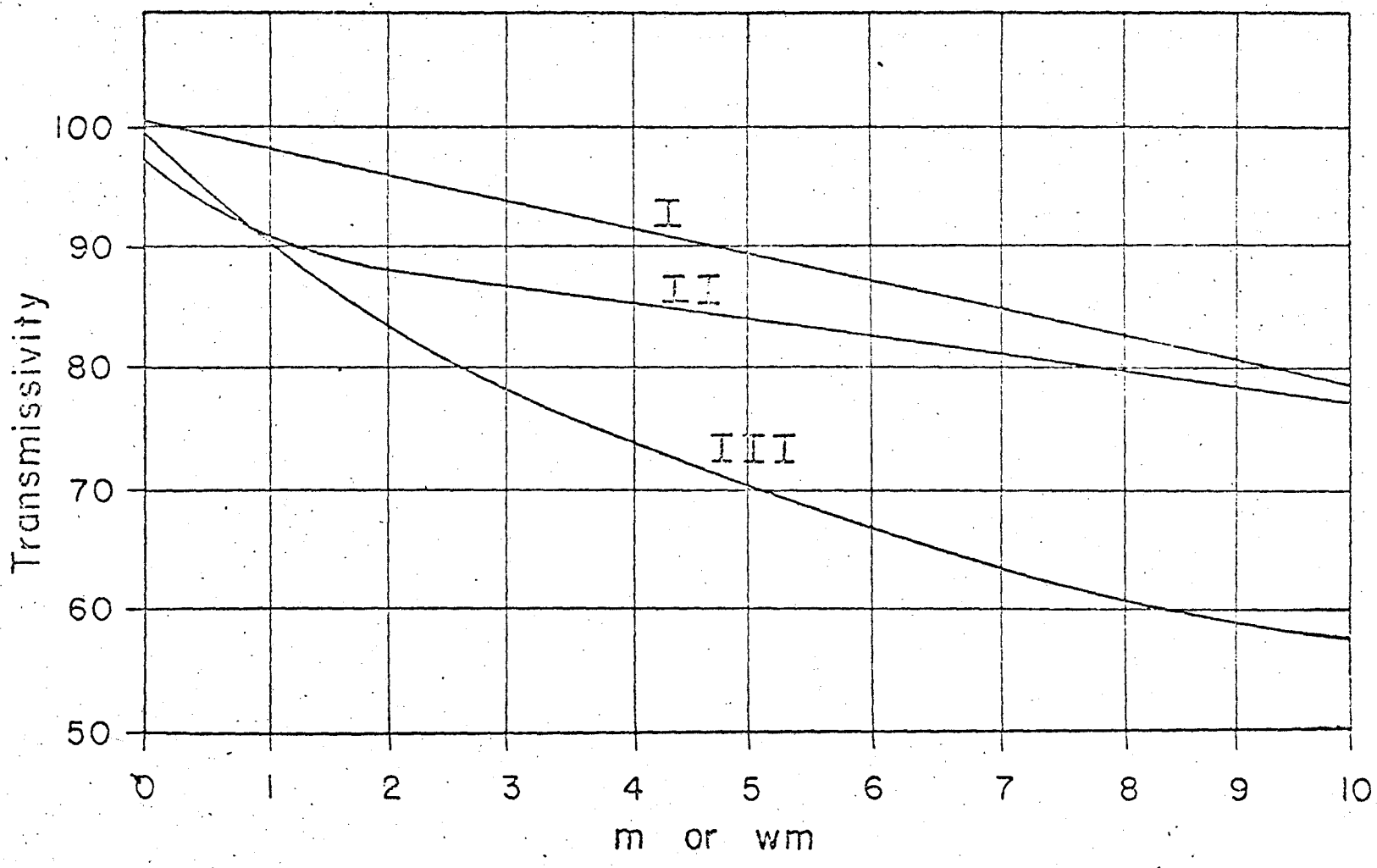

Figure 1: Houghton's curves for the tranmissions $\phi Ws(I)$, $\phi Wa(II)$ and $\phi Rs(III)$.

$$\Theta_\lambda = \int_o^\infty k_\lambda \rho \, dh + \int_0^\infty a_{w,\lambda} \rho_w \, dh + \int_0^\infty a_{d,\lambda} \rho a \, dh \quad (11)$$

where K_λ = *mass coefficient of molecular scattering*

ρ = *air density*

$a_{w,\lambda}$ = *mass coefficient of absorption by water vapour*

ρ_w = *water vapour density (specific humidity)*

$a_{d,\lambda}$ = *mass coefficient of radiation attenuation by dust*

ρa = *dust concentration*

h = *height in the atmosphere*

From this the monochromatic turbidity factor can be determined by

$$\Theta_\lambda = T_\lambda \int_0^\infty k_\lambda \rho \, dh, \quad (12)$$

where T_λ is the ratio between the vertically directed Θ_λ and the corresponding optical thickness determined for a Rayleigh atmosphere. For such a case

$$T_\lambda = \Theta_\lambda \Big/ \int_o^\infty k_\lambda \rho \, dh \quad (13)$$

The total attenuation of a given wavelength of direct beam radiation at a specific zenith angle and air mass can be shown as

$$S_{m,\lambda} = S_{o\lambda} \left(\exp\left[-T_{\lambda m} \int_0^\infty k\lambda \rho \, dh\right]\right) \quad (14)$$

where $S_{m,\lambda}$ = *the attenuated monochromatic solar radiant flux*

$S_{o,\lambda}$ = *the monochromatic solar radiant flux outside the atmosphere*

m = *air mass*

Alternatively,

$$S_{m,} = S_o \; q_\lambda^{mT\lambda} \tag{15}$$

where $q_\lambda = exp\left(\int_o^\infty k \; \rho \; dh\right)$

T_λ can now be defined as the number of times the monochromatic wavelength must pass through an ideal atmosphere to be attenuated to the same extent as the real atmosphere $S_{m,\lambda}$.

By integrating equation (15) over the solar spectrum a turbidity factor T can be defined as the number of clean dry atmospheres the solar beam must pass through to achieve the real attenuation in a turbid atmosphere. Hence

$$S_m = S_o \; q_m^{mT} \tag{16a}$$

alternatively,

$$S_m = p_m^{\,m} \int_o^\infty S_{o\lambda} \; \partial_\lambda \tag{16b}$$

$$= S_o \; p_m^{\,m} \tag{16c}$$

where p_m = *the integral transparency coefficient*

p_m can be calculated emperically for an ideal atmosphere by the theory of molecular light scattering.

By combining (16a) and (16c), T can be expressed in terms of q_m and p_m

$$T = \frac{In \; p_m}{In \; q_m} = \frac{\Theta}{\Theta_o \; ideal} = \frac{\Theta_o \; (o)}{\Theta_o \; ideal(o)} \tag{17}$$

where Θ_o = *optical thickness of the real atmosphere determined by the air mass m*

Θ_o *ideal* = *optical thickness of the ideal atmosphere determined by the air mass m*

Θ_o *(o)* = *optical thickness of the real atmosphere in a vertical direction*

Θ_o *ideal (o)* = *optical thickness of an ideal atmosphere in the vertical direction*

(Kondratyev, 1969)

Empirical Formulations of Turbidity

By rearranging equation (16a) the Linke T can be alternatively defined by using the expression *P(m)*

$$T = P(m)\ (\log S_o - \log S_m - \log r) \qquad (18)$$

where S_o = *solar constant*

S_m = *attenuated solar radiant flux*

r = *sun-earth distance correction factor*

$P(m)$ = $(m \times \bar{a}_r(m) \times \log e)^{-1}$

in which $\bar{a}_r(m)$ = *mean extinction coefficient for a Rayleigh atmosphere, weighted for the distribution of the transmitted spectral irradiance.*

Values of *P(m)* are tabulated (e.g. IGY Manual, 1956), but are usually those calculated by Feussner and Dubois (1930) using the solar spectral irradiance given by Fowle (1915). Hoyt (1975) used the Thekaekara (1972) spectrum to produce the most accurate determinations of *P(m)* now available. Using these values an empirical formula was derived for $\bar{a}_r(m)$

by a least squares regression line:

$$\overline{a}_r(m) = exp[-2.12362 - 0.31289\ In(m) + 0.0197\ (In(m))^2 - 0.01862(In(m))^3] \qquad (19)$$

From equations (18) and (19) $P(m)$ can be determined for any air mass within the range 1.0 to 5.0. Once evaluated T can be readily calculated using direct beam measurements.

This method has been widely used (e.g. Heidel, 1972) as a measure of atmospheric turbidity. However, it suffers the serious drawback that it not only reflects aerosol content in the atmosphere, but also ozone and water vapour content.

Because of the inclusion of water vapour content in the Linke Turbidity model, a "wet" turbidity factor was developed. This incorporated 10 mm of precipitable water in 'the evaluation of the turbidity factor' to reduce water vapour influence.

Sivkov (1968) developed a function for $P(m)$ dependent only opon the ideal atmosphere. When determining T for a clean dry Rayleigh atmosphere this method should approximate those values ascertained by Hoyt (1975). However, unlike Hoyt, the clean dry atmosphere can be replaced by substituting a more complex ideal atmosphere. $P(m)$ is defined

$$P(m) = (log\ S_{o,c} - log\ S_{i,m})^{-1} \qquad (20)$$

where $S_{i,m}$ = *a modelled ideal direct beam radiation*

$S_{o,c}$ = *the corrected solar constant*

Substituting equation (20) into equation (18)

$$T = (\log S_{o,c} - \log S_m)(\log S_{o,c} - \log S_{i,m})^{-1} \qquad (21)$$

In this form, both terms can be independently evaluated to determine the turbidity due to any one or more processes. In this study T will be evaluated using the same air mass and precipitable water parameters as the real atmosphere to determine the attenuation due to aerosols.

Unsworth and Monteith Turbidity Factor

Unsworth and Monteith (1972) in formulating their attenuation coefficient τ_a, also begin with Beer's Law, but in the more general form of

$$S_{m,\lambda} = S_{o,\lambda} \exp[- \int_o^\infty a_\lambda \rho \, dh] \qquad (22)$$

where a = *a mass attenuation coefficient*

ρ = *the density of an unchanging atmospheric column.*

In a similar manner to the general theory, this is related to air mass by

$$S_{m,\lambda} = S_{o,\lambda} \exp(- \tau_\lambda m) \qquad (23)$$

where $\tau_\lambda = \int_0^\infty a_\lambda \rho \, dh$ *for a vertical beam*

Thus τ_λ compared to Θ_λ as the monochromatic optical thickness of the atmosphere. However, unlike Θ_λ, Unsworth and Monteith describe τ_λ as a function of 4 atmospheric components,

$$\tau_\lambda = \tau_{g\lambda} + \tau_{s\lambda} + \tau_{aa\lambda} + \tau_{as\lambda} \qquad (24)$$

where $\tau_{g\lambda}$ = *the optical atmospheric thickness due to gaseous absorption*

$\tau_{s\lambda}$ = *the optical atmospheric thickness due to molecular scattering*

$\tau_{aa\lambda}$ = *the optical atmospheric thickness due to aerosol absorption*

$\tau_{as\lambda}$ = *the optical atmospheric thickness due to aerosol absorption.*

From this one is able to see that τ_λ is strongly wavelength dependent, both gaseous absorption and Rayleigh being so effected. Gaseous absorption is selectively dependent on wavelength, while Rayleigh scattering is proportional to the negative fourth power of wavelength.

By integrating over the entire optical thickness:

$$\tau = -m^{-1} \left[\int_0^\infty S_{o,\lambda} \exp(-\tau_{\lambda m}) d\lambda \right] / \int_0^\infty S_{o,\lambda} \, d\lambda \qquad (25)$$

Although τ is now a composite function of the optical thickness, it still suffers from the problems of being air mass dependent. As has been shown, both Linke's T (Linke 1942) and atmospheric transparency (Kondratyev, 1969) suffer from the same problem and thus are not totaly effective/

By manipulation, Unsworth and Monteith (1972) derive a form to express $S_{m,\lambda}$ as

$$\begin{aligned} S_{m,\lambda} &= S_{o,\lambda} [\exp -(\tau_{g\lambda} + \tau_{s\lambda})m] \cdot \\ &\quad [\exp -(\tau_{aa\lambda} + \tau_{as\lambda})m] \\ &= S_{o,\lambda}(o) \, [\exp -(\tau_{a\lambda} m) \end{aligned} \qquad (26)$$

where $S_{o,\lambda}(o)$ = *the irradiance below an atmosphere free of aerosol*

$\tau_{a\lambda}$ = *a spectral coefficient for aerosol.*

By doing this the wavelength dependence of $\tau_{g\lambda}$ and $\tau_{s\lambda}$ is contained in $S_{o,\lambda}(o)$. Integrating this over the spectral range one is able to determine a turbidity factor free of air mass and wavelength dependence,

$$\tau_a = -m^{-1} \left[\int_0^\infty S_{o,\lambda}(o) \exp -(\tau_{a\lambda m}) \, d\lambda \right] / \int_0^\infty S_{o,\lambda}(o) \, d\lambda$$
$$= -m^{-1} \, ln[S_m(\tau) | S_o(o)] \qquad (27)$$

where $S_m(\tau)$ = *the measured value of irradiance over the spectrum, normal to the solar beam*

$S_o(o)$ = *a modelled expression of irradiance over the atmosphere excluding aerosol, calculated normal to the solar beam.*

CHAPTER 3

EXPERIMENTAL BACKGROUND

The measurements of direct beam solar radiation were taken on the upper roof of the Burke Memorial Science Building, McMaster University, Hamilton, Canada (latitude 43°15.5'; longitude 79°54.5'). Hamilton, with a population of 300,000 is a two-tiered city. The central business district, the industrial heartland and the older residential areas are located at the level of Lake Ontario. The newer portion of the city, mostly residential, is located on the top of the Niagara Escarpment, south of the older sector. Hamilton is the major steel-producing centre of Canada and thus is a highly industrialized region. The main body of the industry is located along the lake shore on the northeast side of the city. The university is on the opposite side of the central business district from the harbour, approximately 3.5 kilometers west. McMaster University is situated in the Dundas Valley which runs west to east through the Niagara Escarpment. Further west in the valley is the feeder community of Dundas (population 11,000). On top of this escarpment and behind the Dundas Valley, the area is of a market gardening nature. This area is in a portion of Canada which is not typical of the general climatic conditions, particularly when concerned with how man has affected these conditions. It is equally important to note that a relatively large percentage of the population of Canada lives in the area surrounding Lake Ontario. Because of this, the climatic influences affecting Hamilton are very important in understanding the influences of man on climate in Canada.

The general climate of the area is that of a modified continental type, with temperatures in the months of study reaching as high as 36°C. The prevailing wind bears down the Dundas Valley. This blows most of the industrial pollution out over the lake. Days in which the predominant wind is an onshore breeze is not uncommon however. It is believed that this wind is responsible for days of high turbidity and is, therefore, an important local factor.

The meteorological data for the study has been provided by the Meteorological Branch of the Department of Transport from the station at the Hamilton Civic Airport (Hamilton A). It is located 14.5 kilometres south of the experimental site on the top of the Niagara Escarpment. An intercomparison between data taken for prevailing winds from Hamilton A and the Royal Botanical Gardens recording site, located in the Dundas Valley, show good similarity over 5 years (Table 1), 56% of the recorded values being identical. The data is a result of determining the number of hours of a given wind direction over a period of a month. Even with the intercomparison, it is difficult to determine the exact error in observations over time, but it will be assumed to be negligible when dealing with wind and cloud observations. The problem will be especially small in the latter observations since the Civic Airport overlooks the sky of the Dundas Valley and the net radiation measurements will provide a secondary check on cloud conditions.

The upper air data needed to determine the precipitable water was taken at Buffalo International Airport, situated approximately 80.5 kilometres south southeast of Hamilton. The 1200 GMT radiosonde ascents

Month	1970		1971		1972		1973		1974		1975	
	RBG	HAM A	RBG	HAM A	RBG	HAM A	RBG	HAM A	RBG	HAM A	RBG	HAM A
Jan.	SW	----	SW	SW	SW	SW	SW	SW	SW	SW	SW	SW
Feb.	SW	----	SW	SW	SW	W	NE	NE	W	W	SW	SW
Mar.	SW	W	SW	W	NE	W	NE	NE	NE	SW	SW	W
Apr.	SW	NE	NW	NW	NE	E	NE	NE	SW	SW	NW	NW
May	SW	NE	SW	S	NE	NE	SW	NE	SW	W	SW	NE
June	SW	SW	NE	NE	SW	NE	SW	SW	SW	SW		
July	SW	SW	SW	W	SW	SW	SW	SW	SW	SW		
Aug.	SW	W	SW	SW	SW	SW	SW	SW	SW			
Sept.	SW	NW	SW	NE	SW	SW	SW	SW	SW			
Oct.	NE	NE	----	NE	SW	SW	NE	NE	SW			
Nov.	SW	SW	SW	W	SW	NE	SW	SW	SW			
Dec.	SW	SW	SW	W	SW	W	SW	SW	SW			

TABLE 1. Comparison of prevailing winds between Hamilton mountain station (HAM A) and Dundas Valley recording wind station (RBG).

were taken as representative of atmospheric conditions during the day in which observations were being made. This site has been successfully utilized to determine precipitable water data over the entire Lake Ontario region during IFYGL in which Burlington radiation station, only a few kilometres from the experimental site, was taking part (Schertzer, 1975) (see Map 1).

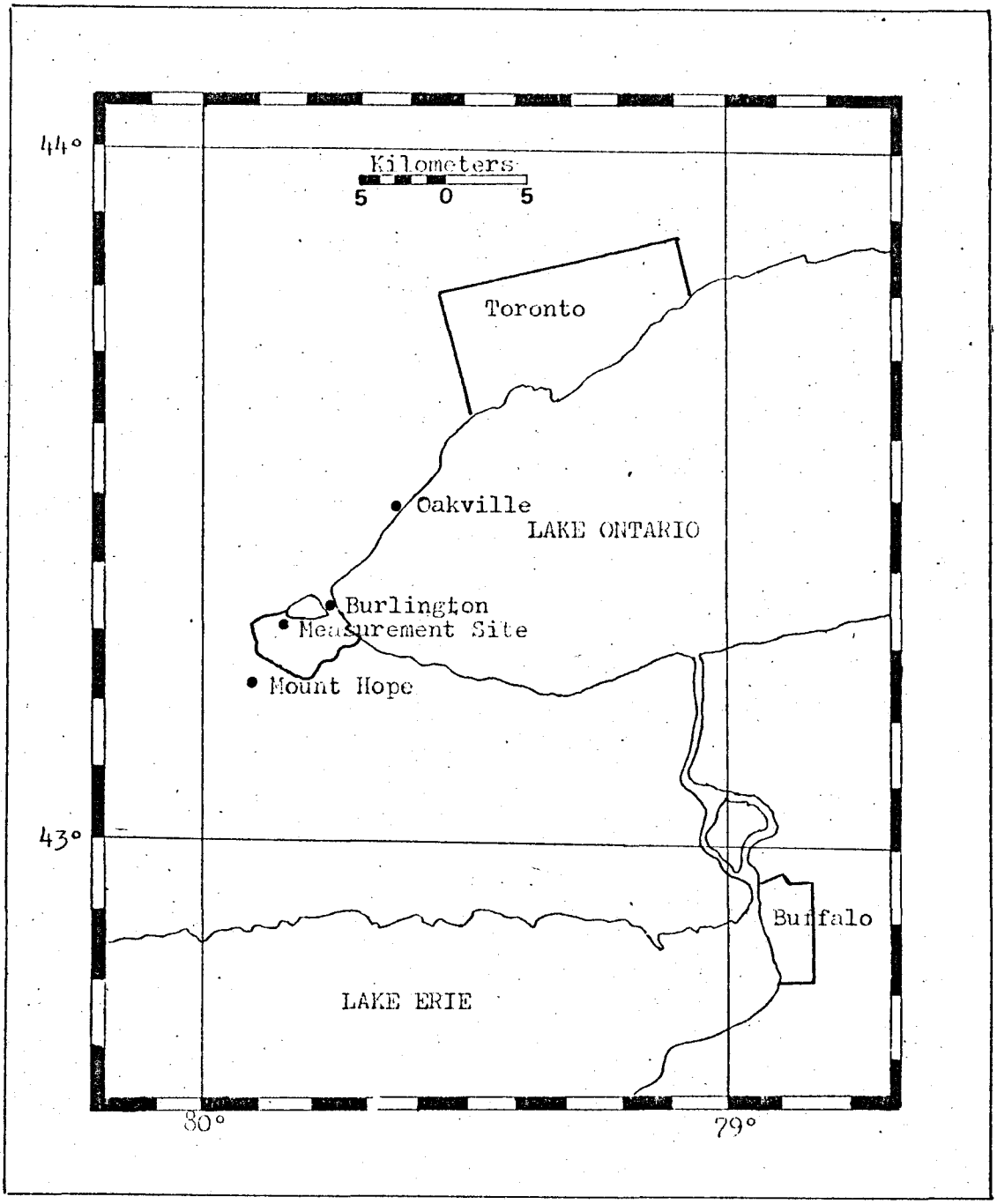

Map 1. Region surrounding the Measurement Site. Includes the location of the major centres of regional pollution, site of the meteorological station, and site of the upper air station.

CHAPTER 4

METHODOLOGY

The radiation instruments were located on the uppermost roof of the Burke Memorial Science Building. From this vantage, the trajectory of the sun could be accurately tracked for the entire portion of the day when measurements were being made. The hour after sunrise and before sunset were not utilized because of the large air mass the solar radiation had to pass through and the declining accuracy of the instruments at large angles. The diffuse radiation was blocked out at several points before the horizon, but this was not important in that only the direct beam component of the solar radiation was of interest.

The experiment utilized two methods of determining the direct beam component. The primary method was by direct beam measurement using the Linke-Feussner Actinometer. The secondary method was by residual of the net and diffuse components of the radiation.

To determine the second method, the Precision Eppley Pyranometer (Model 2) was used. This measured the net radiation except when occulted to give the diffuse component. To occult the pyranometer, a hand-helt, flat-black disc of a 100 mm diameter was positioned 1 m away from the thermopiles. During the occulting, the entire sensing area was in shade. This method was similar to that used by Unsworth and Monteith (1972), on a Kipp solarimeter. It was found that by holding it at this distance for 30 seconds, the response of the instrument and recorder was complete, giving an accurate determination of diffuse solar radiation.

Both radiation instruments were wired into a Honeywell Electronic 194 2-pen Strip Chart Recorder. The response of each instrument driving 1 pen, giving a comparison between direct and net radiation. For a short period at the beginning of the experiment, the actinometer was connected to a Kiethley Digital Multimeter. This was replaced because of the difficulty of accurately determining the read-out during periods of high wind or bright sunshine, which adversely affected the stability and clarity of the read-out. No such problems were encountered with the Honeywell.

A Cole-Palmer recorder was wired in series with the Eppley and placed on the roof as a monitor to check net radiation and indicate the effect of cloud on the observations. The Honeywell was located in an air-conditioned office so that it would not be adversely affected by changing temperature.

The experiment was carried out only on clear sky or nearly clear sky days. The latter can be defined as days when between one and four tenths cloud cover was present. The exact amount of cloud cover was dependent on its location in the sky and the wind velocity. If a full set of measurements, as described below, could be carried out without any cloud occulting the area of the sun or the circumsolar sky radiation, the determiminations were made. Before the equipment was set up for a given day, the meteorological forecast had to predict clear sky conditions and under one-tenth cloud cover had to be present in the sky.

The experiment was set up each day; the radiation instruments being susceptible to lightening during the evening. The location of instruments allowed both the pyranometer to "see" the full sky, being located on a stand approximately 6.25 m above the roof-top, and the

actinometer to track the sun without interference.

Measurements of direct beam radiation were taken every hour about the hour; time being LAT. Before each set of observations were taken, the strip-chart recorder was zeroed and time checked. The observational sequence for the actinometer consisted of one-minute periods of measurement for each of five filters; the order being open, red, yellow, green, zero, open. At the time of the second open measurement for each sequence, the occulting of the Eppley pyranometer was carried out. It was assumed that this period would be representative of the diffuse radiation for the five-minute period of incoming radiation directly preceding it.

Before each sequence of actinometer measurements, the temperature of the thermopile was recorded to an accuracy of 0.5°C. This was also done at the end of a set of measuring sequences to check for change. Although a large error in measurement may be encountered, this error becomes negligible when used to calculate the correction factor.

Each sequence of measurements took approximately seven minutes to complete and the procedure is repeated. At the beginning of the season, the measurements were repeated three times every half-hour. This was then decreased to a set of five consecutive measurements about the solar hour. These measurements were supplemented by observations being taken throughout the entire hour. The difference between these two types of measurement frequencies is negligible; the change in atmospheric turbidity conditions between a 15-minute and a 30-minute interval between observations being very minor.

From the raw data collected over 21 days throughout the experiment (from May 23 to August 20), only the open and zero filters were used from the actinometer in the study (Table 2). This was converted according to the proper correction factor and along with the corrected pyranometer data was used to determine the Linke Turbidity Factor (Linke, 1922) and the Unsworth and Monteith τ_a (1972).

A comparison was also made to determine the accuracy of the residual method of determining the direct beam component with that of actinometer measurements. This was carried out by using a Biomedical (BMD) program to compute the correlation coefficients and standard errors between the two methods for daily and overall observations.

DATE	TIME (DECIMAL HOURS) First Observation	Last Observation
May 12	10.66 (LAT)	14.91 (LAT)
May 27	09.56	17.93
May 28	06.49	16.91
June 02	09.32	10.32
June 04	05.95	08.41
June 09	05.90	17.44
June 23	08.37	12.87
June 26	06.12	15.00
June 30	06.04	15.97
July 01	06.07	17.01
July 04	06.22	10.88
July 05	07.13	18.04
July 17	07.04	14.90
July 22	06.98	17.96
July 23	05.68	10.97
July 25	05.97	06.98
July 26	11.10	16.94
July 28	06.98	10.78
July 29	07.99	17.96
July 30	06.06	13.91
July 31	06.98	15.97
August 01	07.98	14.97
August 08	06.98	15.86
August 09	07.01	16.98
August 12	07.99	12.00

Table 2. The date and the meaned time of the first and last set of observations for each day of measurements.

CHAPTER 5

INSTRUMENTATION

The direct beam solar radiation was measured by a Linke-Feussner Actionometer. The actinometer body consists of six copper rings of decreasing radius from 12.6 mm to 10 mm. These serve as diaphragms to reduce air turbulence within the instrument. Between these and the casing is a layer of felt which dampens rapid temperature variations. As added protection against solar heating, a sun screen is placed above the head of the instrument. Since the thermopiles have a temperature dependency, a thermometer is set within the copper rings to determine the temperature of the air surrounding the thermopiles.

With the sighting of a procedure, a pinpoint of light on a bull's eye-type target, it was found that for the one minute periods of readings taken for each of the five lenses, the actinometer did not have to be readjusted. After each reading, it was re-aligned with the sun's beam.

The actinometer is supplied with standard filters as recommended by the International Radiation Commission. These include a yellow filter OG1, a red filter RG2 and a quartz filter. The instrument also has a filter disc for the determination of zero, which is a double-walled screen.

The sensing device consists of a compensated Moll-thermopile composed of 2 x 20 thermocouples of constantan-manganin. This provides a circular sensing surface of a 10 mm diameter with a sensitivity of approximately 10 mv/[Wm^{-2}]. The lag time of the thermopile is 8 seconds.

At an actinometer temperature of 20°C, the sun radiation can read directly in Wm^{-2}. Varying from this, a 0.2% per degree Celcius correction factor must be applied. This temperature correction factor can be expressed as

$$[1. + \alpha(t - 20)] \qquad (28)$$

where $t = 0.002$ *for sun radiation.*

A precision Eppley Pyranometer Model 15 was used in the measurement of the direct and diffuse solar radiation in the determination of the direct beam radiation through residual. This instrument contains a 50-junction, wire-wound, plated thermopile of copper-constantan enclosed in two concentric glass hemispheres of 30 and 50 mm diameters. The sensing surface is recessed beneath these on an equatorial plane and is covered with parson's optical black. The pyranometer contains its own dessication (copper anhydride) to prevent condensation. This was checked regularly through the experiment. A protective white disc about the instrument guarded against radiation reaching the thermopile.

The pyranometer's thermopile has an accuracy of ±0.05% over the ambient temperature range of -20 to 40°C. It further has an accuracy of ±0.05% for input from 0 to 2800 watts m^{-2}. This does not vary by more than ±1% between zenith angles of 0 to 70° and only up to ±3% for zenith angles greater than 70° (see Figure 2). For the entire experiment the zenith angle never exceeded 70°. The calibration factor for the instrument was 4488.14 Wm^{-2} mV^{-1}. Its response time was 1 second to reach 63.2% of the measured value and 3 seconds to reach 95% of the value (Latimer, 1971).

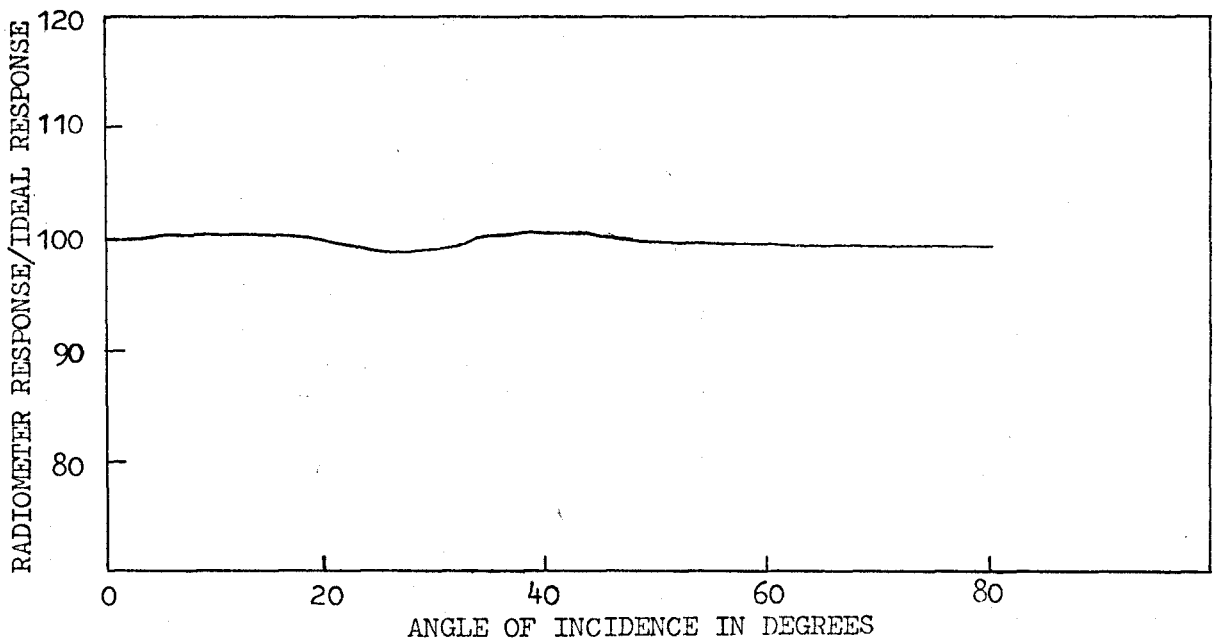

Figure 2. The cosine response of the Eppley precision spectral radiometer (Model 15). (Latimer, 1971)

All measurements were recorded on a Honeywell Electronik 194 strip-chart recorder. This particular model is of multi-range and has two independent pens. The instrument ran at a speed of 1 inch per minute; the actinometer's output being recorded on a full scale of 20 mV and the pyranometer's signal being recorded on a 10 mV range.

The recording accuracy of the instrument is ±0.25% of the span. This gives the actinometer's data a recorded accuracy of ±0.05mV. The pyranometer's recorded data is accurate to ±0.025 mV. Due to the scales used in the recording of the data, an error inherent in the recording is that of removal. For the pyranometer, this would be ±0.01 mV and for the actinometer, ±0.02 mV. This works out to be a 1% error for each.

A further determination of error and cumulative error is found in the section on error analysis. The progression of error between the instrument output and the digitization can be seen in Table 3.

CHAPTER 6

ERROR ANALYSIS

The error stated in the description of the two sensors and the recorder are the manufacturer's quoted accuracy. These will be dependent on care and maintenance of the instruments, but with proper attention this accuracy will be the upper limits of error. The error derived from the strip-chart recorder was taken because it provides the maximum accuracy that one can achieve in data removal. It was determined from the span of the recorder and the diameter of the pen line.

From the instrumental error, the maximum error can be determined by summing the individual errors in the procedure. According to Cook and Rabinowicz (1963), this error is unlikely to occur if all errors are independently derived. Equally unlikely, is the case when all errors cancel out. The most probable error is that of the root mean square (Cook and Rabinowicz, 1963; DeWalle and Parmere, 1974). Consider the individual errors ε_a to ε_d as independently derived components of the total error. The root mean square is

$$\varepsilon_i = (\varepsilon_a^2 + \varepsilon_b^2 + \varepsilon_c^2 + \varepsilon_d^2)^{1/2} \qquad (29)$$

In Table #3, the maximum error and the root mean square are given for both sets of radiation instruments.

The R.M.S. method was also employed in determining the accuracy of the final outcome of the two methods used for determining direct beam

radiation. In the case of the direct beam method, the open filter must be reduced to account for the zeroing of the instrument. For the pyranometer method, the diffuse radiation must be removed from the net radiation.

To reduce experimental error internally in the measurements, for any one time period, up to five separate sets of observations of each variable were recorded. This was accomplished by setting a time period to eclipse the solar hour such that the mean time would be the solar hour. The observations were then averaged to give the working value for each variable. In this manner, spurious fluctuations were reduced to a minimum. These mean values will be used in the discussion.

Instrument	Instrument Error	Recording Error	Data Reduction Error	Maximum Error	Root Mean Square
Eppley (global and diffuse)	1%	0.5%	1%	2.5%	2.25%
Actinometer (direct beam)	1%	0.5%	1%	2.5%	2.25%

Table 3. Accumulative or maximum error and root mean square error of the instrumentation as indicated by the manufacturers.

CHAPTER 7

COMPARISON OF APPROACHES IN DETERMINING DIRECT BEAM RADIATION

Latimer (1971) determined the calibration of pyranometers by determining the direct beam component of solar radiation by residual and comparing it to a standard actinometer reading. Similarly, Unsworth and Monteith (1972) checked the calibration of a Linke-Feussner Actinometer by comparing it to direct beam values determined from net and diffuse radiation measurements by a Kipp solarimeter. Both comparisons were done for a finite set of measurements on given clear sky days. No such comparisons have been attempted over a longer period of time in varying meteorological conditions.

Linear correlations, using the residual method as the independent variable and measured direct beam radiation as the dependent variable, were performed for each of the 25 days of observations. Of these, June 2 was rejected due to the small sample size. A final regression was then performed on the composite data set. In doing so, a combination of cloud amount, temperature, wind velocity and direction are incorporated into the evaluation of the accuracy of the residual model as a predictor of direct beam radiation.

A further comparison of the data was accomplished by determining the ratio of the direct beam values over the residual determination. By this, any systematic value differences are brought out by the ratio's divergence from 1.0. At low sun angles, it was found that the residual model underestimated the values measured by the actinometer, while for

most of the other parts of the day, the actinometer values were less than the residual values. Several major exceptions to this must be noted however. On days with high turbidities, the actinometric data were larger than the residual data by approximately 0.2 to 8%. When this was combined with low sun angles, the difference was increased to a maximum of 23% late on August 9.

A second exception to this is for days of low turbidity; the values of the measured and residual direct beam are also reversed from the normal. The prime example of this is August 8. Turbidities were never greater than 0.1 for the day and yet from 1000 hours to 1600 hours, the actinometric values range from 0.2 to 8% as the day proceeds.

A general progression of this phenomenum is seen as the season progresses with the exception of several hazy days. For days before July 30, only those hours during low sun angles have residual values less than the measured values. Beginning on July 30, the hours between 1000 and 1400 have the values reversed. At 1400, measurements were abandoned due to cloud cover. On July 31, August 1, 8, 9 and 12, all had higher actinometric values beginning in the middle of the morning and continuing throughout the day. No explanation for this phenomenum can be offered at the present time. All data were recorded in the same manner before and after the phenomenum occurred. A change in experimental procedure cannot, therefore, be linked with this apparent change in values for the two determinations of the direct beam component.

Although these discrepancies bear further investigation their overall effect on the two methods of determining the direct beam

measurement is small. For the 967 measurements of direct beam radiation by each method, only 28 (approximately 3%) are different by greater than 10% of the lesser value. All of these values show that the actinometric measurement is larger. Further, they occur when the zenith angle is very large; the solar time being before 0700 or afer 1700. Of those values under 10% difference, the majority are under 5%. With a R.M.S. error of 2.9%, this variation does not appear to be a limiting factor in using the residual method of determining direct beam radiation.

Twenty-six regressions were run on the data; one for each day and one including all the data. As would be expected, the coefficients of determination were all greater than 0.9 (Table 2); 17 of the first 25 regressions) having an r^2 value greater than 0.98 and only 5 regressions with an r^2 value less than 0.95. The r^2 value for the regression combining all the data was 0.98.

The y-intercept values of the regressions show a large variation, ranging between -150 and 115 Wm^{-2}. As the number of data points increase, the intercept approaches 0.0. Exceptions to this do occur however. At present, no explanation can be offered. Generally, the large intercept values are due to the small scatter of the data for values with only a 200 Wm^{-2} range in the 600 to 800 Wm^{-2} domain. This forces the equation to give values of no physical reality.

The slope term for the individual days approaches 1.0 with a range between 0.86 and 1.29; only two days being less than 1.0. This indicates again that the actinometric measurements were slightly less than residual values.

The final linear correlation was performed using all data, including June 2. The r^2 value of 0.98 indicates that the correlation performed is nearly a perfect fit to the data. This is also shown by a standard error of estimate of only 21.83 Wm^{-2}. The intercept value for the 967 measurements is -31.23 Wm^{-2} which also shows a very close fit to a 1:1 line; the slope of the correlation line being 1.08, nearly 45°.

The negative intercept can be partially explained by the method of obtaining the diffuse measurement. Since the disc was hand-held, slight variations of diffuse readings could be possible. If the diffuse readings were slightly less than the actual diffuse radiation, the residual direct beam radiation would be greater than the actual direct beam radiation. Because accurate estimation of the error involved in this procedure cannot be supplied, attention must be given to the values of the slope and intercept terms of the correlation. The error, as calculated by the intercept over the mean value of the residual method, to approximately 4.25%, which in terms of other micrometeorological measurements (i.e. Swissteco Radiometers) is within the limit of acceptability.

CHAPTER 8

AIR MASS AND PRECIPITABLE WATER DEPENDENCIES FOR THE THREE TURBIDITY FACTORS

The dependency of turbidity on changing air mass and precipitable water is necessary to interpret the meaning of a given turbidity value. A comparison of the two Linke T's and the Unsworth and Monteith τ_a with respect to these variables was therefore carried out to evaluate these dependencies and to determine the most accurate method in calculating turbidity.

A model Houghton atmosphere was determined for a number of different air masses and precipitable water values. Using this model, a 20% attenuation factor was assumed for a unit air mass and a model atmosphere was established. Using these values, the three turbidity values were determined for a given air mass and precipitable water value. The results of these computations can be seen on Tables 4, 5 and 6 for air masses of 1.000 to 3.00, with increments of 0.25 and precipitable water values of 5 to 60 mm, with 5 mm increments. These are presented graphically with turbidity plotted against air mass for varying precipitable water values.

The most effective turbidity factor for determining the amount of atmospheric aerosols is that of Unsworth and Monteith (1972). Unlike Sivkov's (1968) or Hoyt's (1973) determination of Linke's T, τ_a is totally independent of atmospheric water vapour. The second advantage of the τ_a turbidity is that its dependence on air mass is slight. This is readily

Precipitable Water	Air Mass				
	1.00	1.50	2.00	2.50	3.00
0.500	0.2231	0.2378	0.2554	0.2773	0.3054
1.000	0.2231	0.2378	0.2554	0.2773	0.3054
1.500	0.2231	0.2378	0.2554	0.2773	0.3054
2.000	0.2231	0.2378	0.2554	0.2773	0.3054
2.500	0.2231	0.2378	0.2554	0.2773	0.3054
3.000	0.2231	0.2378	0.2554	0.2773	0.3054
3.500	0.2231	0.2378	0.2554	0.2773	0.3054
4.000	0.2231	0.2378	0.2554	0.2773	0.3054
4.500	0.2231	0.2378	0.2554	0.2773	0.3054
5.000	0.2231	0.2378	0.2554	0.2773	0.3054
5.500	0.2231	0.2378	0.2554	0.2773	0.3054
6.000	0.2231	0.2378	0.2554	0.2773	0.3054

Table 4. The dependency of τ_a on precipitable water and air mass.

Precipitable Water	Air Mass				
	1.00	1.50	2.00	2.50	3.00
0.500	3.0694	3.4839	3.9049	4.3741	4.9335
1.000	3.2943	3.7046	4.1261	4.5981	5.1619
1.500	3.4810	3.8935	4.3198	4.7981	5.3691
2.000	3.6502	4.0683	4.5021	4.9889	5.5693
2.500	3.8093	4.2356	4.6788	5.1761	5.7678
3.000	3.9619	4.3983	4.8528	5.3625	5.9676
3.500	4.1101	4.5584	5.0259	5.5499	6.1706
4.000	4.2553	4.7171	5.1994	5.7395	6.3783
4.500	4.3982	4.8751	5.3740	5.9325	6.5919
5.000	4.5396	5.0332	5.5504	6.1297	6.8128
5.500	4.6800	5.1918	5.7293	6.3319	7.0422
6.000	4.8197	5.3514	5.9113	6.5399	7.2814

Table 5. The dependency of the Hoyt determination of the Linke T on precipitable water and air mass.

Precipitable Water	Air Mass				
	1.00	1.50	2.00	2.50	3.00
0.500	2.0696	2.3775	2.6724	2.9851	3.3446
1.000	1.9475	2.2139	2.4679	2.7361	3.0438
1.500	1.8654	2.1019	2.3258	2.5613	2.8307
2.000	1.8024	2.2151	2.2152	2.4245	2.6632
2.500	1.7510	1.9441	2.1242	2.3117	2.5248
3.000	1.7076	1.8839	2.0470	2.2159	2.4070
3.500	1.6699	1.8317	1.9801	2.1326	2.3046
4.000	1.6367	1.7857	1.9211	2.0593	2.2142
4.500	1.6071	1.7447	1.8685	1.9938	2.1334
5.000	1.5804	1.7078	1.8211	1.9347	2.0604
5.500	1.5561	1.6742	1.7780	1.8810	1.9940
6.000	1.5339	1.6435	1.7386	1.8319	1.9330

Table 6. The dependency of the Sivkov determination of the Linke T on precipitable water and air mass.

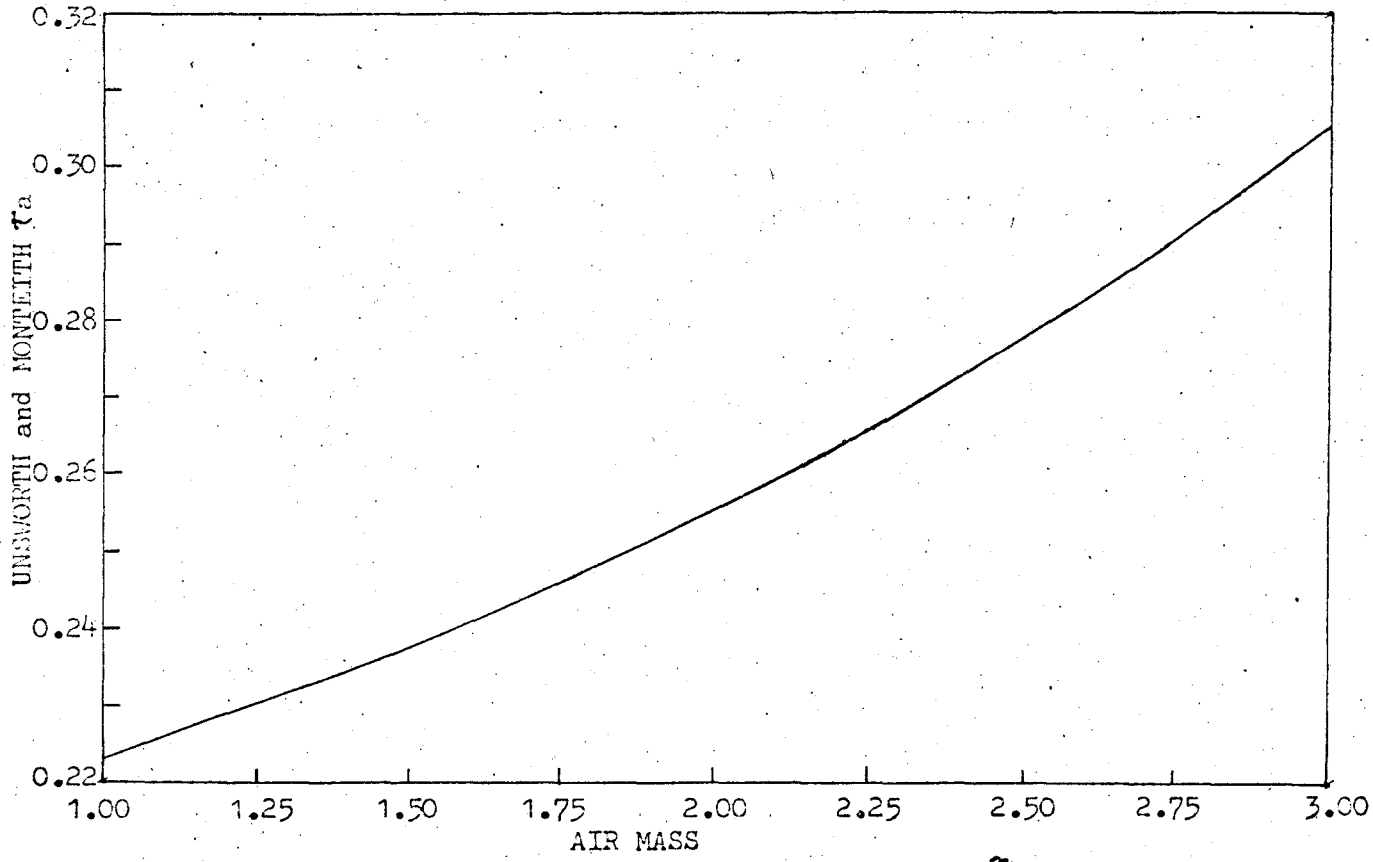

Figure 3. The dependency of the Unsworth and Monteith τ_a on air mass.

observed on Figure 3 with a change of 0.0823 or 37% due to an air mass change of 200% from 1.0 to 3.0.

The Hoyt (1975) version of the Linke T is seriously affected by precipitable water when considering aerosol alone as an aerosol factor. *P(m)* is derived using a Rayleigh atmosphere. By introducing increasing amounts of preciptable water in the calculation, T increases linearily. A further complication in using the Linke T is its dependence on air mass. By varying air mass in a similar manner to the τ_a calculation, T was found to increase by 60.73% for 10 mm of precipitable water, but only 51.07% when preciptiable water reached 60 mm (Figure 4). Precipitable water over Hamilton never exceeds 40 mm, but the figures illustrate the interdependency of air mass and precipitable water on the Linke T.

In attempting to reduce the interdependencies, the Sivkov (1968) "wet" turbidity was evaluated. This allowed the input of precipitable water into the ideal atmosphere to reduce turbidity dependency on this parameter. Figure 5 illustrates the results from Table 6 for varied precipitable water values. Because of the logarithmic influence of precipitable water in the wet turbidity factor, the dependency of T on precipitable water increases as air mass increases and decreases as precipitable water increases with air mass held constant.

When holding precipitable water constant and allowing air mass to increase (Figure 6), T behaves unexpectedly. For large amounts of precipitable water, the variation in T over varying air masses is only 26%, the least of all three turbidity indices. However, as precipitable water decreases, for the same variation in air mass, T changes more drastically. The change in turbidity, with a precipitable water of 10 mm and with a

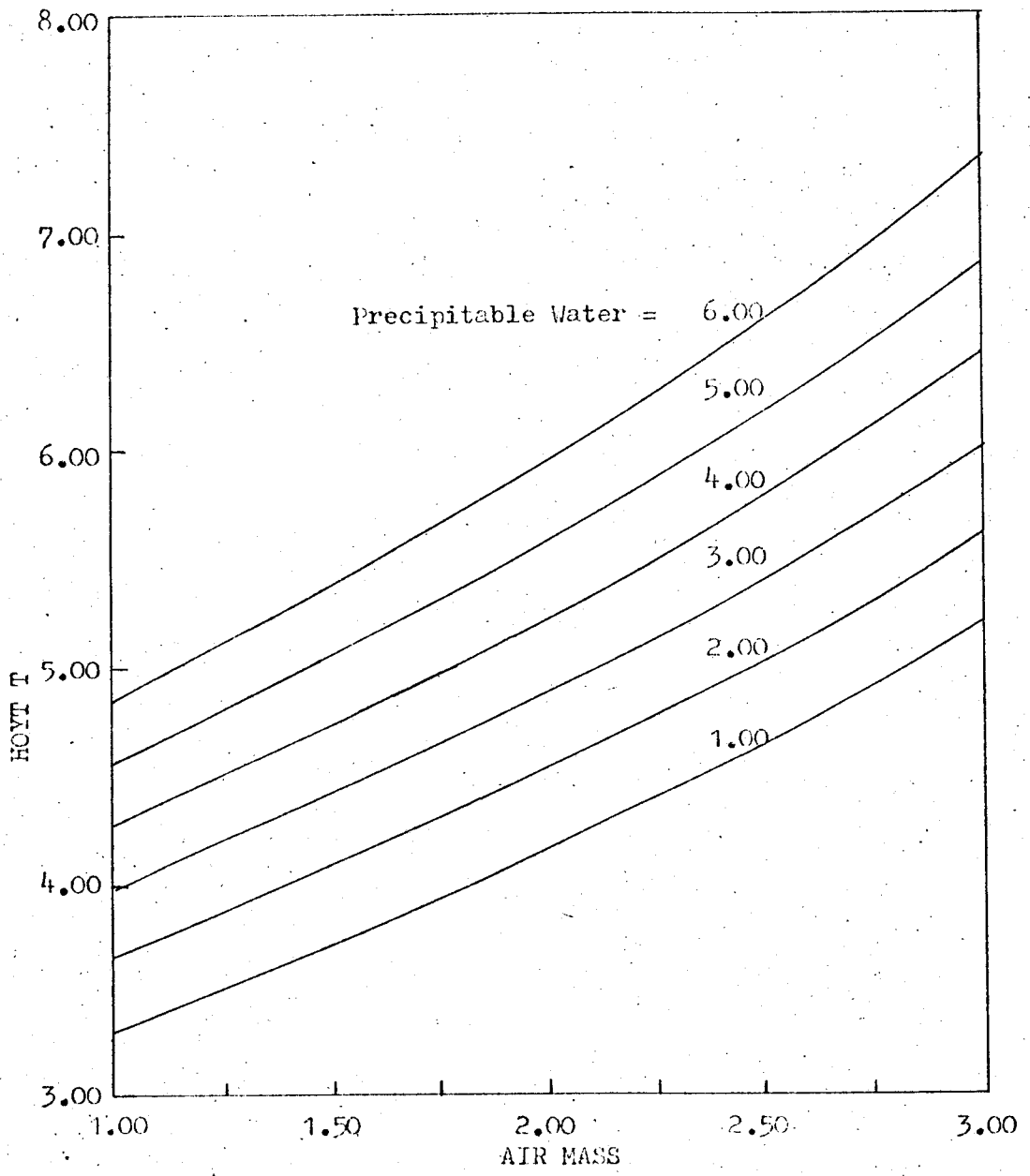

Figure 4. The dependency of the "Hoyt T" on air mass for given precipitable waters.

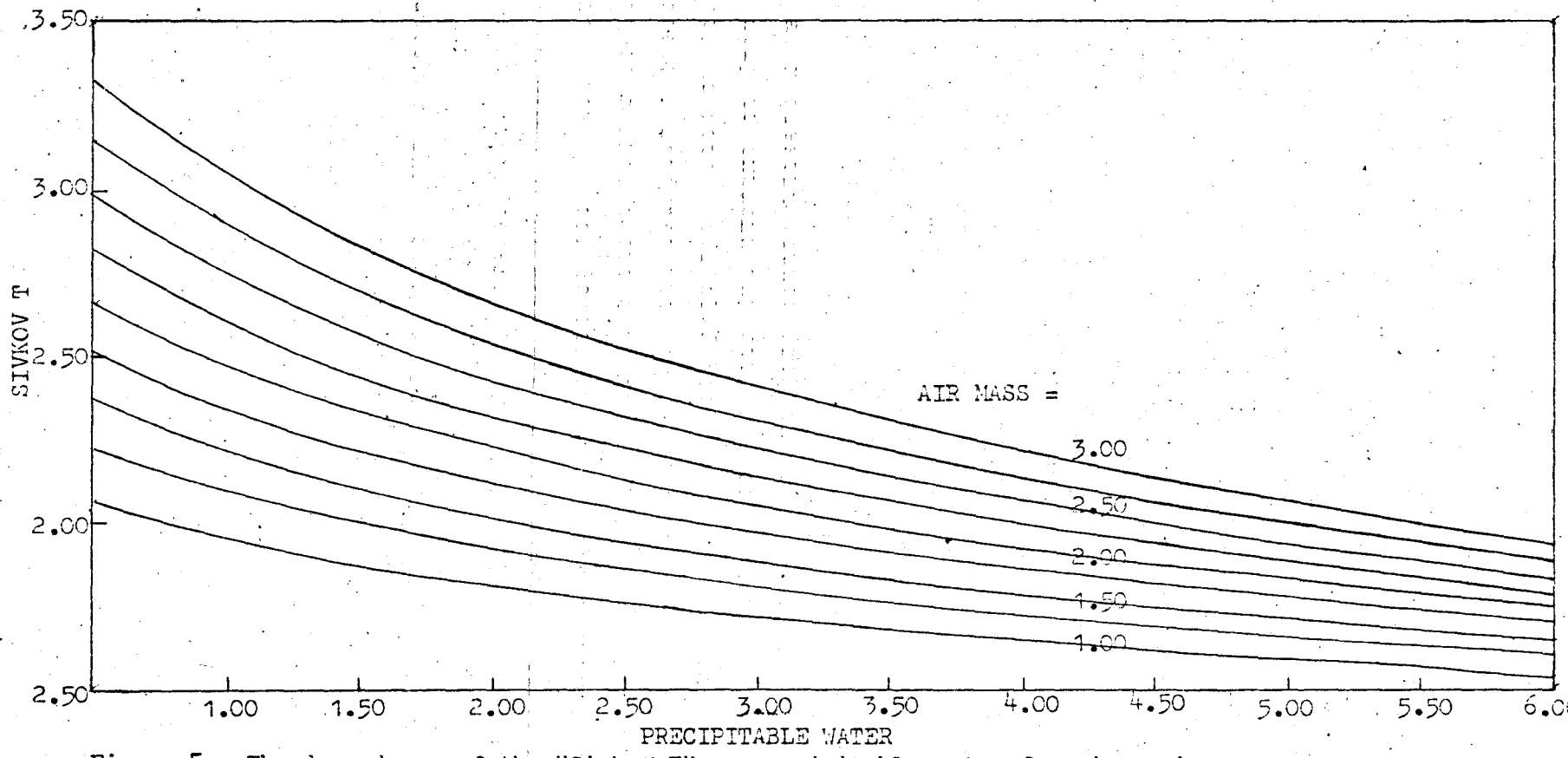

Figure 5. The dependency of the "Sivkov T" on precipitable water for given air masses.

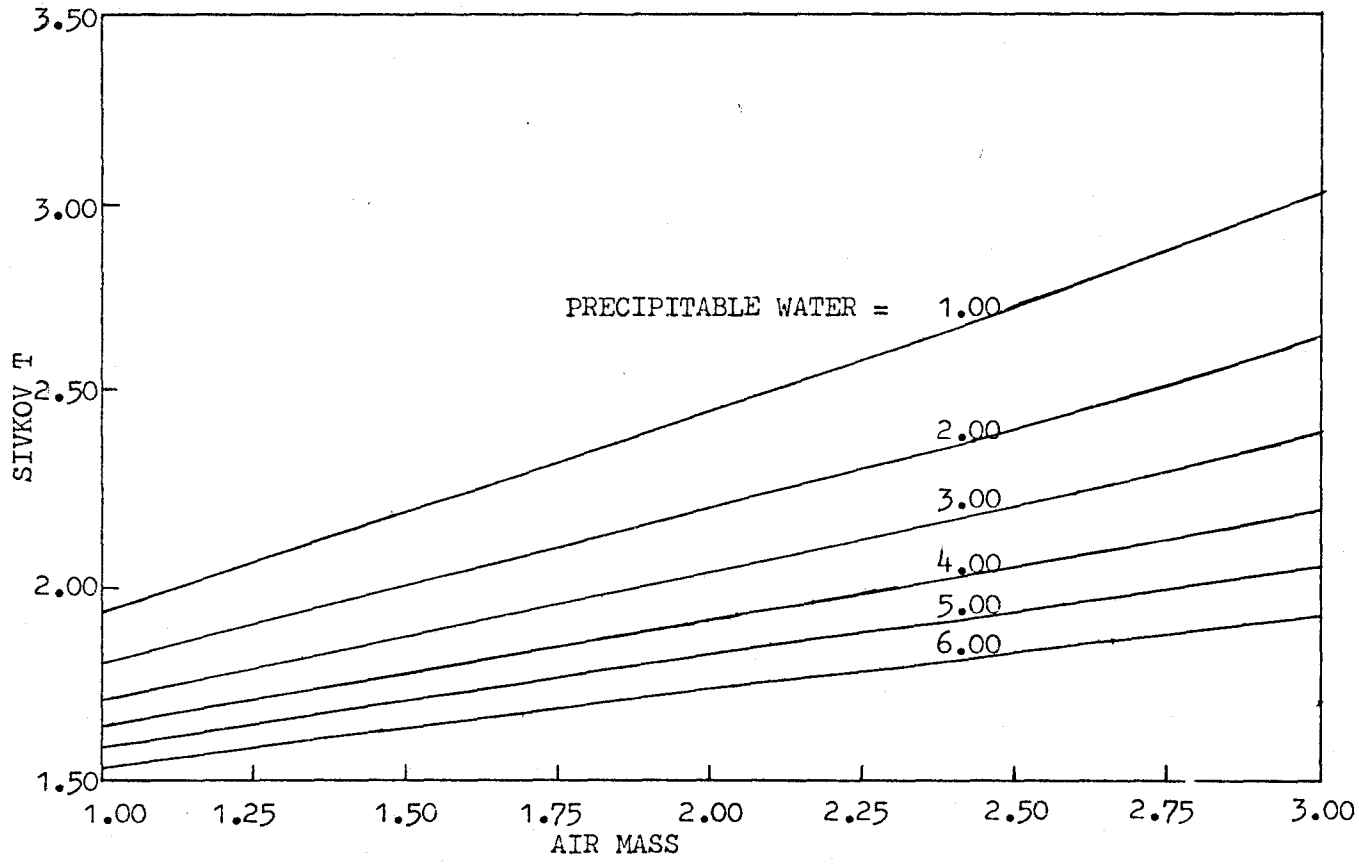

Figure 6. The dependency of the "Sivkov T" on air mass for given precipitable waters.

changing air mass from 1.0 to 3.0, is 61.61%. This is virtually identical to that of Hoyt's (1975) calculation of T.

The average precipitable water over Hamilton during the time that measurements were taken was approximately 20 mm. The percent change of the Sivkov T and the Hoyt T for this precipitable water value, with varying air mass, are 47.75% and 52.58% respectively. Because of the lesser variation of the Sivkov T with air mass for the summer measurement period, results obtained will be a more accurate indicy of aerosol turbidity in Hamilton than that of the Hoyt T. Therefore the Sivkov T is the preferred method of determining the Linke Turbidity Factor for this study.

CHAPTER 9

SYNOPTIC DEPENDENCIES

Many sources (Kondratyev, 1969; Joseph and Manes, 1971; Manes, 1972; Unsworth and Monteith, 1972) show that the turbidity of a site is dependent on local sources of pollution and the history of the prevailing air mass. The latter determines the input of aerosols from distant sources and their distribution in the atmosphere (Unsworth and Monteith, 1972). To evaluate the exact nature of the synoptic influence on aerosols in Hamilton, two methods were utilized. The first method was to take all periods of coverage of two or more consecutive days and study changes in turbidity with respect to synoptic conditions, wind direction and wind speed. The second method was to plot turbidity against wind direction. In this manner, local effects and synoptic effects can be determined by the origin of the air mass with respect to the relative locations of local pollutant sources to the measurement site.

Synoptic Pattern Analysis

All turbidities discussed are of the Unsworth and Monteith derivation because it is the least dependent on optical air mass and precipitable water. Plots of τ_a indicate the calculated values of turbidity and ± Root Mean Square of these values. Appendix 3 contains similar graphs for the Sivkov T for comparison.

May 27, May 28

On May 27, a high pressure system was centred south of Lake Michigan drawing air from the northwest over Hamiton with a speed of 6.75 ms^{-1} to

10.75 ms^{-1}. These winds were accentuated by a low pressure system centred to the northeast of James Bay (Map 2). Throughout May 26, rainstorms were washing the larger aerosols out of the air (Williamson, 1973) keeping turbidity low. This is seen on the morning of May 27. At 10.00 LAT, the turbidity was 0.144 (Figure 7). Throughout the day, turbidity was decreased reaching a minimum value of 0.047 at 18.00 LAT. The NW wind forced the local influence out over Lake Ontario replacing the local air mass with clean polar air from the Hudson Bay region.

May 28's synoptic pattern was similar to that of May 27 (Map 3). Winds continued to be from the northwest, but with a greater westerly component. By noon, the winds shifted to the west or west northwest. Wind speed decreased to between 2.24 ms^{-1} to 4.48^{-1}. However, even with this lesser wind speed, turbidity remained low, varying between 0.089 and 0.122 (Figure 8). A slight increase in τ_α is apparent throughout the day. This could be due to a build-up of local aerosols not apparent with the stronger winds of May 27. With westerly winds, a small amount of dust from the Niagara Peninsula may also increase the turbidity of Hamilton slightly.

June 30, July 1

On June 29, thunderstorms moved across the region washing out particulate matter. This would clean the atmosphere to a base level from which turbidity would increase. The atmospheric conditions throughout June 30 were stable; no pressure systems bring within a 2000 km radius (Map 4). Breezes of 2.70 ms^{-1} up to 5.40 ms^{-1} were present throughout the day. Early morning winds were northerly, shifting to the north northeast or northeast by 08.00.

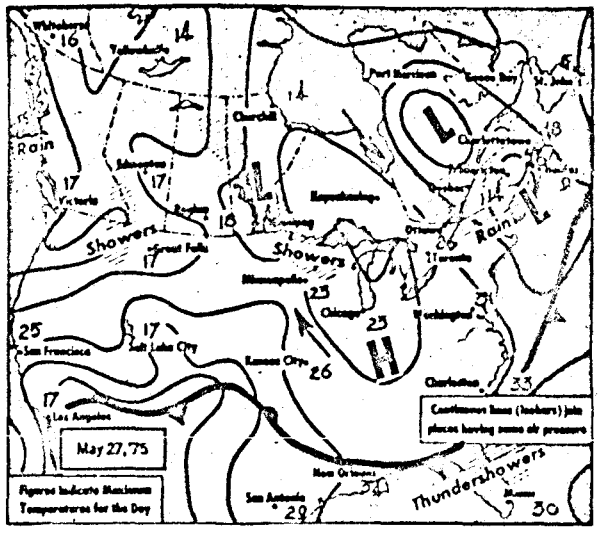

Map 2. Synoptic patterns for May 27.

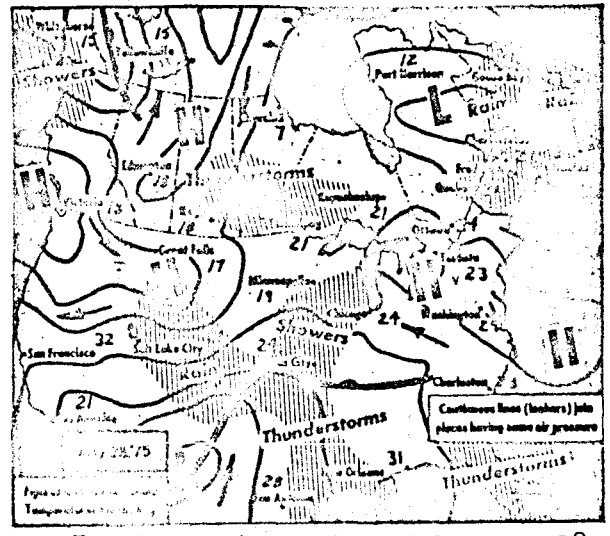

Map 3. Synoptic patterns for May 28.

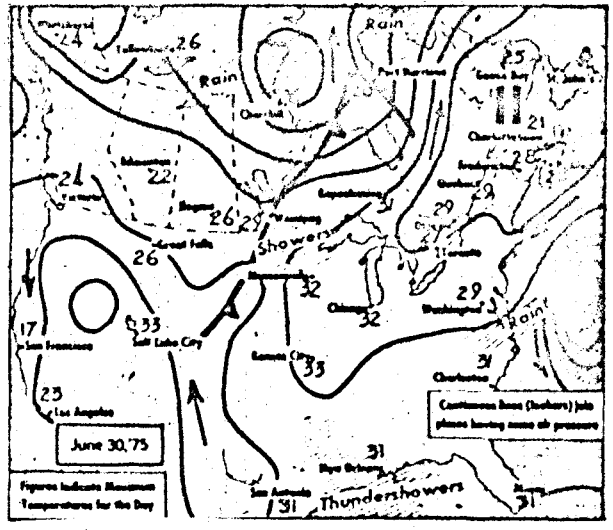

Map 4. Synoptic patterns for June 30.

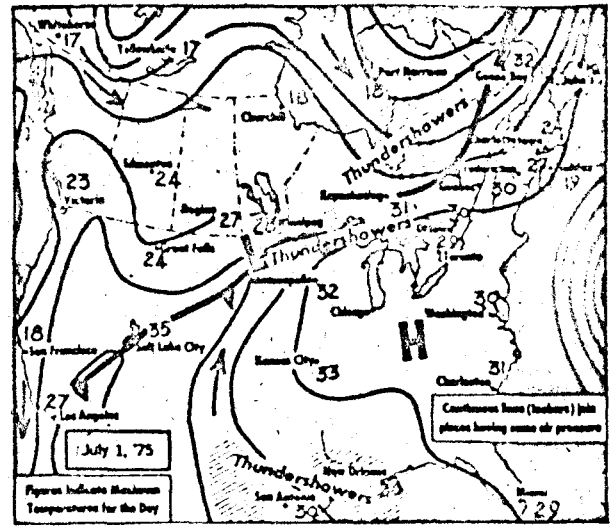

Map 5. Synoptic patterns for July 1.

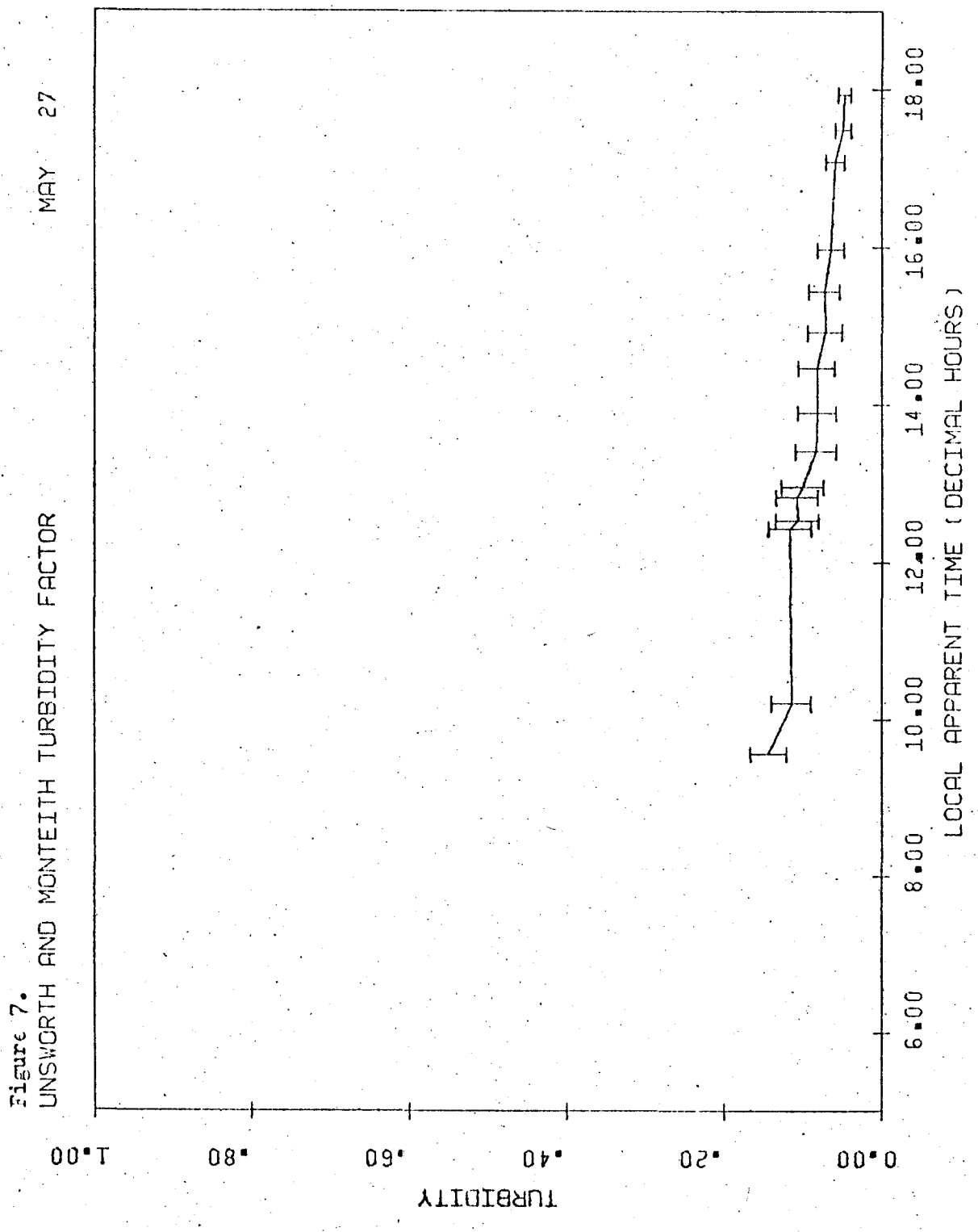
UNSWORTH AND MONTEITH TURBIDITY FACTOR
MAY 27
TURBIDITY
0.00
.20
.40
.60
.80
1.00
6.00
8.00
10.00
12.00
14.00
16.00
18.00
LOCAL APPARENT TIME (DECIMAL HOURS)

Figure 7.

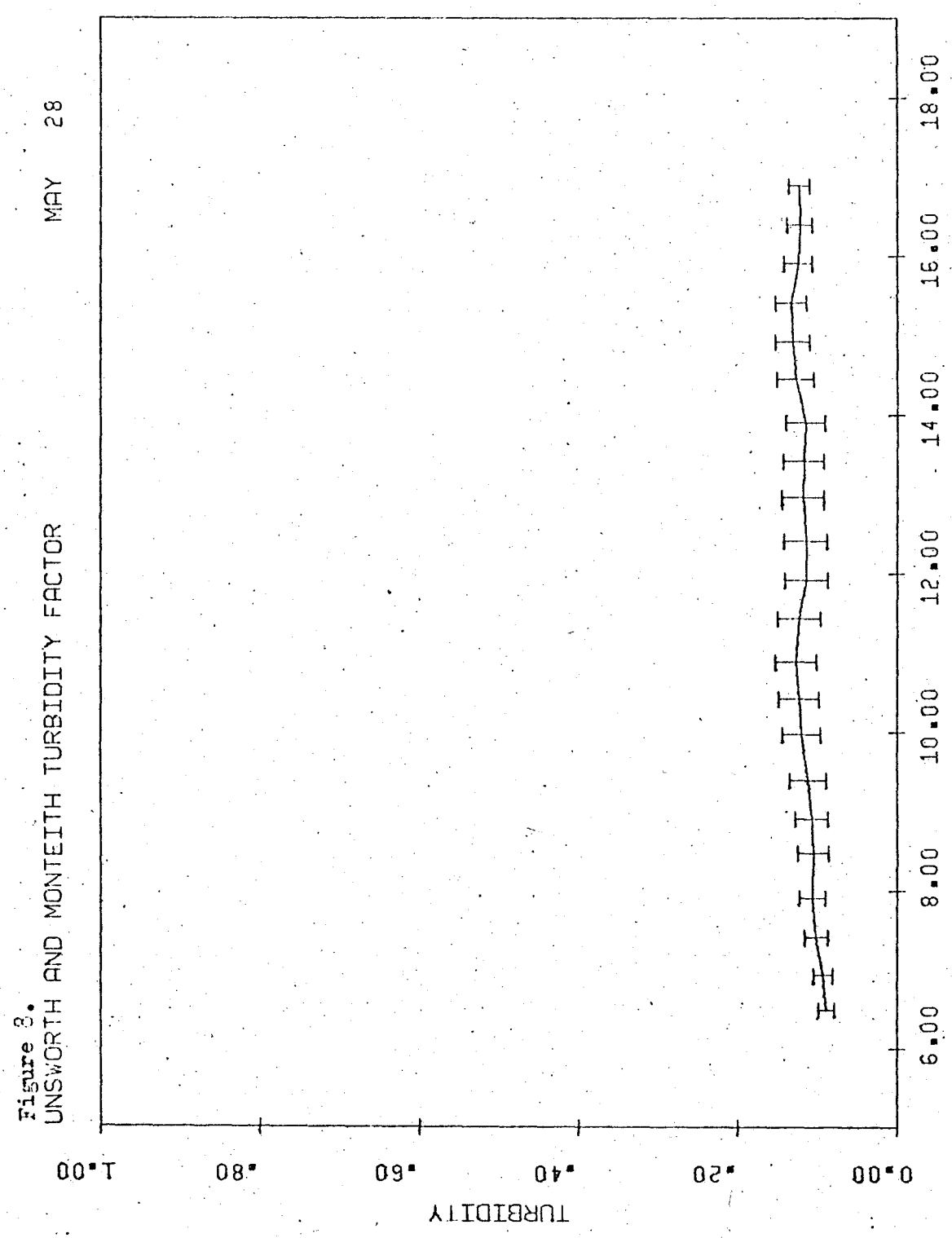
UNSWORTH AND MONTEITH TURBIDITY FACTOR
MAY 28
TURBIDITY
0.00
.20
.40
.60
.80
1.00
6.00
8.00
10.00
12.00
14.00
16.00
18.00
LOCAL APPARENT TIME (DECIMAL HOURS)

Figure 3.

Turbidity at 0600 was evaluated at 0.113 (Figure 9). This increased very slowly throughout the morning to a maximum value of 0.140 at 1400. The turbidity then decreased slightly and remained constant at approximately 0.133.

The effects of the winds are apparent. With a northeast wind, pollutants will be blown toward Hamilton from the industrial areas of Oakville and Toronto. These, as expected, increased turbidity throughout the day while conditions remained stable. The slight reduction in turbidity during the period after 1400 could be due to the sun's position with respect to the aerosol sources and the wind direction. The sun is to the northeast of the measurement site while the major aerosol sources are to the northeast. With a northeast wind, the full effects of these aerosols cannot be measured during latter periods of the day.

Conditions remained stable July 1 (Map 5). Winds were still from the northwest during the early morning, slowly shifting toward the southeast after 1700. Wind speed was 2.44 ms^{-1}.

Until 0700 LAT, the aerosol build-up continues in the manner of June 30 (Figure 10). As the wind direction changes toward the east, more aerosol is blown into the city. τ_a rapidly increases from 0.148 to 0.323. The local nature of this turbidity is evident in its reduction as the solar path moves toward the south and away from the direct influence of the harbour front. By solar noon, the turbidity has been reduced to a value of 0.249.

The rapid rise in turbidity between 1350 and 1500 LAT can be partially attributed to a build-up of cloud affecting the observations. After 1500 the turbidity once again begins to decrease as the presence of cloud dissipates.

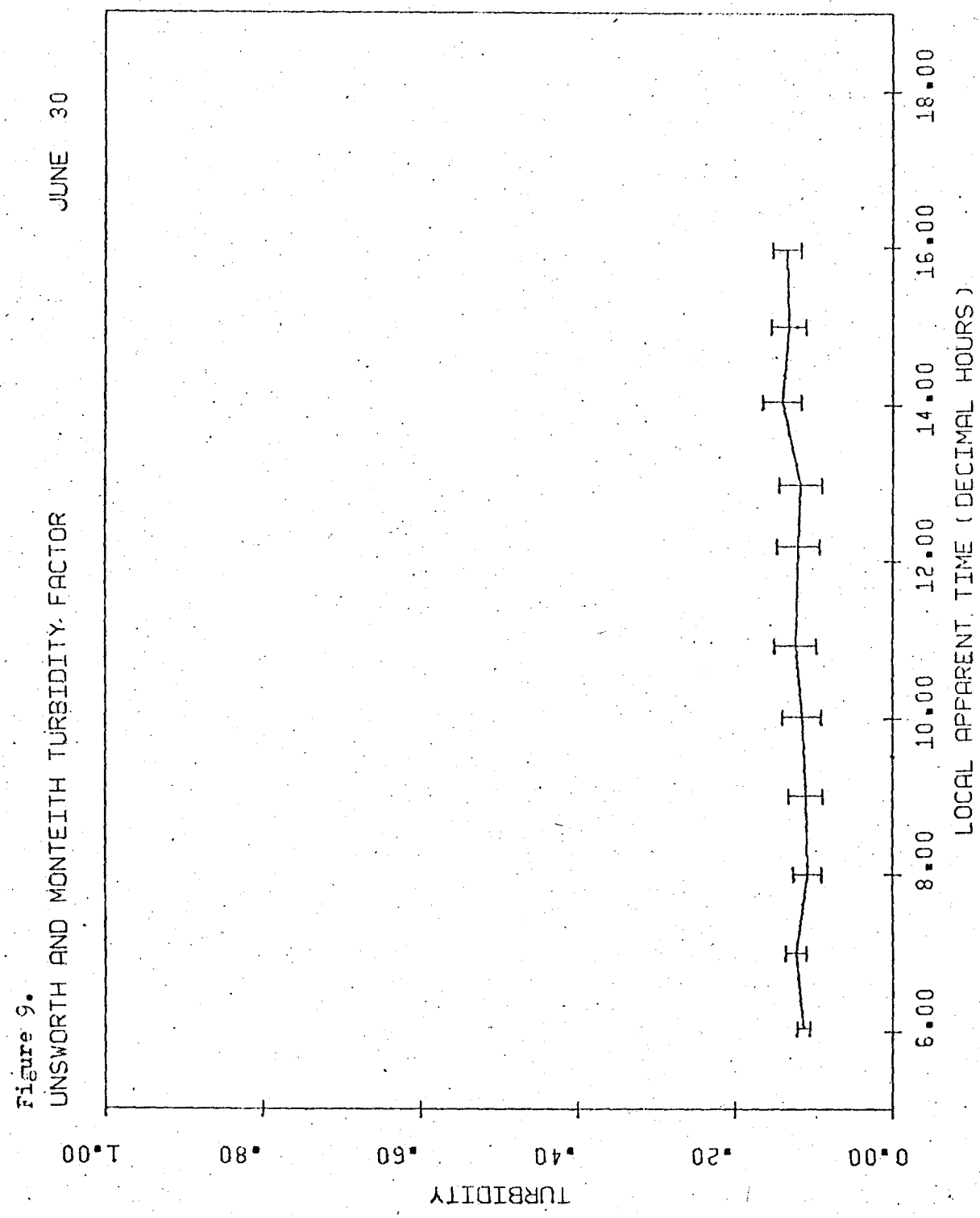

Figure 9.
UNSWORTH AND MONTEITH TURBIDITY FACTOR

Figure 10.

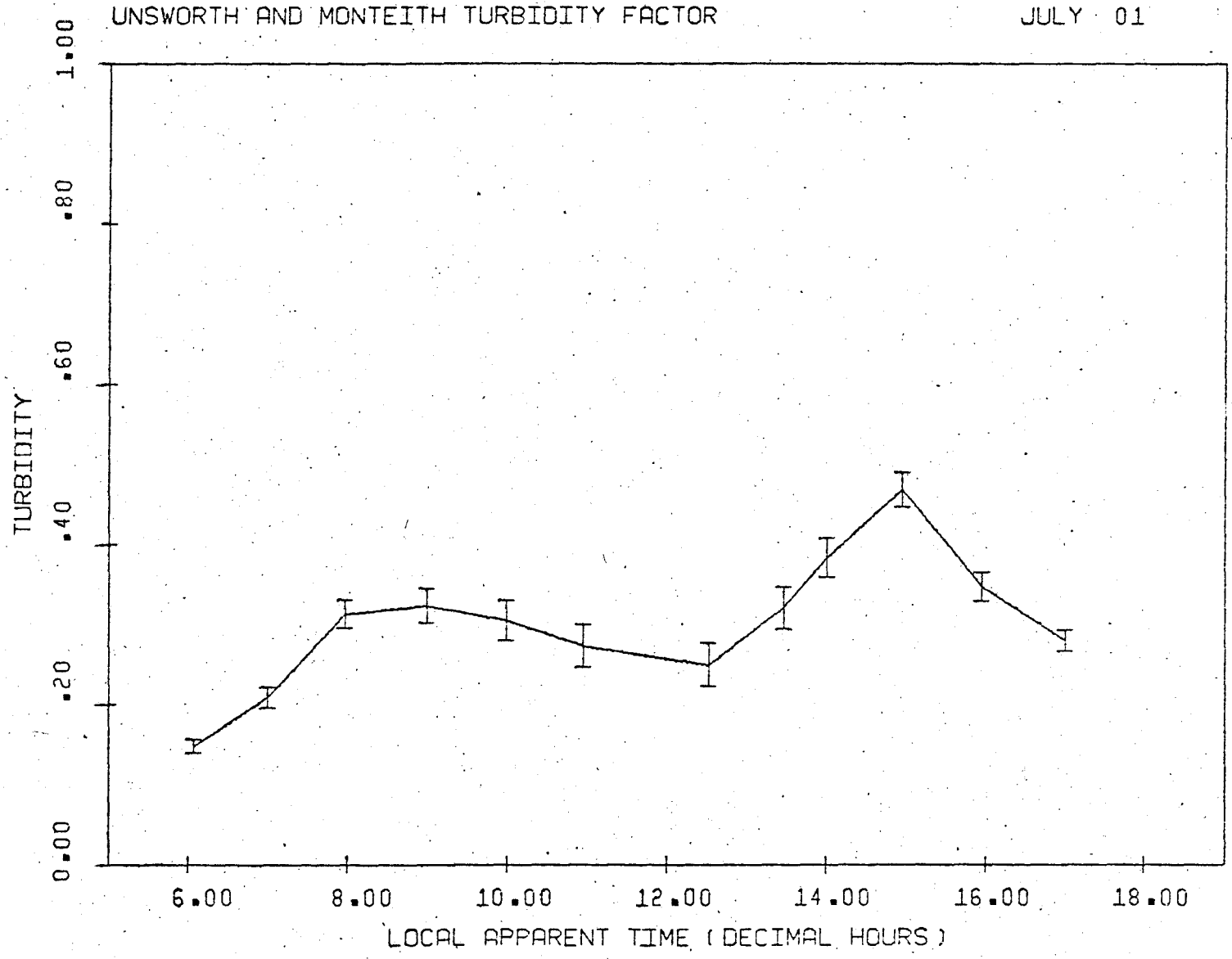
UNSWORTH AND MONTEITH TURBIDITY FACTOR
JULY 01
TURBIDITY
1.00
.80
.60
.40
.20
0.00
6.00
8.00
10.00
12.00
14.00
16.00
18.00
LOCAL APPARENT TIME (DECIMAL HOURS)

July 4, July 5

July 3 was also a day of rain over Hamilton. The measurements for July 4 consisted only of a morning period (Figure 11). As can be seen from Map (6), the synoptic conditions for the area were stable. From 06.00 LAT, a steady build-up of particulate matter was occurring from 0.129 to 0.175 by 09.00 (Figure 11). During this period, wind of 3.15 ms^{-1}, from the northeast were transporting aerosol from the Oakville and Toronto areas. The sudden reduction in turbidity at 10.00 coincides with a wind shift from the northeast to the east. This effectively eliminates the aerosol input from the north shore of Lake Ontario, leaving only local sources of aerosols as contributors. From these observations, it becomes apparent that the movement of particulate matter from the industralized region of the northeast exerts a definite influence on the turbidity of Hamilton.

The synoptic conditions for July 5 remained stable. Wind velocities were approximately 2.5 ms^{-1} shifting from the west northwest to the south southwest as the day progressed.

Turbidity was at least twice as high as July 4, with the early morning turbidity being 0.323 (Figure 12). It increased only slightly to 0.391 by 14.00. After this, turbidity began to decrease. This decrease corresponds with a wind shift to the south southwest; the wind blowing up the Niagara Peninsula. Areas south of Hamilton were under low pressure conditions including rain showers, as can be seen from the low pressure system moving across the northern states from July 4 to July 6 (Map 7). This would explain the reduction of turbidity with the changing wind direction, the cleaned air from the south moving into the area.

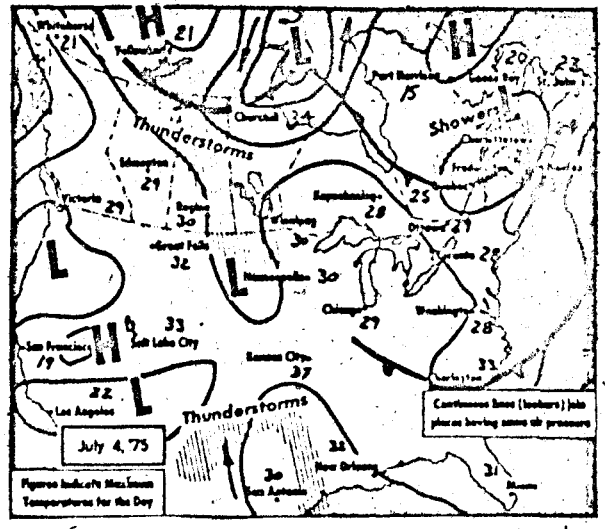

Map 6. Synoptic patterns for July 4.

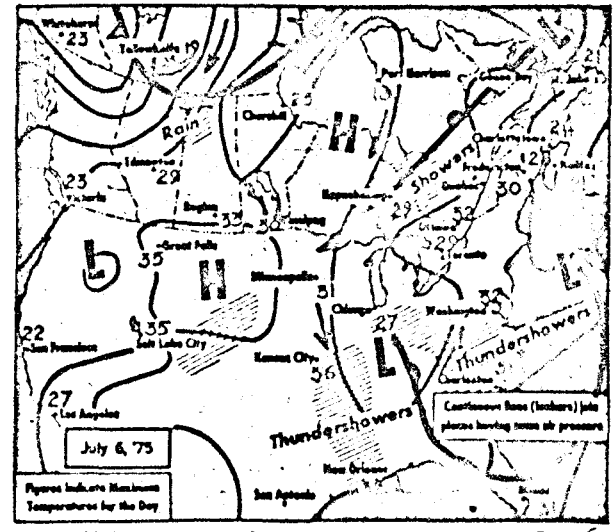

Map 7. Synoptic patterns for July 6.

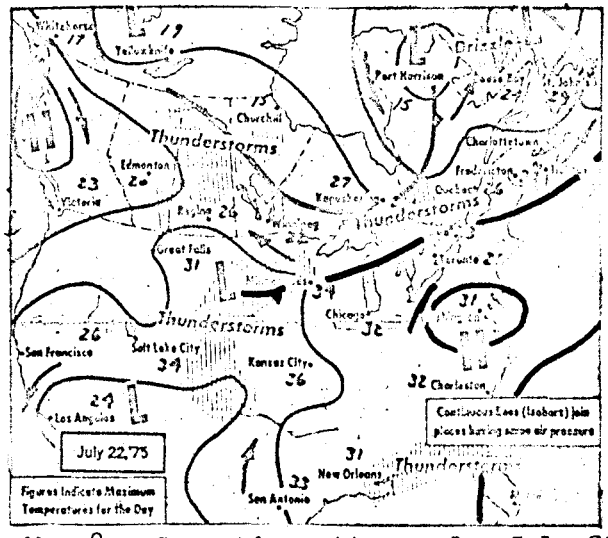

Map 8. Synoptic patterns for July 22.

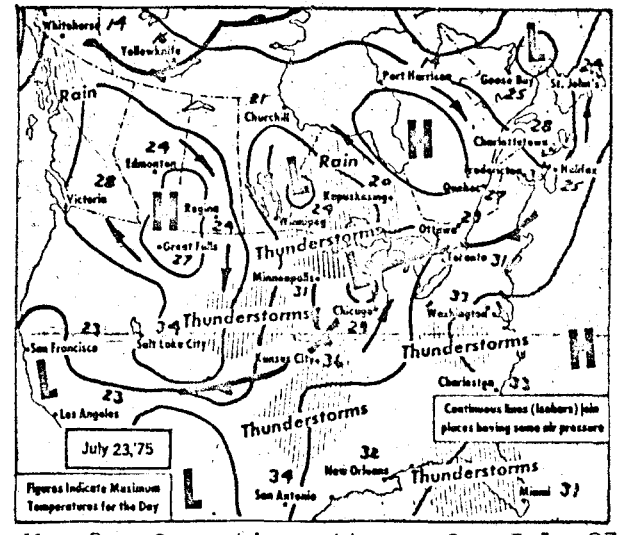

Map 9. Synoptic patterns for July 23.

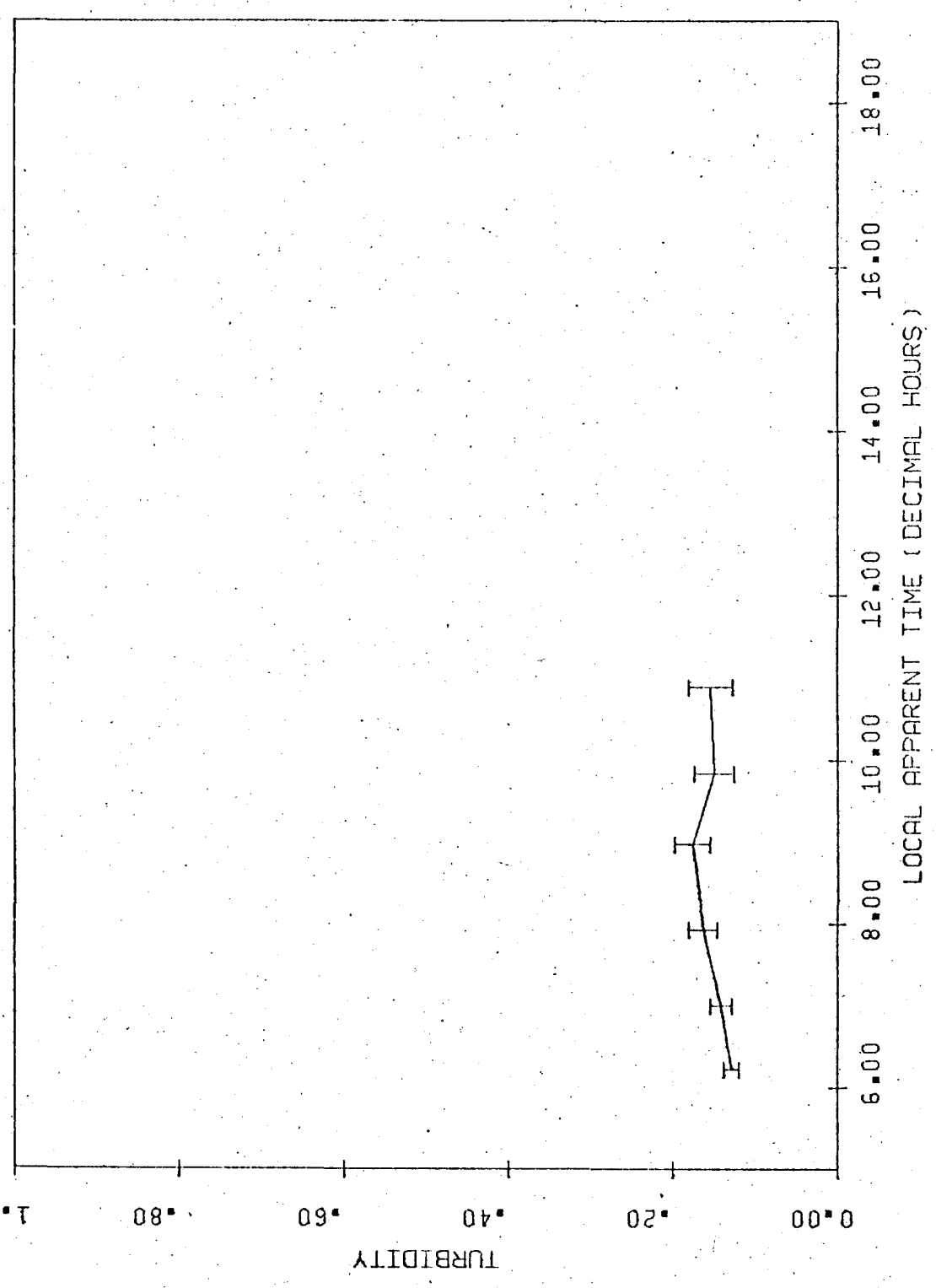

Figure 11.
UNSWORTH AND MONTEITH TURBIDITY FACTOR

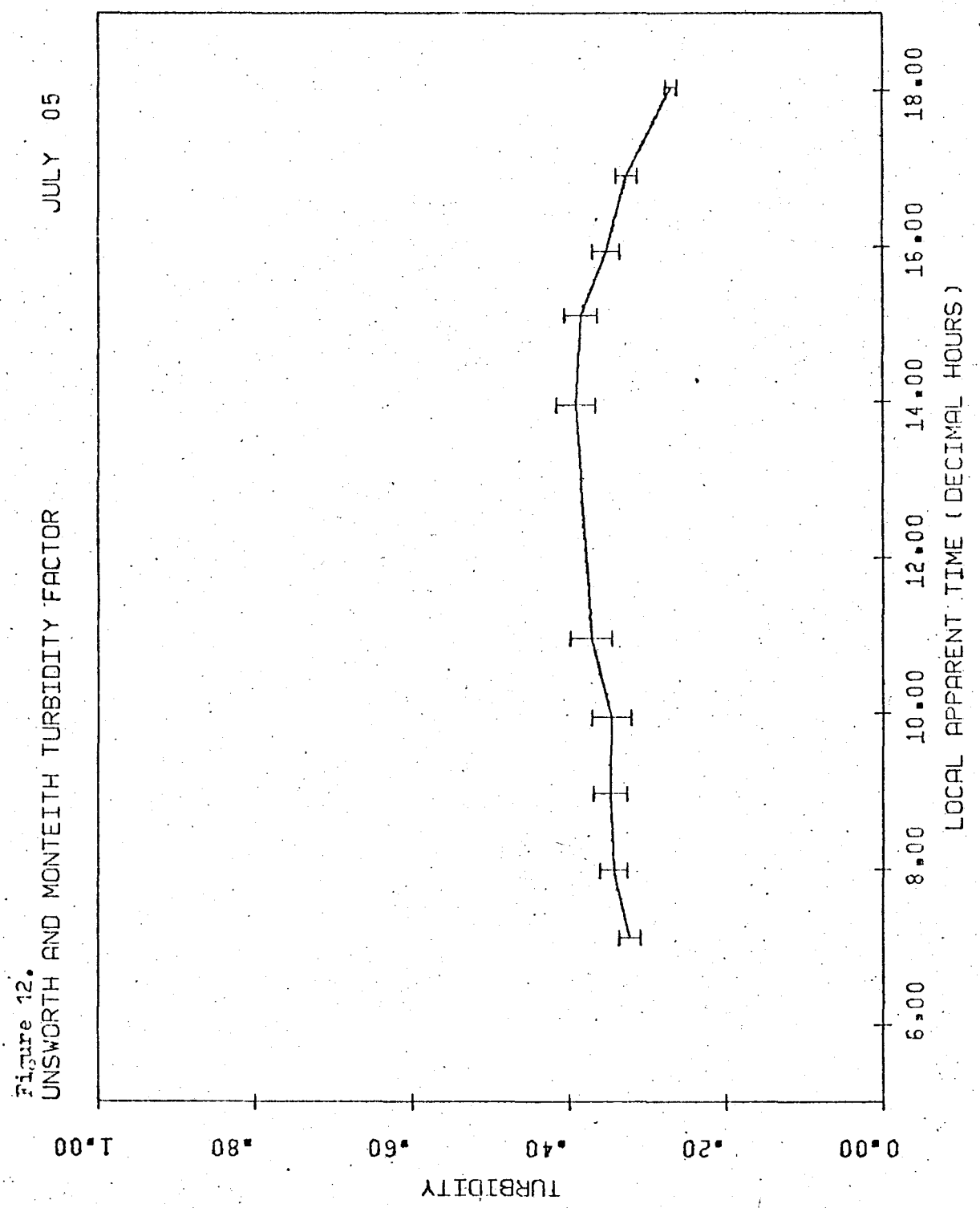

Figure 12.
UNSWORTH AND MONTEITH TURBIDITY FACTOR

July 22, July 23

On both July 20 and July 21, rain fell over Hamilton and area. By July 22, a high pressure system was located south of Washington, D.C. (Map 8) with major air masses moving northeast. Local winds were from the west until 11.00 LAT, swinging to the south southwest after this time. The turbidity increased gradually from 0.128 at 07.00 to 0.177 at 10.00, one hour before the change of wind is detected (Figure 13). In the next two hours, the turbidity jumped to 0.240 and then rapidly increased to 0.278 by 16.00 LAT. During the last two hours of measurements, turbidity dropped significantly. The winds did not change in direction or speed so no explanation can be given. One possible reason could be inaccuracies due to increased air mass as previously discussed. This inaccuracy may also be found on other days, such as July 5 (Figure 12).

On July 23, a cold front was moving toward Hamilton from the north. This was a trough extending from a low pressure system west of Lake Michigan (Map 9). Further, a warm air mass was moving from the Kansas City region toward Lake Huron. During the day, winds were from the west northwest almost without exception with speeds increasing from 1.35 ms^{-1} at 06.00 LAT to 3.6 ms^{-1} at 11.00 LAT (Figure 14).

By comparing July 22 and July 23, it becomes apparent that the decrease in turbidity in the late afternoon of July 22 was not due to error but to actual change. This is substantiated by the low turbidities of July 23, τ_a being 0.106, indicating a possible diurnal cycle (Kondratyev, 1969). During the day of July 23, a gradual increase in turbidity was observed for the morning measurement period. This corresponded with increasing wind velocities. Since no continental air masses were in

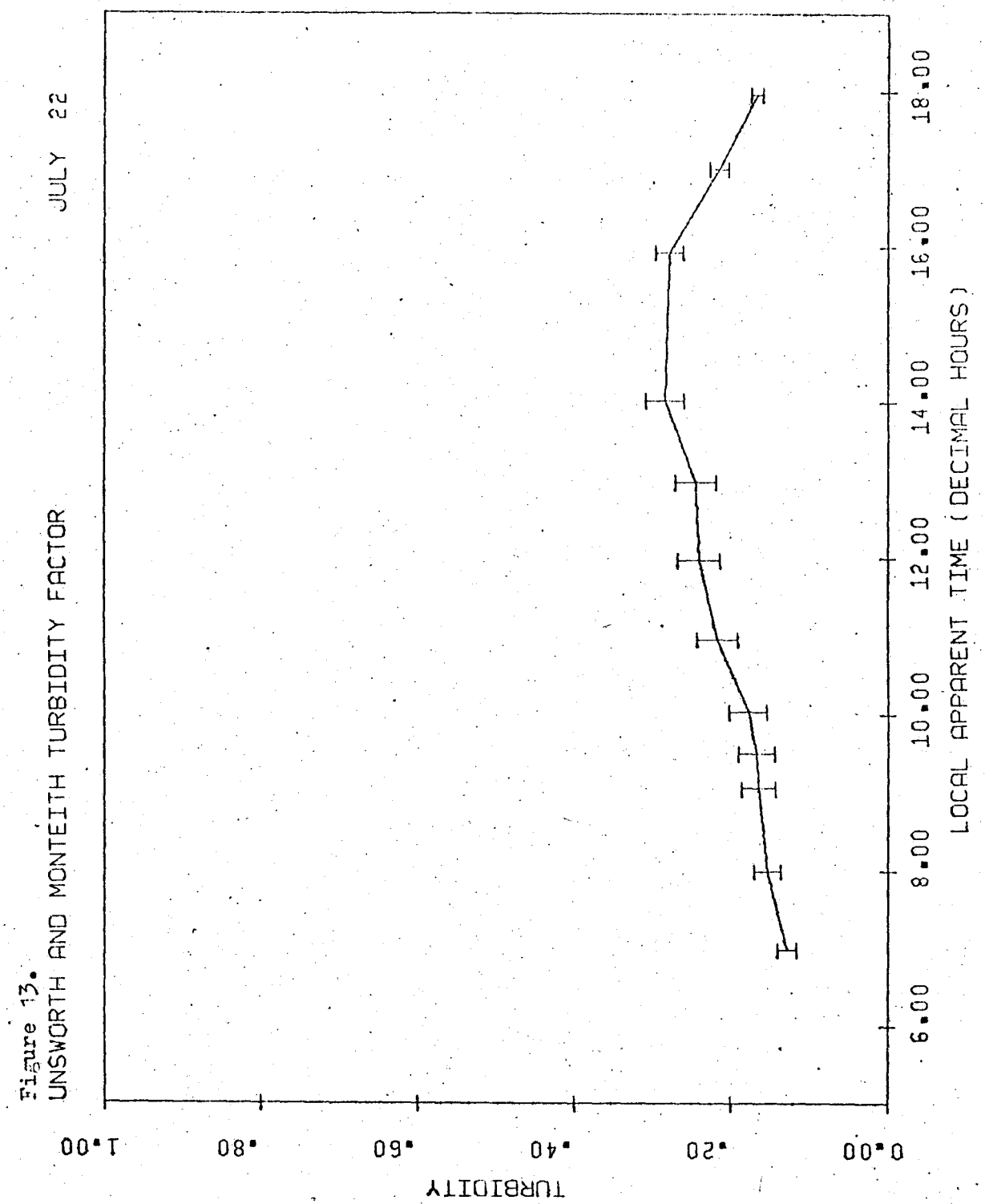
UNSWORTH AND MONTEITH TURBIDITY FACTOR
JULY 22
TURBIDITY
0.00
.20
.40
.60
.80
1.00
6.00
8.00
10.00
12.00
14.00
16.00
18.00
LOCAL APPARENT TIME (DECIMAL HOURS)

Figure 13.

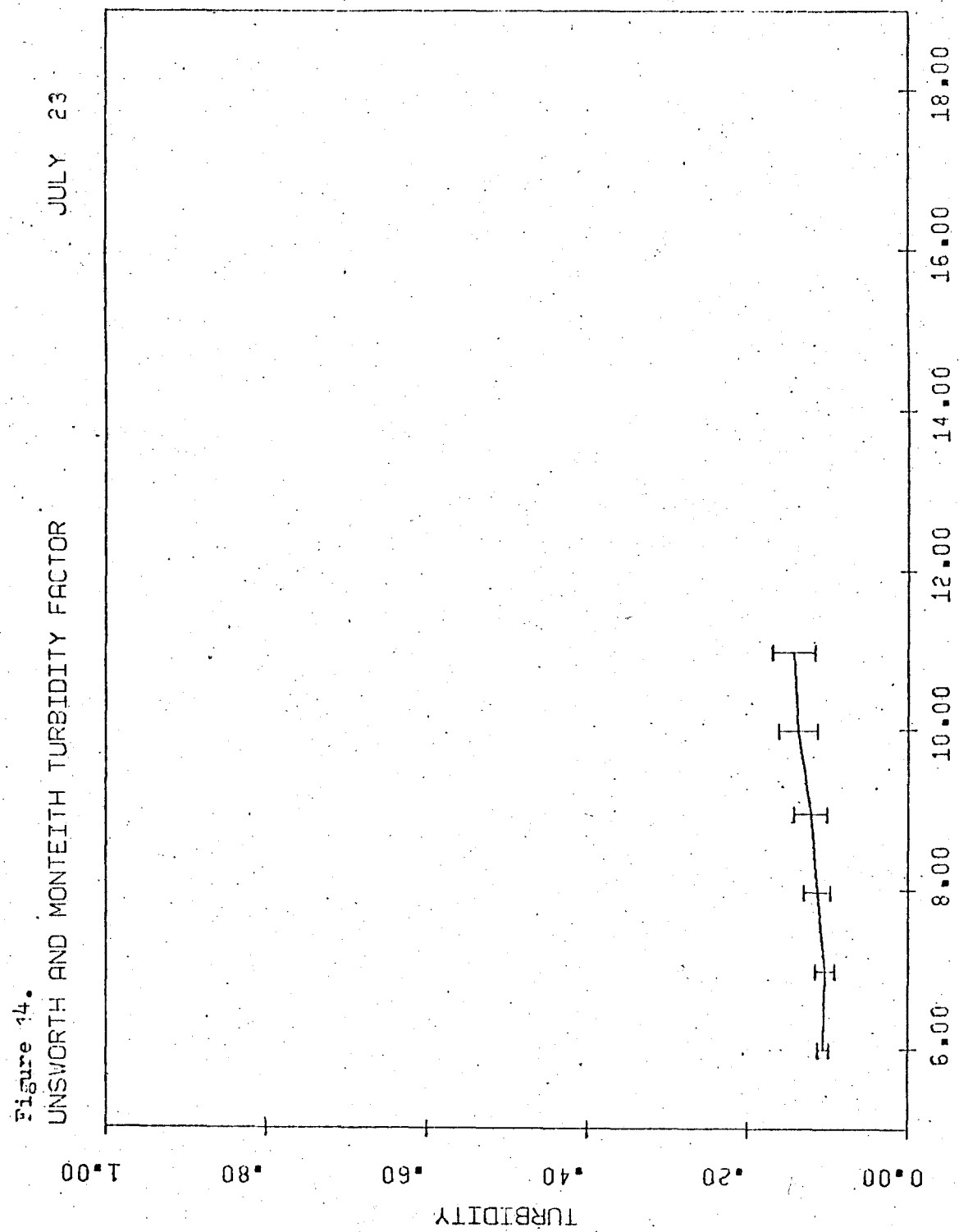
UNSWORTH AND MONTEITH TURBIDITY FACTOR
JULY 23
TURBIDITY
0.00
.20
.40
.60
.80
1.00
6.00
8.00
10.00
12.00
14.00
16.00
18.00
LOCAL APPARENT TIME (DECIMAL HOURS)

Figure 14.

the region of the west northwest winds, two possible reasons can be put forward for the increasing turbidity. The first reason is that aerosols were being entrained over agricultural land across Southern Ontario. If this is the case, it indicates that aerosols in the form of natural particulate matter is equal to the magnitude of local pollutants.

Secondly, if wind during this period is assumed too weak to disperse or entrain aerosols, the build-up might be explained by local sources. The direct solar beam passes through the atmosphere above the source area during the time period in question substantiating this possibility. Data for August 9, however, does not fully support this argument. During the early morning, calm conditions prevailed, yet τ_a never exceeded the value 0.10. It was also found that there was no variation in turbidity in the manner found on July 23. This will be more fully discussed under the section dealing with August 8 and 9.

July 28 to August 1

This set of observations was the longest period of clear sky and partially clear sky days over the duration of the experiment. The synoptic record over this period can be seen progressing on Maps 10-14. During these few days, two high pressure systems moved across the eastern half of the continent. On July 28, a low pressure system was centred on the Manitoba - Saskatchewan border with stationary front passing through it. The high pressure system moved over the Western Atlantic on July 29 and remained stationary during July 30. By July 31, it had moved into the mid-Atlantic and been replaced by another located over Lake Huron which had moved up from the Gulf of Mexico. On August 1, this high pressure system was found to be located just south of Washington, D.C. on the

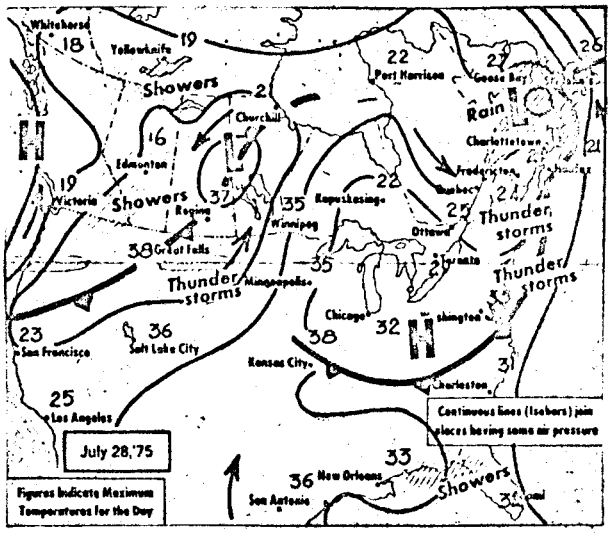

Map 10. Synoptic patterns for July 28.

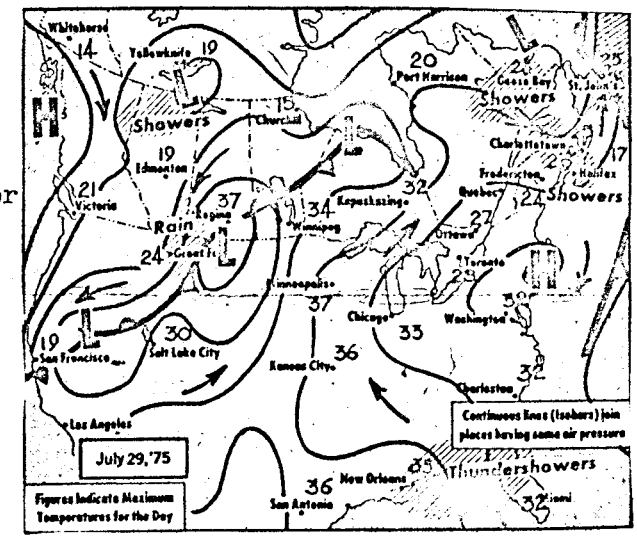

Map 11. Synoptic patterns for July 29.

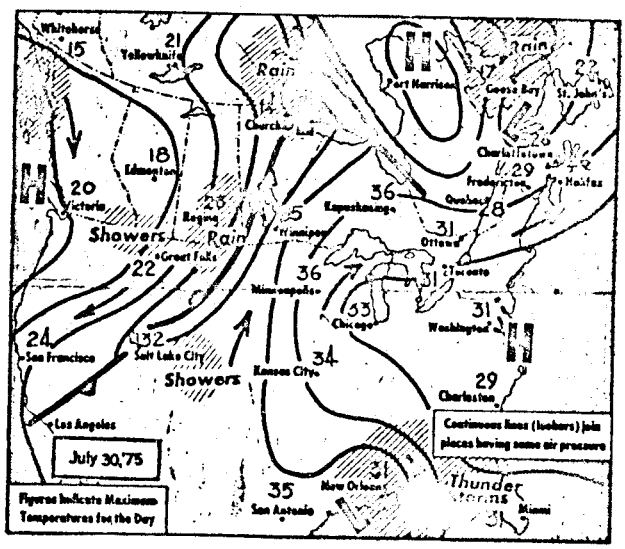

Map 12. Synoptic patterns for July 30.

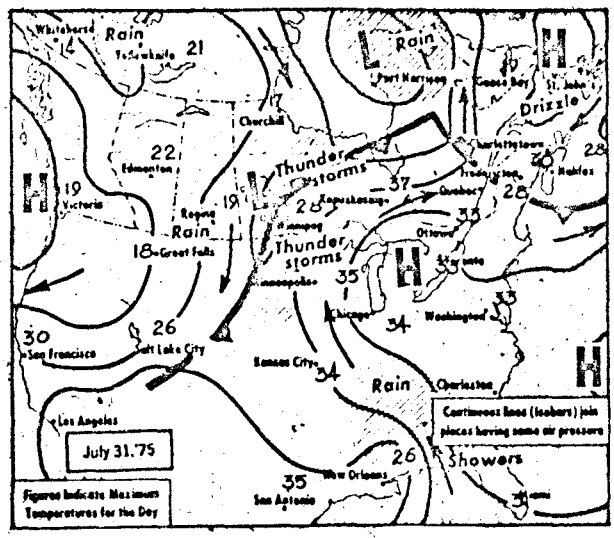

Map 13. Synoptic patterns for July 31.

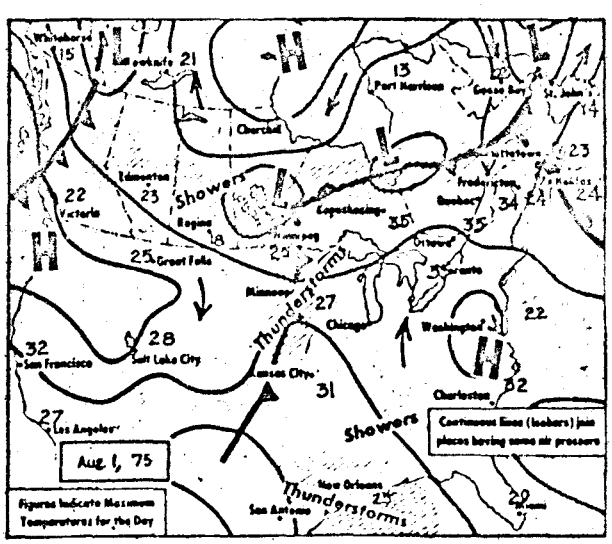

Map 14. Synoptic patterns for August 1.

Atlantic coast. For the entire period, temperatures were unseasonally high. Winds were predominantly from the west to southwest during this period.

Measurements began at 07.00 LAT on July 28 and ended at 10.75 LAT because of cloud. For the first two hours of the day, turbidity increased from 0.127 to 0.151 (Figure 15). After this period, τ_α remained stable until the cloud cover forced measurements to be terminated. The wind during the period was between 3.4 ms^{-1} to 6.85 ms^{-1} in an easterly direction down the Dundas Valley. The increase in wind speed corresponds to the stabilization of the turbidity factor. This indicates that the aerosol is likely of local origin and that the increase is due to a build-up of aerosol before the stronger winds are able to disperse the particulates.

July 29 presented a special set of problems in the analysis. Cirrus cloud cover cleared to allow observations to begin at 09.00 LAT and continue for the entire day. Over eleven observations, the wind direction did not remain constant for more than two hours at a time. Further, there was no progression of wind direction, but situations of complete reversal. An example is at 14.00 LAT. The wind was blowing from the east and one hour later, the wind was from the west. The reason for this can be attributed to the nature of windspeed. From 08.00 LAT to 16.00 LAT, the wind never exceeded a speed of 1.8 ms^{-1}. At this low speed, conditions can be assumed to be only local breezes.

The day began with a turbidity value of 0.129 which did not change noticeably until solar noon when it jumped from 0.129 to 0.158 (Figure 16). This corresponds to a wind with an easterly component. As the wind shifted from the southeast at 12.00 LAT to the east at 13.00 LAT, the

Figure 15.

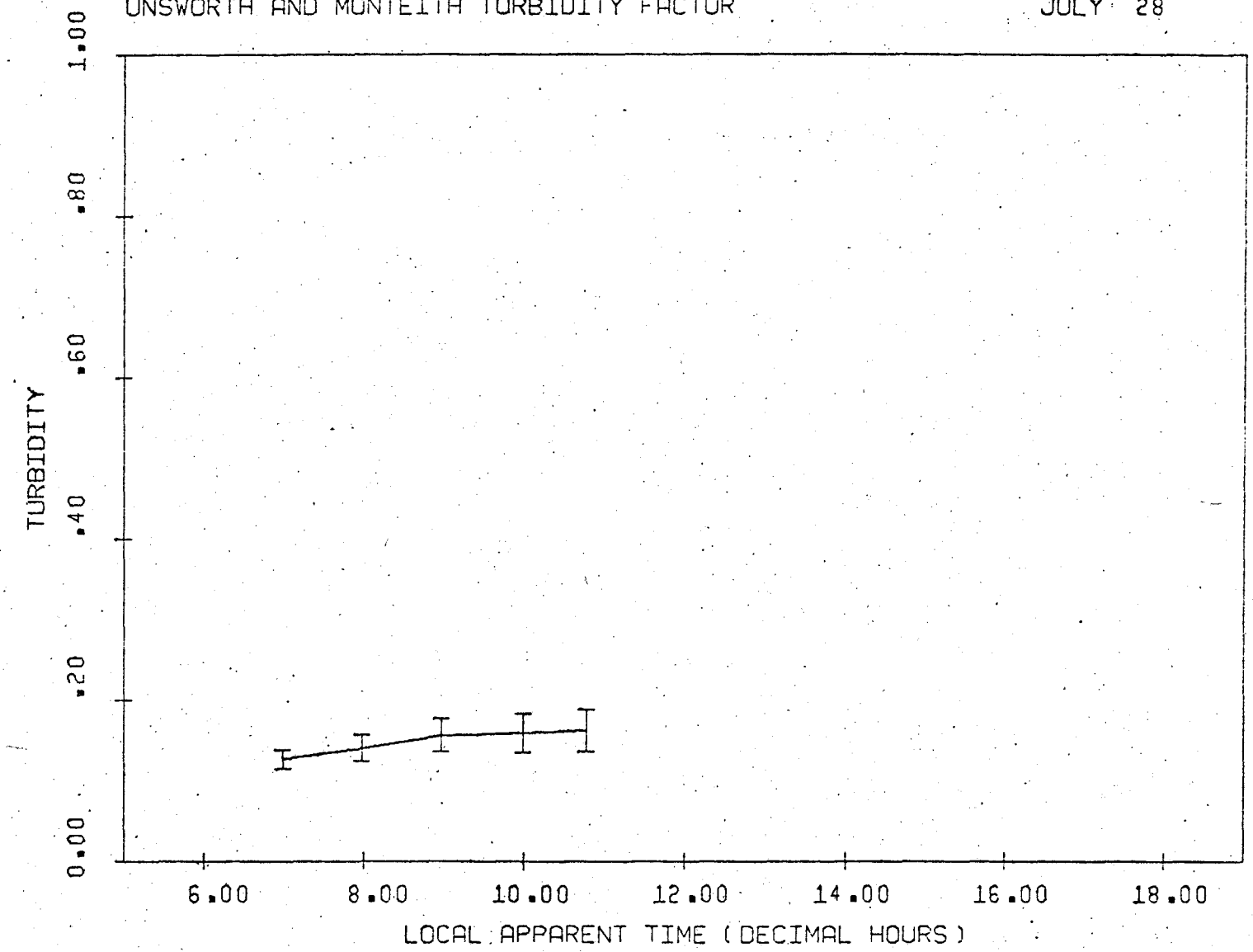
UNSWORTH AND MONTEITH TURBIDITY FACTOR
JULY 28
TURBIDITY
1.00
.80
.60
.40
.20
0.00
6.00
8.00
10.00
12.00
14.00
16.00
18.00
LOCAL APPARENT TIME (DECIMAL HOURS)

Figure 16.

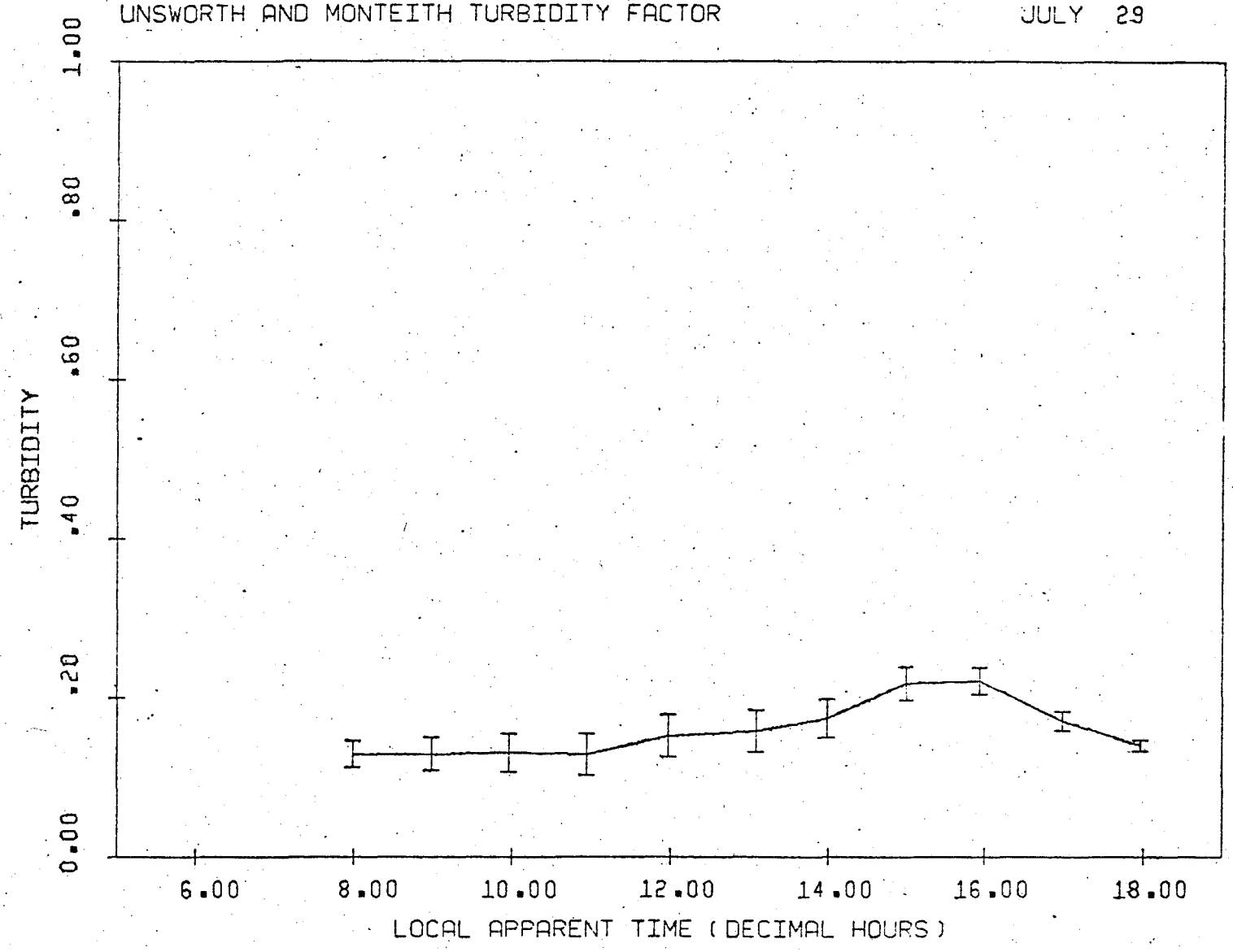
UNSWORTH AND MONTEITH TURBIDITY FACTOR
JULY 29
TURBIDITY
1.00
.80
.60
.40
.20
0.00
6.00
8.00
10.00
12.00
14.00
16.00
18.00
LOCAL APPARENT TIME (DECIMAL HOURS)

turbidity increased only fractionally. However, over the next hour with an east wind, turbidity increased to 0.174. This jump is poorly explained by the wind shift, since the turbidity increases rapidly to a value of 0.218 with a shift of wind to the west between 14.00 and 15.00 LAT. This latter increase may be explained from dust being drawn down the valley over the measurement site. A second explanation for the overall increase could be that it was due to a thin band of cirrus cloud which was not detected. However, this also is not a satisfactory explanation.

Although no explanation can be given for these changes, it is apparent that as wind direction changes, even at low wind speeds, turbidity values are highly correlated. Throughout the day, the aerosol increase was local in nature. This indicates that local sources are important when the wind is of a local nature. However, they are not major contributors of aerosols when compared to the movement of particulate matter by large air masses.

By 17.00 LAT, the wind speed had increased to 3.60 ms^{-1} from the south. This forced air from along the Niagara Peninsula into Hamilton to disperse the concentration. From Figure 16, one is able to see that turbidity is reduced to 0.140 by 18.00 LAT.

July 30 is a continuing build-up of aerosol. Unlike July 29, however, the turbidity peaks by 10.00 LAT (Figure 17) and then remains stable for the rest of the observations, varying by less than 10%. The winds were from the southwest at 3.00 ms^{-1} for the entire period. This may have had an influence on the turbidity, but the exact nature cannot be determined. Assuming little outside influence by foreign air masses, it appears that a certain upper limit may be reached each day by local aerosols. This upper limit is approximately 0.218 according to the last

Figure 17.

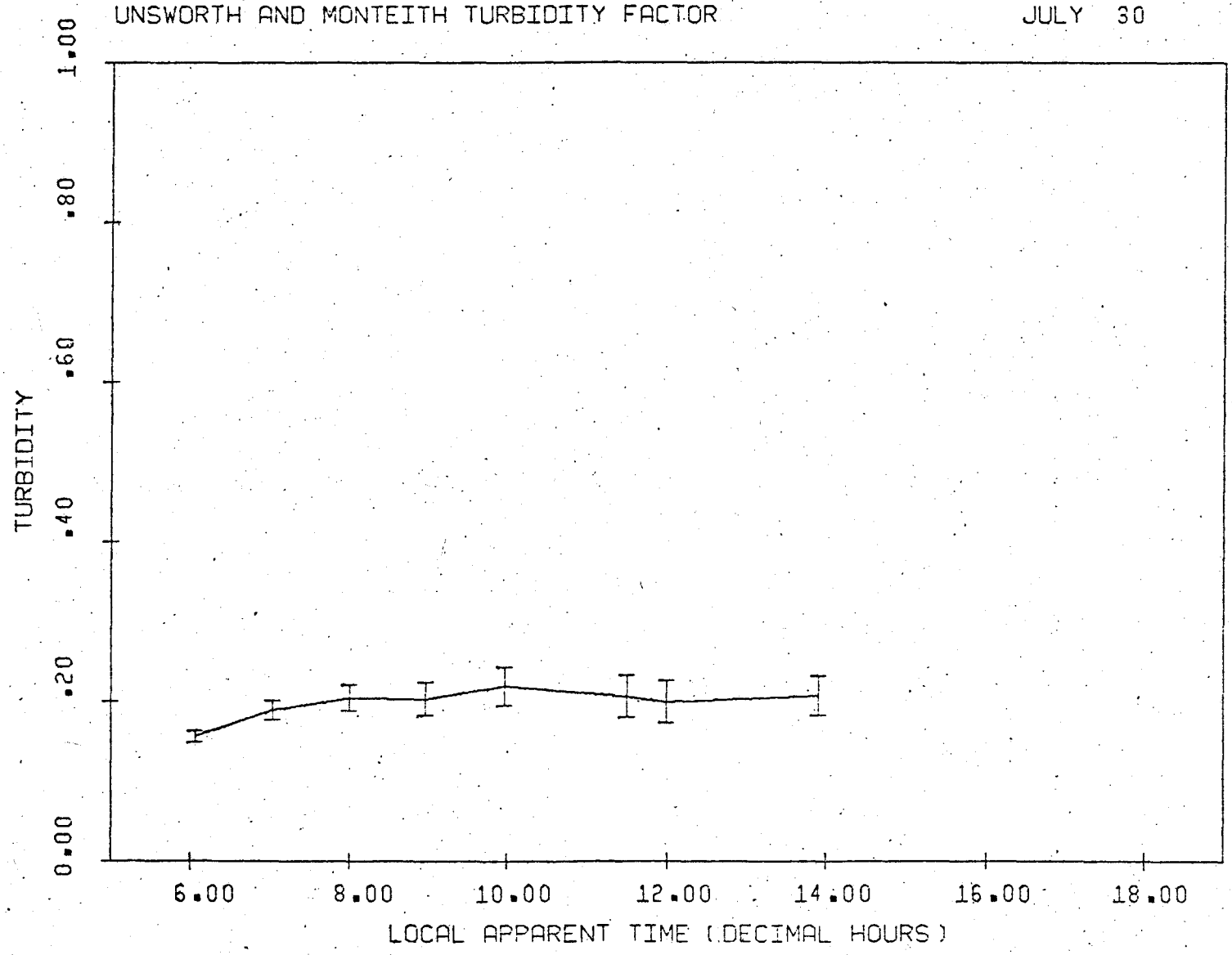
UNSWORTH AND MONTEITH TURBIDITY FACTOR
JULY 30
TURBIDITY
1.00
.80
.60
.40
.20
0.00
6.00
8.00
10.00
12.00
14.00
16.00
18.00
LOCAL APPARENT TIME (DECIMAL HOURS)

two days of observations.

Conditions on July 31 remained stable; aserosols building up to give a τ_a of 0.250 at 07.00 LAT. Winds were from the west until 11.00 LAT at approximately 3.20 ms^{-1}. During this period, turbidity slowly increased to a value of 0.307 (Figure 18). There are good indications that the aerosols originated from the southeast U.S.A. and were transported north by winds associated with a high pressure system that was centred over Lake Huron during this period (Map 13). As the day progressed, the wind began to fluctuate to the west northwest and west southwest. Turbidity rapidly increased to 0.421 over this period. The turbidity is nearly as great as values obtained when only local sources were present. Not until 15.00 LAT when windspeeds decreased to 2.24 ms^{-1} did turbidity begin to decline. By 16.00 LAT, turbidity had decreased to 0.403, but was still considerably greater than any of the previous days.

The last day of the clear weather for this period was August 1. Turbidity remained high, increasing during the afternoon but never reaching values greater than 0.3 (Figure 19). The high pressure system had moved to the southeast of Washington and the system was beginning to disintegrate. As this occurred, it is apparent that reduced turbidities resulted.

A definite cycle can be seen over the five-day period. For the first three days, local sources of aerosol predominate, being most prevalent July 29. By July 31, the local effects have been dominated by continental air masses moving north from the industrialized region around the southern Great Lakes. It is during this time, that turbidity reaches its greater values. August 1 sees the system rapidly deteriorating as the high pressure system moves farther east. As indicated, this reduces

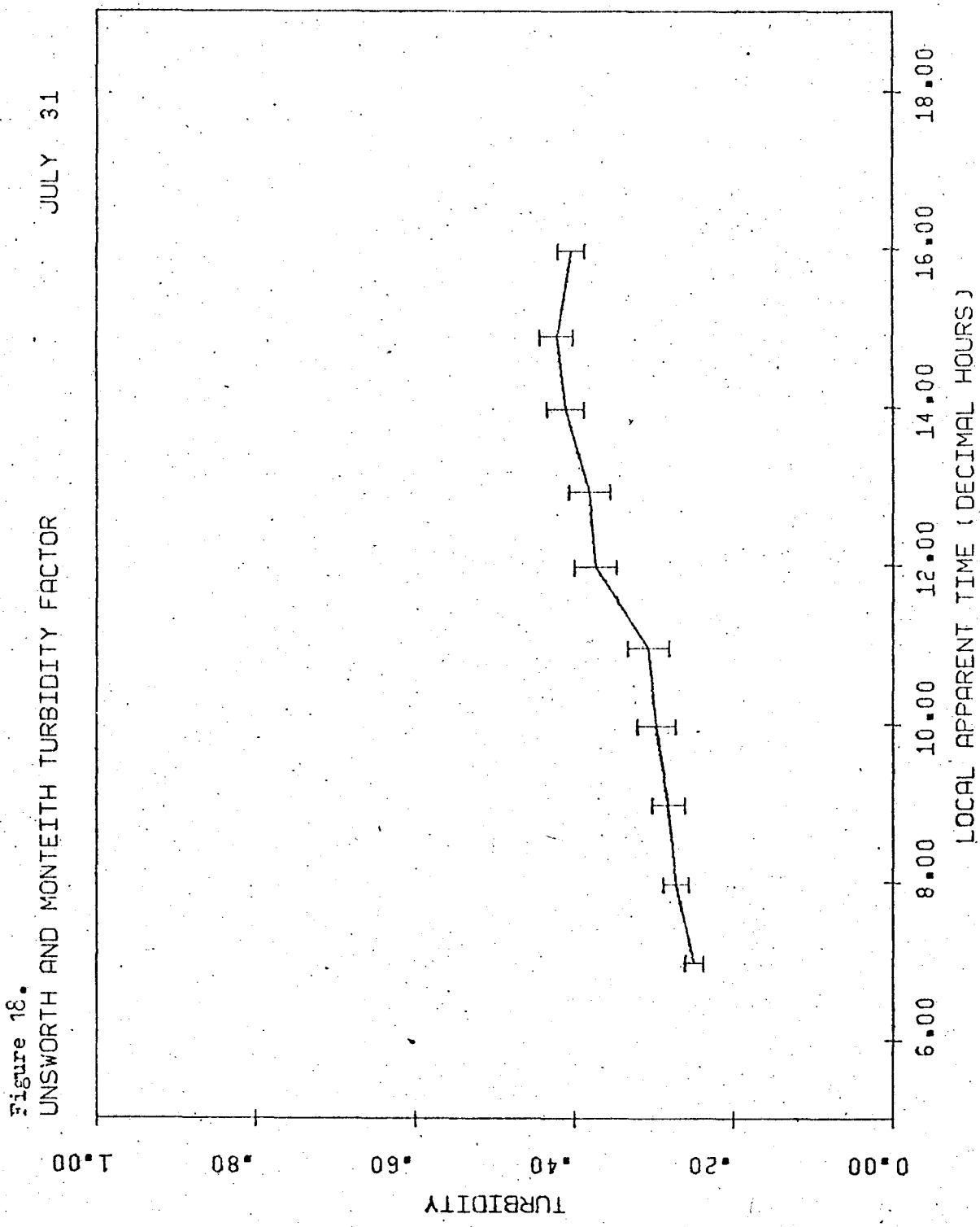
UNSWORTH AND MONTEITH TURBIDITY FACTOR
JULY 31
TURBIDITY
0.00
.20
.40
.60
.80
1.00
6.00
8.00
10.00
12.00
14.00
16.00
18.00
LOCAL APPARENT TIME (DECIMAL HOURS)

Figure 18.

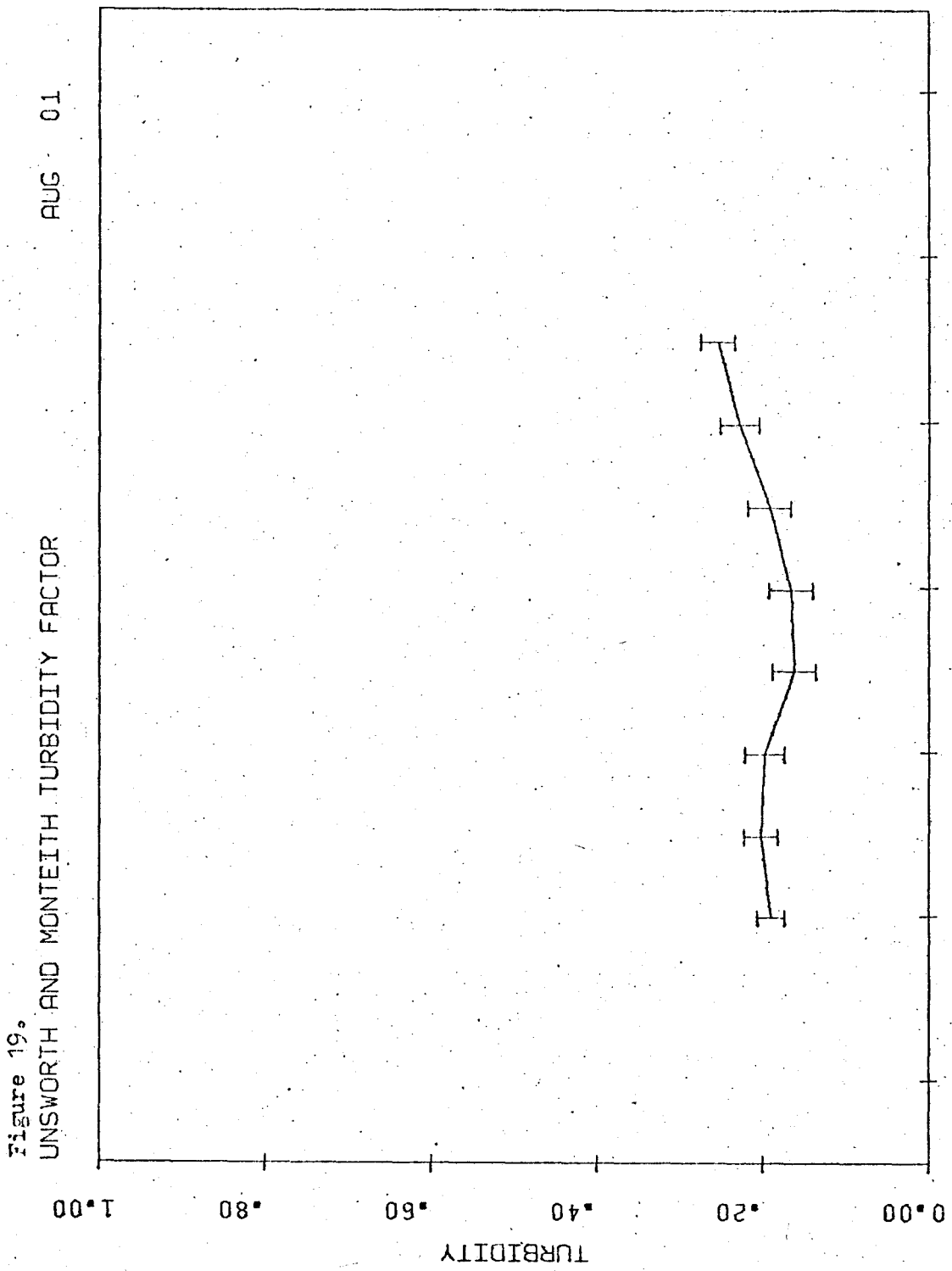

Figure 19.
UNSWORTH AND MONTEITH TURBIDITY FACTOR

turbidity by 25% from the previous day's peak.

The turbidities reached on July 28 and 29 were of a maximum value of 0.219. If this can be attributed only to local sources, it becomes necessary to consider these local sources as major contributors to the turbidity of Hamilton. However, the results must first be duplicated in a less complex situation than the one accompaning these observations. Previous observations have not indicated turbidities due to local sources alone, except in situations where a build-up of other sources have first occurred.

August 8, August 9

August 8 is the only day when observations were taken for a period of time during calm conditions. For both August 7 and 8, a high pressure cell was located over Lake Erie stabilizing conditions in the area (Map 15). Observations began at 07.00 LAT and continued until 16.00 LAT. Winds were generally in a westerly direction throughout the day at a speed of 3.50 ms^{-1} when blowing.

The first three sets of observations for the day were taken in calm conditions. Over the time span of two hours, 07.00 to 09.00 LAT, the variation in turbidity was a maximum of 0.005 increasing to 0.061 at 08.00 LAT and then decreasing to 0.056 at 09.00 LAT. The azimuth of the sun does not affect turbidity measurements with respect to its position and the location if the aerosol sources. Secondly, this indicates that build-ups of aerosol such as those on July 28 and 29, were not solely due to local effects.

Throughout the day, turbidity remained low and nearly constant. A slight trend can be seen during the latter part of the day (Figure 20) as

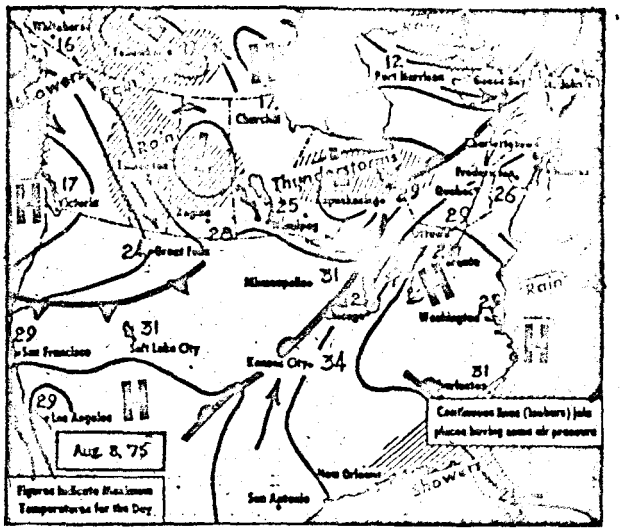

Map 15. Synoptic patterns for August 8.

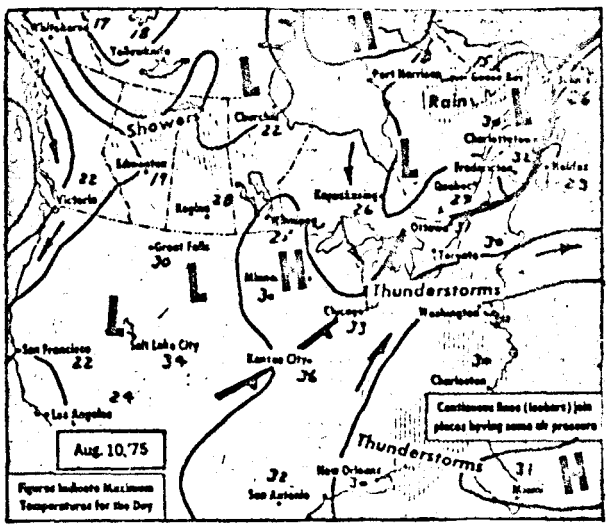

Map 16. Synoptic patterns for August 10.

Figure 20.

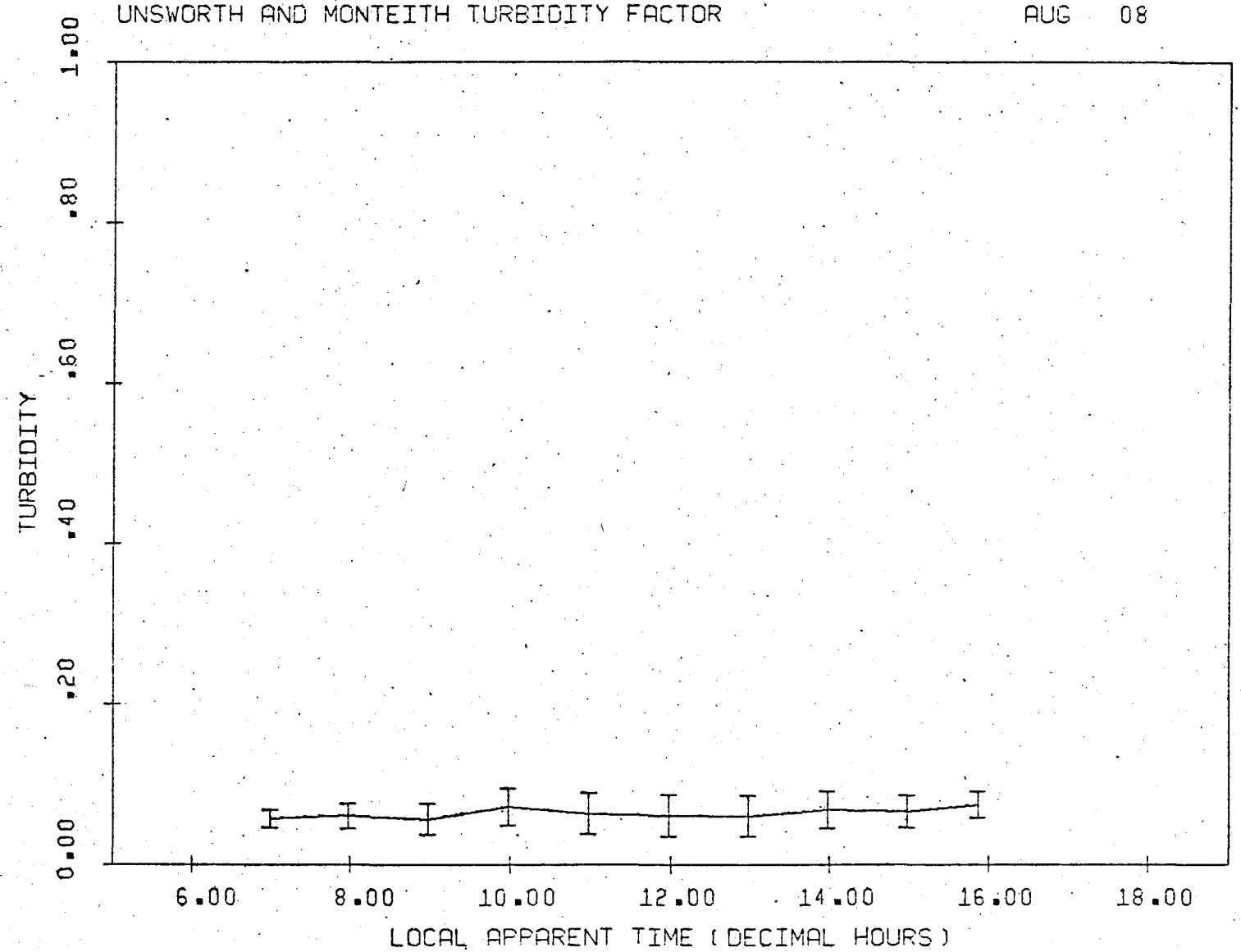
UNSWORTH AND MONTEITH TURBIDITY FACTOR
AUG 08
TURBIDITY
1.00
.80
.60
.40
.20
0.00
6.00
8.00
10.00
12.00
14.00
16.00
18.00
LOCAL APPARENT TIME (DECIMAL HOURS)

winds were from the west to west southwest and aerosol content increased. The maximum turbidity was attained; 0.074 at 15.85 LAT.

During August 8 and 9, the high pressure cell began moving west drawing air north from the south central United States (Map 15). The generally unsettled conditions brought an increase in turbidity during the night. By 07.00 LAT, August 9, the turbidity value was 0.166, a 0.042 increase over the 15.85 LAT value of August 8. Winds for August 9 were from the west southwest between 4.05 ms^{-1} and 7.15 ms^{-1} increasing as the day progressed. Following the increase in wind velocity was a continuous increase in turbidity (Figure 21). By 17.00 LAT, turbidity had reached a value of 0.360. This is more than 2.5 times as great as eleven hours before.

August 8 and 9 indicate the effect that unstable conditions have on turbidity, compared to pollution alone. This compared with Unsworth and Monteith (1972) who found that when synoptic conditions were stable τ_a changed by less than ± 10%, but on days of synoptic change, turbidity sometimes changed by a factor of 2 between sunrise and sunset.

Wind Direction Analysis

As has been implied from the previous section, wind direction, turbidity and synoptic air masses are interrelated. Figure 22, a polar graph of turbidity (τ_a) versus wind direction further indicates these relationships. The scatter was determined by taking the degree direction of the wind from the hourly weather observation nearest the actual time of measurement of the direct beam radiation.

Values of τ_a are well defined for each sector of the circle. The southeast quadrant having only 7 observations and be omitted from the

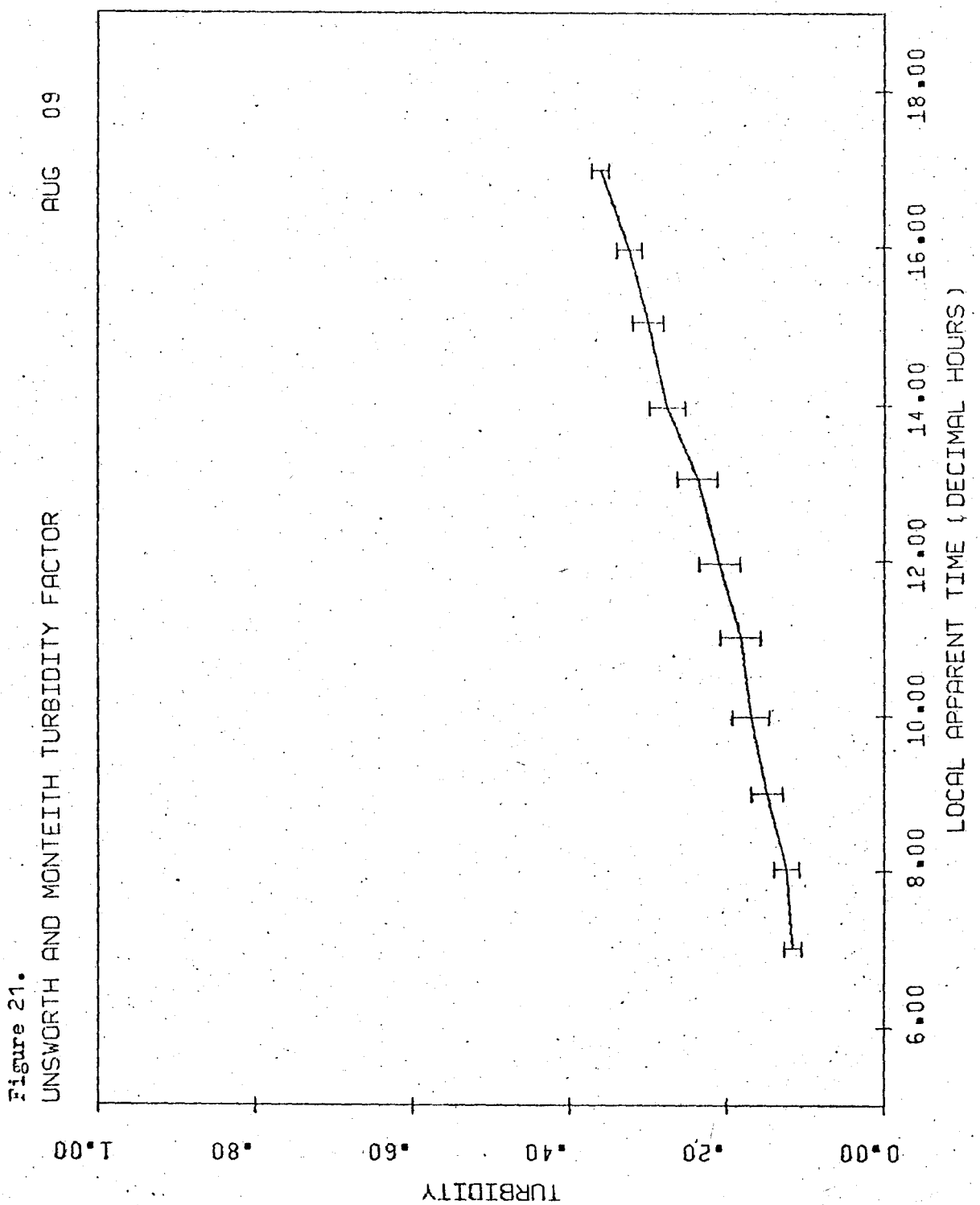
UNSWORTH AND MONTEITH TURBIDITY FACTOR
AUG 09
TURBIDITY
0.00
.20
.40
.60
.80
1.00
6.00
8.00
10.00
12.00
14.00
16.00
18.00
LOCAL APPARENT TIME (DECIMAL HOURS)

Figure 21.

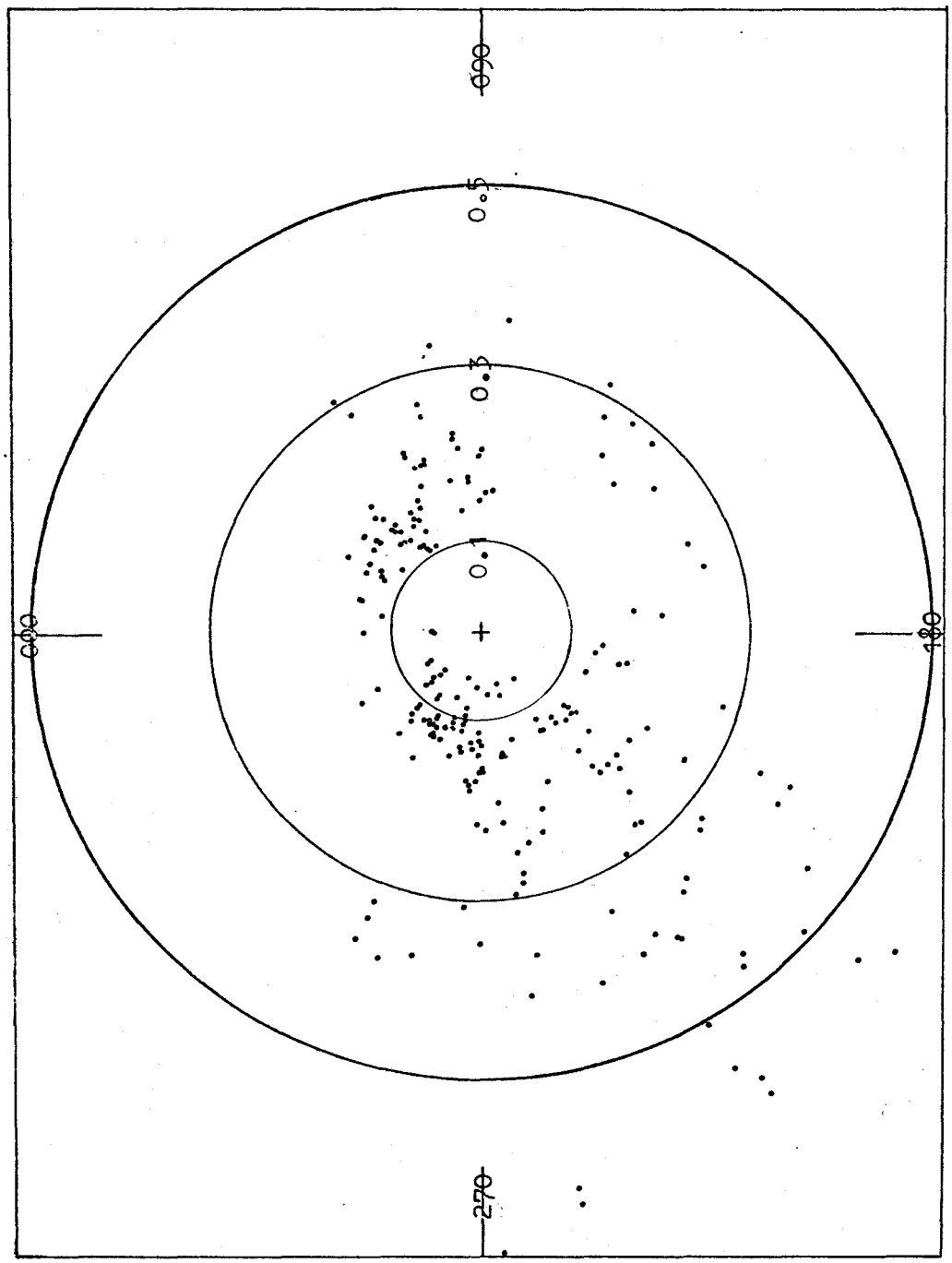

Figure 22. Turbidity (τ_a) versus wind direction.

discussion since no generalization can be adequately formed.

The largest turbidities are found on the southwest quadrant. This is expected since these winds carry highly turbid air masses from the industrialized mid-west United States. With turbidities reaching values of over 0.45 on occasion the continental air masses are the major sources of pollutants. Approximately 33% of the time when southwest winds were blowing turbidities were greater than 0.3. These values compare favourably to the daily averages of Unsworth and Monteith (1972) where values of up to 0.6 were found on occasion from tropical continental air masses. Values of 0.3 were frequently observed.

The second largest turbidities occur when winds blow from the west northwest. Values again are periodically greater than 0.3, most values being greater than 0.15. Two reasons can be put forward for those values. These greater than 0.3 occurred when high pressure systems were located over Lake Huron. These high pressure systems would also have moved across the industrial United States and entrained aerosols in the same manner as the pressure systems creating winds from the southwest.

The lower values of turbidity during westerly winds appear to be a combination of diffusion of point source aerosols from industry and removal of material from agricultural land. These values were detected during days when no high pressure systems could effect the observations, yet turbidity values could not be assessed as being from local sources. Two examples of this situation are July 26 and August 12.

Although, winds are from the southwest during July 26 no synoptic patterns (Map 17) are effecting the region and the diffusion process is similar to that of west northwest winds. Once again the air passes over

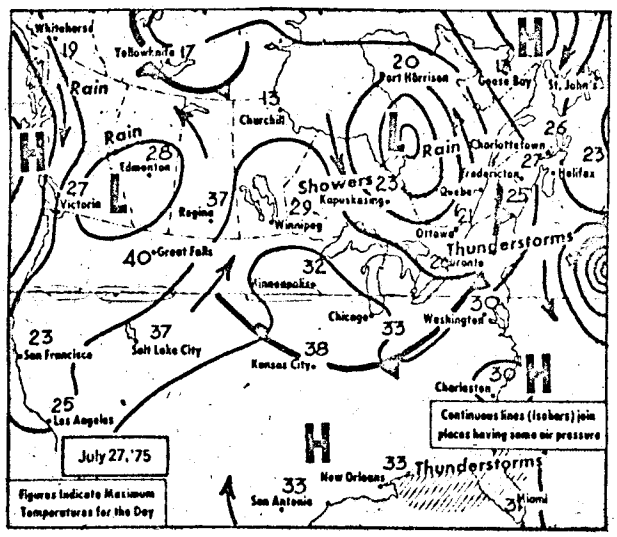

Map 17. Synoptic patterns for July 27.

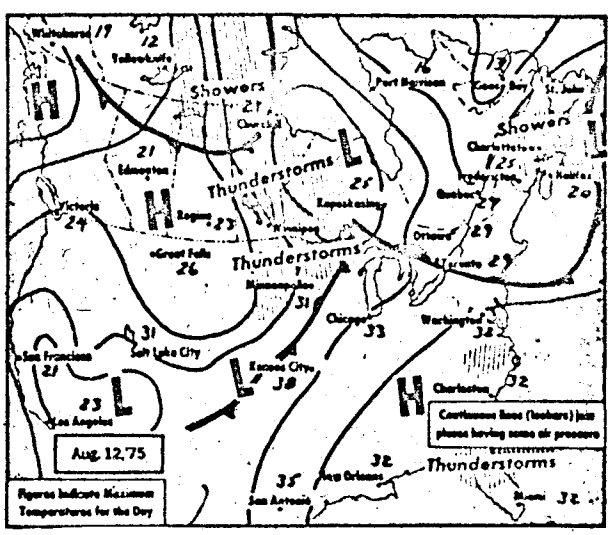

Map 18. Synoptic patterns for August 12.

the same type of region before reaching Hamilton, entraining the same type of aerosols. Turbidity varies little over the observation period, τ_α values of 1.28 and 1.27 being observed at 11.00 LAT and 17.00 LAT respectively, the first and last observations. The peak value of 0.136 being reached at 16.00 LAT, one hour after the highest wind speed was recorded. Interestingly the turbidity, at the time the wind reached its maximum velocity (4.0 ms^{-1}), had increased from 0.130 to 0.135 over the previous hour Figure 23.

A similar situation occurred on August 12 when no synoptic conditions were effecting the region (Map 17). Winds were from the west and west northwest at 2.5 ms^{-1}. Turbidities for the four hours of observations varied from 0.138 to 0.117 Figure 24. These low values are to be expected with the wind velocities. The reduction in turbidity in the morning was the removal of local aerosols from the region.

Industry throughout the southwestern portion of Ontario is mostly of the light variety and is sporadically distributed. This leaves only natural materials from the farmed and forested areas to be major sources for aerosols. Compared to the values of turbidity when winds were light or from the east producing "local" turbidity, these values indicate that agricultural pollutants are an equally important factor.

Turbidities are generally low when a directional component of the wind is from the north. As can be seen from Figure 22 the turbidity values are noticeably reduced in the northern half of the graph. The lowest turbidities were found when winds were from the northwest. Air masses sweeping down from the Arctic draw in every clean air, the only aerosols being those of the global background and natural materials

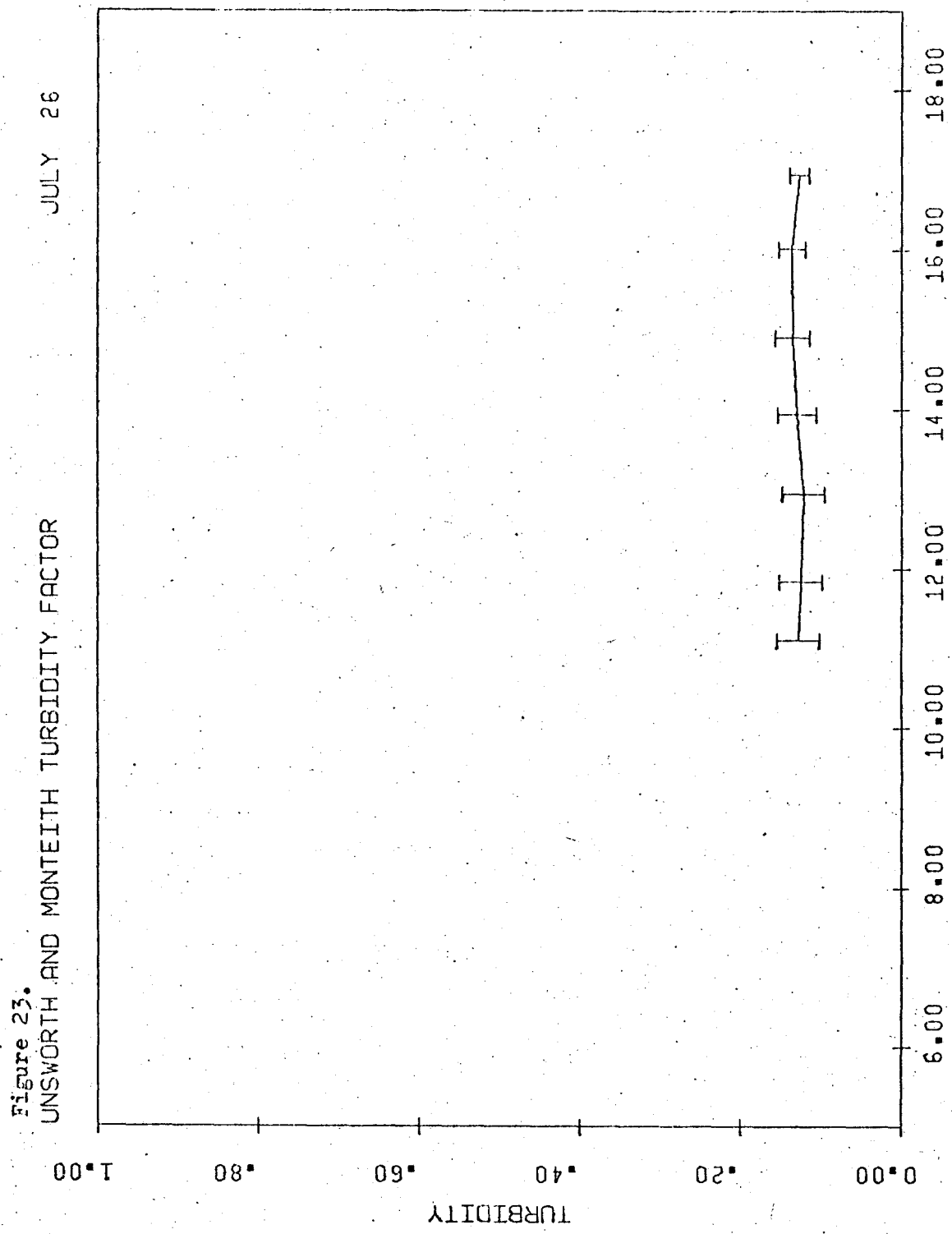

Figure 23.
UNSWORTH AND MONTEITH TURBIDITY FACTOR

Figure 24.

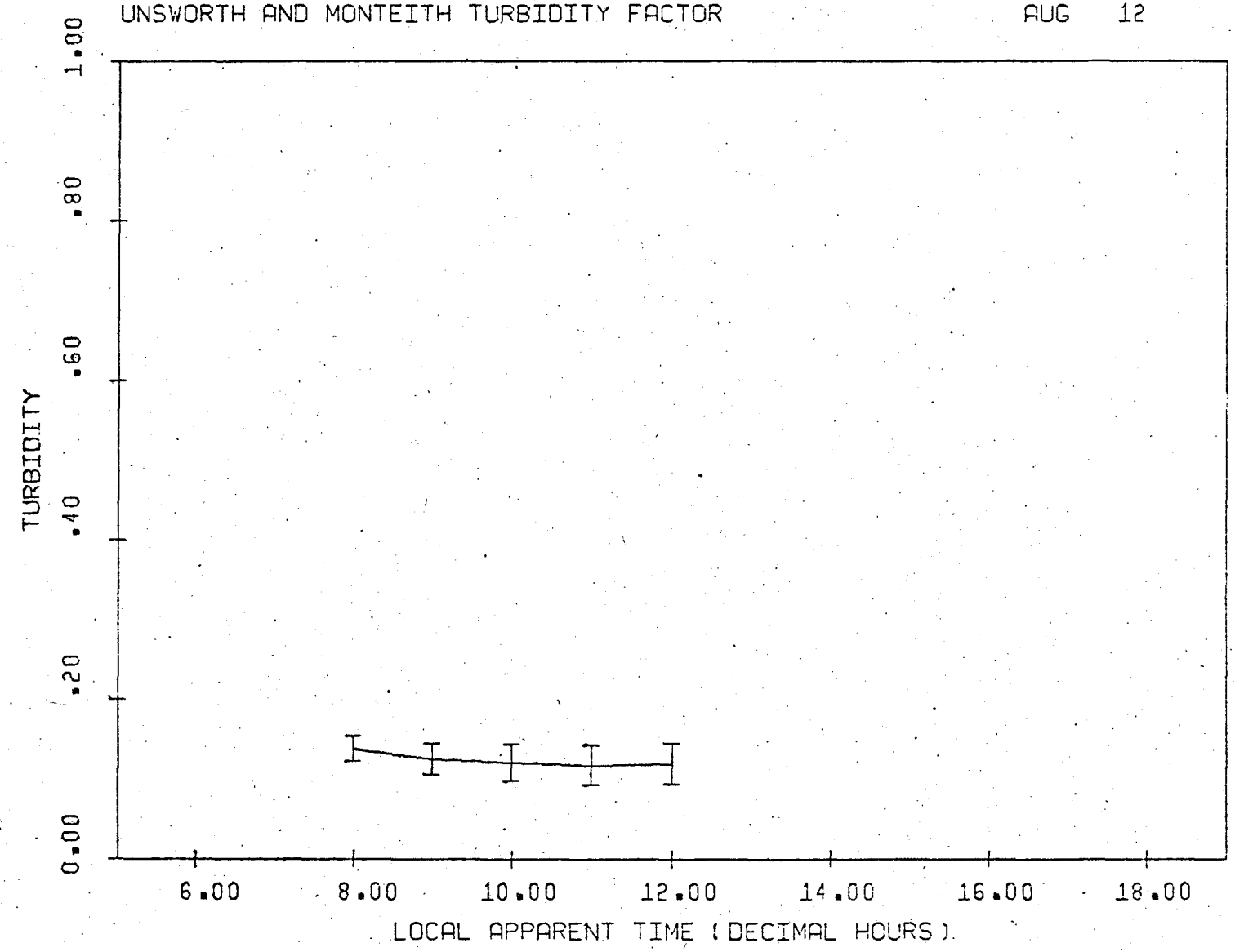
UNSWORTH AND MONTEITH TURBIDITY FACTOR
AUG 12
TURBIDITY
1.00
.80
.60
.40
.20
0.00
6.00
8.00
10.00
12.00
14.00
16.00
18.00
LOCAL APPARENT TIME (DECIMAL HOURS)

entrained over dense forest. During days of northwest winds, turbidities seldom reached values of greater than 0.15. Comparing these values to those of Unsworth and Monteith (1972) the same effects are found when Arctic Maritime or Polar Maritime air masses move over Britain.

The most complex factors effecting aerosol movement are found when winds are being directed from the northeast. Generally air masses from this direction are relatively clean, originating as Arctic Maritime air masses. These being forced south, entrain aerosols from dense forest areas. Winds which move in from the east northeast cross an area of heavy industry before reaching Hamilton. Turbidities when winds are in this direction are slightly greater than when winds are from either further north or east. These are identified by a slight peak in the northeast sector of Figure 22.

Winds blowing from the east remain clean until reaching Hamilton, having blown across Lake Ontario. These winds are also mixed with on-shore breezes during the early morning. It appears that when blowing, the turbidity being measured is that from local sources alone. On two occasions the "local" turbidity values are greater than 0.3, but usually are found to be approximately 0.2. The values compare with the effect of the aerosol blowing in from agricultural sources from the west.

Besides direction, wind speed must also be considered when dealing with values of turbidity. The direction of the wind indicates the type of air mass moving toward the area. The wind speed indicates the volume of air that will move over the area, and is a reasonable indicator of the amount of aerosol in the air. An example will indicate how turbidity is a function of windspeed as well as direction. On May 28 a northwest wind

blew at between 6.75 and 10.75 ms^{-1}. Throughout the day turbidity decreased as large volume of clean air moved across the region. Conversely, on August 8 wind speed was light during the day and turbidities remained low. On August 9, however, winds reached velocities of up to 7.15 ms^{-1}. By the end of the day turbidity had increased from 0.116 at 07.00 LAT to 0.360 by 16.97 LAT, as more airborne material was entrained in the air mass by the increased turbulence present with these winds.

CHAPTER 10

CONCLUSIONS

Krondratyev (1969), Unsworth and Monteith (1972) and Joseph and Manes (1971) have documented the effect of synoptic air masses on local turbidity conditions. Only work documented by Kondratyev (1969) though, has been in industrialized regions. The results put forward here further indicate that turbidities produced by the movement of synoptic air masses predominate. Local sources of pollutants in Hamilton appear to be effective only in a site specific manner (Rouse and McCutcheon, 1970) and do not effect the entire area unless winds are blowing from the east. The largest turbidity values were encountered with strong southwest winds when high pressure systems were moving north from the mid-west U.S.A. The lowest values were observed during periods of strong northwest winds. Unexpectedly, the turbidity values resulting from air moving over the agricultural region of Southern Ontario and down the Dundas Valley were of equal or greater magnitude than the turbidity indicies from winds moving the local sources westward. Furthermore the frequency of these occurrences was several times greater. Only when the wind direction brought aerosols from the industrialized region of Toronto were the regional industrial sources greater than rural sources of aerosols. This indicates that concern about the atmosphere may need review concerning the entrainment of aerosol over highly mechanized farming areas.

Unsworth and Monteith τ_a was found to far superior than either the dry or wet turbidity factors modelled after Linke. However, more work

must still be done on the removal of air mass dependence in this model if accurate results of turbidity are to be calculated over large variations in optical air mass. The independence of τ_a from water vapour in mid-latitude regions is essential for meaningful results of aerosol turbidities.

The effects of a moving source of radiation have not been fully determined. In cases where synoptic air masses are the chief factors in local turbidity it does not seem to be a factor. However, when only local sources are present, or are predominant in the atmosphere, the position of the sun could drastically effect turbidity calculations. This is especially the case in cities such as Hamilton where the industrial sector is found in one section of the city.

The determination of the accuracy of the residual method of deriving direct beam radiation allows turbidity calculations to be carried out at all radiation stations with minimal problems. This would allow a full and accurate index of atmospheric pollution for a region which could be easily incorporated into all synoptic reports. Since the need for accurate determinations of precipitable water is low, because of the insensitivity of the Houghton model (Davies et al, 1975), surfaced based approximations or radiosone ascents from neighbouring meteorological stations could be utilized with little loss of accuracy. The determination of when direct beam radiation was received can be derived from sunshine records.

By evaluating a large number of turbidities over a wide area, the actual importance of local agricultural and air mass related turbidities could be determined. Using this method on past records, for any given region, the determination of increasing or decreasing aerosol amounts could be evaluated without long term actinometric measurements. The high

correlation between the residual and actinometric measurements over a longer period of time idnicates the applicability of this method to the problems presented.

REFERENCES

Ångström A., 1964: The parameters of atmospheric turbidity, *Tellus*, 16, 64-75.

Cook, N.H. and E. Rabinowicz, 1963: *Physical Measurement and Analysis*, Adison-Wesley Publishing Co. Inc., Reading Mass., 312 pages.

Davies, J.A., W. Schertzer and M. Nunez, 1975: Estimating global solar radiation, *Boundary Layer Meteorology*, 9, 33-52.

De Walle, D.R. and L.H. Parmele, 1974: Application of error analysis to surface temperature determination by radiation budget techniques. *J. Appl. Meteor.*, 13(4), 430-434.

Dilley, A.C., 1968: On the computer calculation of vapour pressure and specific humidity gradients from psychrometric data, *J. Appl. Meteor.*, 7, 717-719.

Feussner, K. and P. Dubois, 1960: Trübungsfaktor, precipitable water, stuab, *Gerlands Beitr. Z. Geophys.*, 27, 132-175.

Flowers, E.C., R.A. McCormick and K.R. Kurfis, 1969: Atmospheric turbidity over the United States, *J. Appl. Meteor.*, 8(6), 955-962.

Fowle, F.E., 1915: The transparency of aqueous vapour, *Astrophys. J.*, 42, 394.

Heidel, K., 1972: Turbidity trends in Tuscon, Arizona, *Science*, 177, 882-883.

Houghton, H.G., 1954: On the annual heat balance of the Northern Hemisphere, *J. Met.*, 11, 1-9.

Hoyt, D.V., 1975: New calculations of the Linke Turbidity Coefficient, *Q.J. Roy. Meteor. Soc.*, 101(428), 383-385.

IGY Instruction Manual, 1958: *Annals of IGY* 5, Part 6, "Radiation Instruments and Measurements, Pergamon Press, N.Y., 371-466.

Joseph, J.H. and A. Manes, 1971: Secular and seasonal variations of atmospheric turbidity at Jerusalem, *J. Appl. Meteor.*, 10(3), 453-462.

Kasten, F., 1966: A new table and approximation formula for the relative optical air mass, *Arch. Met. Geoph. Biokl. B.*, 14, 206-223.

Kondrat'yev, K. Ya., 1969: *Radiation in the Atmosphere*, Academic Press, 912 pages.

Latimer, J.R., 1971: Radiation Measurement. *International Field Year for the Great Lakes, Technical Manual Series,* No.2, 53 pages.

Linke, F., 1922: Transmissionkoeffizient and trubungsbaklor, *Beitr. 7. Phyd. fr. Atm.,* 10, 91-111.

Manes, A., 1972: *Atmospheric Turbidity over Jerusalem, State of Israel, Ministry of Transport - Israel Meteorological Service, Research and Development Division Series A, Meteorological Note No.26,* 81 pages.

Mamontova, L.I. and S.P. Khromov, 1933: Turbidity factors in different types of trospheric air masses over Moscow. *Meteorol.* Z.1.

McDonald, J.E., 1960: Direct absorption of solar radiation by atmospheric water vapour, *J. Meteor.,* 17, 319-328.

Poliakova, M.N., S.I. Sivkov and K.V. Ternovskaya, 1935: Actinometric characteristics of tropospheric air masses as observed at Slutzk and Kursk, *Geophys (Moscow),* 5(1).

Rouse, W.R. and J.R. McCutcheon, 1970: The effect of the regional wind on air pollution in Hamilton, Ontario, *Canadian Geographer,* 14(4), 271-285.

Schertzer, W.M., 1975: A model for calculating daily totals of global solar radiation in cloudless and cloudy sky conditions, *M.Sc. Thesis, Department of Geography, McMaster University,* 143 pages.

Sellers, W.D., 1965: *Physical Climatology,* University of Chicago Press, 272 pages.

Sivkov, S.I., 1968: *Computation of Solar Radiation Charactieristics,* Israel Program for Scientific Translations, 185 pages.

Smithsonian Institution, 1963: Smithsonian Meteorological Tables, R.J. List ed., Washington, 527 pages.

Thekaekara, M.P., 1972: Evaluating the light from the sun, *Optical Spectra,* 6, 32-35.

Unsworth, M. and J.L. Monteith, 1972: Aerosol and solar radiation in Britain, *Q.J. Roy. Meteor. Soc.,* 98(418), 778-797.

Valko, P., 1963: Uber das Verkalten des atmospherischen Dunstes am Alpensudfuss, *Archiv. Met. Geophys. Bioklim,* 12, 458-473.

Williamson, S.J., 1973: *Fundamentals of Air Pollution,* Addison-Wesley Pub. Co., Don Mills, Ontario, 472 pages.

Appendices

Appendix 1

LIST OF SYMBOLS

LIST OF SYMBOLS

τ_a	Unsworth and Monteith attenuation coefficient
T	Linke Turbidity Factor
d	earth sun distance
ϕ_{wa}	transmission due to water vapour absorption
ϕ_{ws}	transmission due to water vapour scattering
ϕ_{RS}	transmission due to Rayleigh Scattering
S	modelled direct beam radiation
S_o	solar constant
m	air mass
z	zenith angle
ϕ	latitude
δ	solar declination
h	hour angle
LAT	local apparent time
P	precipitable water
g	gravitational acceleration
q	specific humidity
p_o	pressure at the surface
p_u	the pressure measurement immediately preceding the pressure at which the dew point depression becomes unmeasureable
p	pressure
e	water vapour pressure

T_d	dew point temperature
$(\overline{q_i})$	mean specific humidity at layer i
(Δp_i)	pressure thickness of layer i
$(\overline{p_i})$	mean pressure at layer i
O_w	corrected optical depth
Θ_λ	atmospheric optical thickness for wavelength λ
K_λ	mass coefficient of molecular scattering
ρ	air density
$a_{w,\lambda}$	mass coefficient of absorption by water vapour
ρ_w	water vapour density
$a_{d,\lambda}$	mass coefficient of radiation attenuation by dust
ρ_a	dust concentration
h	height
$S_{m,\lambda}$	the attenuated monochromatic solar radiant flux
$S_{o,\lambda}$	the monothcromatic solar flux outside the atmosphere
p_m	integral transparency coefficient
Θ_o	optical thickness of the real atmosphere determined by the air mass m
$\Theta_{o\ ideal}$	optical thickness of the ideal atmosphere determined by the air mass m
r	sun-earth distance correction factor
$\overline{a}_r(m)$	mean extinction coefficient for a Rayleigh atmosphere, weighted for the distribution of the transmitted
	spectral irradiance
$S_{c,m}$	modelled ideal direct beam radiation

$S_{o,c}$	the corrected solar constant
$\tau_{g\lambda}$	the optical atmospheric thickness due to gaseous absorption
$\tau_{s\lambda}$	the optical atmospheric thickness due to molecular scattering
$\tau_{aa\lambda}$	the optical atmospheric thickness due to aerosol absorption
$\tau_{as\lambda}$	the optical atmospheric thickness due to aerosol scattering
$S_{o,\lambda}(o)$	the irradiance below an atmosphere free of aerosol
$\tau_{a\lambda}$	a spectral coefficient for aerosol

Appendix 2

Measured and calculated data for a representative day (July 31, 1975).

JULY 31 12 18.49

P	T	TD	Q	DW	PW
850.	20.0	6.0	6.870		
				.605	.780
700.	10.2	-5.8	3.336		
				.215	.359
500.	-8.5	-38.5	.186		

OPTICAL DEPTH IS .820CM PRECIPITABLE WATER IS 1.139CM

TM	Z	AM	WM	WA	WS	RS	AT	ST	DB
6.75	1.211	2.618	2.199	.902	.957	.794	.902	.760	874.21
6.87	1.183	2.561	2.077	.904	.959	.802	.904	.770	886.94
6.98	1.157	2.532	1.975	.906	.962	.809	.906	.778	897.63
7.08	1.148	2.425	1.892	.907	.963	.814	.907	.784	906.63
7.21	1.124	2.301	1.795	.909	.966	.821	.908	.792	917.40
				MEANED VALUES OVER THE TIME SPAN					
6.98	1.168	2.547	1.968	.905	.961	.808	.905	.777	895.56

EVALUATION OF RANGES OF DIRECT BEAM RADIATION BY ACTINOMETER AND RESIDUAL

TM	MIN	MEAS	MAX	MIN	MEAS	MAX
6.75	430.61	442.92	455.82	431.05	443.98	456.92
6.87	446.65	460.25	473.66	446.08	459.47	472.35
6.98	462.66	476.54	490.42	461.72	475.58	489.43
7.08	478.61	490.91	505.21	488.37	503.02	517.68
7.21	492.44	507.21	521.99	502.00	517.06	532.13
			MEANED VALUES OVER THE TIME SPAN			
6.98	461.71	475.57	489.42	465.84	479.82	493.80

LINKE TURBIDITY CALCULATED FOR ACTINOMETER AND RESIDUAL MEASUREMENTS

TM	MIN	CALC	MAX	MIN	CALC	MAX
6.75	2.393	2.454	2.518	2.388	2.449	2.513
6.87	2.385	2.448	2.513	2.388	2.452	2.517
6.98	2.371	2.436	2.503	2.375	2.440	2.507
7.08	2.357	2.423	2.492	2.300	2.367	2.435
7.21	2.345	2.413	2.484	2.299	2.368	2.438
			MEANED VALUES OVER THE TIME SPAN			
6.98	2.370	2.435	2.502	2.350	2.415	2.482

UNSWORTH AND MONTEITH TURBIDITY FACTOR CALCULATED FOR ACTINOMETER AND RESIDUAL MEASUREMENTS

TM	MIN	CALC	MAX	MIN	CALC	MAX
6.75	.231	.241	.252	.230	.240	.251
6.87	.236	.247	.258	.236	.247	.258
6.98	.239	.251	.262	.240	.251	.263
7.08	.241	.253	.265	.231	.243	.255
7.21	.245	.258	.270	.237	.249	.262
			MEANED VALUES OVER THE TIME SPAN			
6.98	.238	.250	.261	.235	.246	.258

TM	Z	AM	WM	WA	WS	RS	AT	ST	DB
7.75	1.021	1.906	1.488	.913	.972	.842	.913	.819	953.34
7.86	1.000	1.844	1.439	.914	.974	.846	.914	.823	959.27
7.97	.979	1.787	1.395	.915	.975	.849	.915	.827	964.82
8.08	.958	1.734	1.353	.916	.976	.852	.915	.831	970.03
8.21	.934	1.677	1.308	.917	.977	.855	.917	.835	975.76
				MEANED VALUES OVER THE TIME SPAN					
7.97	.978	1.790	1.397	.915	.975	.849	.915	.827	964.64

EVALUATION OF RANGES OF DIRECT BEAM RADIATION BY ACTINOMETER AND RESIDUAL

TM	MIN	MEAS	MAX	MIN	MEAS	MAX
7.75	553.35	569.96	586.56	576.54	593.84	611.14
7.86	563.32	580.23	597.13	584.94	602.50	620.05
7.97	572.66	592.34	609.99	593.10	610.90	628.70
8.08	588.05	605.69	623.34	608.39	626.65	644.91
8.21	601.02	619.06	637.09	621.71	640.36	659.02
			MEANED VALUES OVER THE TIME SPAN			
7.97	576.17	593.46	610.74	596.94	614.65	632.76

LINKE TURBIDITY CALCULATED FOR ACTINOMETER AND RESIDUAL MEASUREMENTS

TM	MIN	CALC	MAX	MIN	CALC	MAX
7.75	2.275	2.351	2.428	2.168	2.243	2.321
7.86	2.265	2.342	2.421	2.165	2.241	2.320
7.97	2.245	2.323	2.403	2.161	2.239	2.319
8.08	2.217	2.296	2.377	2.123	2.202	2.283
8.21	2.192	2.272	2.355	2.096	2.178	2.261
			MEANED VALUES OVER THE TIME SPAN			
7.97	2.239	2.317	2.397	2.143	2.221	2.301

UNSWORTH AND MONTEITH TURBIDITY FACTOR CALCULATED FOR ACTINOMETER AND RESIDUAL MEASUREMENTS

TM	MIN	CALC	MAX	MIN	CALC	MAX
7.75	.255	.270	.285	.233	.248	.264
7.86	.257	.273	.289	.237	.252	.268
7.97	.257	.273	.290	.240	.256	.272
8.08	.255	.272	.289	.235	.252	.269
8.21	.254	.271	.289	.234	.251	.269
			MEANED VALUES OVER THE TIME SPAN			
7.97	.256	.272	.288	.236	.252	.268

TM	Z	AM	WM	WA	WS	RS	AT	ST	DB
8.75	.833	1.484	1.158	.920	.960	.867	.920	.849	995.53
8.86	.813	1.452	1.133	.920	.960	.869	.920	.852	998.86
8.97	.793	1.422	1.110	.921	.961	.870	.921	.854	1002.02
9.08	.773	1.395	1.088	.921	.961	.872	.921	.856	1004.99
9.21	.750	1.364	1.065	.922	.962	.874	.922	.858	1008.26
				MEANED VALUES OVER THE TIME SPAN					
8.97	.782	1.424	1.111	.921	.961	.870	.921	.854	1001.93

EVALUATION OF RANGES OF DIRECT BEAM RADIATION BY ACTINOMETER AND RESIDUAL

TM	MIN	MEAS	MAX	MIN	MEAS	MAX
8.75	647.31	666.73	685.16	654.85	674.51	694.16
8.86	650.27	669.78	689.29	654.59	674.23	693.87
8.97	650.93	670.47	690.00	654.20	673.98	693.77
9.08	653.36	672.99	692.59	654.59	675.38	696.17
9.21	655.94	676.66	696.37	661.03	680.87	700.70
			MEANED VALUES OVER THE TIME SPAN			
8.97	651.77	671.32	690.88	657.85	677.59	697.33

LINKE TURBIDITY CALCULATED FOR ACTINOMETER AND RESIDUAL MEASUREMENTS

TM	MIN	CALC	MAX	MIN	CALC	MAX
8.75	2.103	2.188	2.275	2.068	2.153	2.241
8.86	2.110	2.196	2.284	2.090	2.176	2.265
8.97	2.127	2.214	2.303	2.089	2.176	2.265
9.08	2.135	2.222	2.312	2.106	2.193	2.284
9.21	2.139	2.228	2.319	2.120	2.209	2.300
			MEANED VALUES OVER THE TIME SPAN			
8.97	2.123	2.210	2.299	2.095	2.181	2.271

UNSWORTH AND MONTEITH TURBIDITY FACTOR CALCULATED FOR ACTINOMETER AND RESIDUAL MEASUREMENTS

TM	MIN	CALC	MAX	MIN	CALC	MAX
8.75	.251	.270	.290	.243	.262	.282
8.86	.255	.275	.296	.251	.271	.291
8.97	.262	.282	.303	.253	.274	.294
9.08	.267	.288	.309	.260	.281	.302
9.21	.271	.292	.314	.267	.288	.309
			MEANED VALUES OVER THE TIME SPAN			
8.97	.261	.282	.302	.255	.275	.296

TM	Z	AM	WM	WA	WS	RS	AT	ST	DB
9.75	.637	1.262	.965	.923	.984	.880	.923	.866	1019.55
9.86	.639	1.245	.971	.924	.984	.881	.924	.867	1021.45
9.97	.622	1.229	.959	.924	.984	.882	.924	.869	1023.22
10.08	.605	1.214	.948	.924	.985	.883	.924	.870	1024.87
10.21	.585	1.198	.935	.925	.985	.884	.925	.871	1026.68
				MEANED VALUES OVER THE TIME SPAN					
9.97	.622	1.230	.960	.924	.984	.882	.924	.869	1023.15

EVALUATION OF RANGES OF DIRECT BEAM RADIATION BY ACTINOMETER AND RESIDUAL

TM	MIN	MEAS	MAX	MIN	MEAS	MAX
9.75	677.92	698.26	718.60	679.00	699.37	719.75
9.86	682.18	702.65	723.12	682.98	703.48	723.97
9.97	686.14	708.79	729.43	687.28	707.90	728.52
10.08	690.59	717.49	738.40	693.15	713.95	734.75
10.21	703.27	724.38	745.48	699.20	720.18	741.17
		MEANED VALUES OVER THE TIME SPAN				
9.97	689.62	710.31	731.01	688.32	708.98	729.63

LINKE TURBIDITY CALCULATED FOR ACTINOMETER AND RESIDUAL MEASUREMENTS

TM	MIN	CALC	MAX	MIN	CALC	MAX
9.75	2.115	2.207	2.301	2.110	2.202	2.296
9.86	2.102	2.200	2.295	2.104	2.196	2.291
9.97	2.091	2.184	2.279	2.095	2.188	2.283
10.08	2.083	2.156	2.252	2.089	2.172	2.258
10.21	2.043	2.137	2.234	2.062	2.156	2.252
			MEANED VALUES OVER THE TIME SPAN			
9.97	2.084	2.177	2.272	2.090	2.183	2.278

UNSWORTH AND MONTEITH TURBIDITY FACTOR CALCULATED FOR ACTINOMETER AND RESIDUAL MEASUREMENTS

TM	MIN	CALC	MAX	MIN	CALC	MAX
9.75	.277	.300	.323	.276	.299	.322
9.86	.277	.301	.324	.277	.300	.323
9.97	.275	.299	.323	.276	.300	.324
10.08	.270	.294	.318	.274	.298	.322
10.21	.267	.291	.316	.272	.296	.321
			MEANED VALUES OVER THE TIME SPAN			
9.97	.273	.297	.321	.275	.298	.322

TM	Z	AM	WM	WA	WS	RS	AT	ST	DB
10.73	.515	1.148	.896	.925	.986	.888	.925	.875	1032.44
10.83	.504	1.141	.890	.926	.986	.886	.925	.876	1033.29
10.95	.491	1.133	.884	.926	.986	.889	.925	.876	1034.22
11.07	.479	1.126	.878	.926	.986	.869	.926	.877	1035.04
11.19	.468	1.119	.874	.926	.986	.890	.926	.877	1035.76
				MEANED VALUES OVER THE TIME SPAN					
10.95	.491	1.133	.884	.926	.986	.889	.926	.876	1034.15

EVALUATION OF RANGES OF DIRECT BEAM RADIATION BY ACTINOMETER AND RESIDUAL

TM	MIN	MEAS	MAX	MIN	MEAS	MAX
10.73	709.51	730.60	752.09	704.89	726.04	747.19
10.83	719.21	740.80	762.38	705.13	726.29	747.45
10.95	714.43	735.87	757.30	698.97	719.94	740.92
11.07	704.85	726.00	747.15	692.22	712.99	733.76
11.19	698.40	719.35	740.31	686.06	706.64	727.23
		MEANED VALUES OVER THE TIME SPAN				
10.95	709.28	730.56	751.85	697.45	718.38	739.31

LINKE TURBIDITY CALCULATED FOR ACTINOMETER AND RESIDUAL MEASUREMENTS

TM	MIN	CALC	MAX	MIN	CALC	MAX
10.73	2.052	2.147	2.246	2.074	2.169	2.267
10.83	2.013	2.108	2.207	2.078	2.174	2.272
10.95	2.041	2.137	2.236	2.114	2.210	2.309
11.07	2.091	2.188	2.287	2.152	2.248	2.347
11.19	2.127	2.224	2.323	2.187	2.283	2.383
			MEANED VALUES OVER THE TIME SPAN			
10.95	2.065	2.161	2.259	2.121	2.217	2.316

UNSWORTH AND MONTEITH TURBIDITY FACTOR CALCULATED FOR ACTINOMETER AND RESIDUAL MEASUREMENTS

TM	MIN	CALC	MAX	MIN	CALC	MAX
10.73	.276	.301	.327	.282	.307	.332
10.83	.267	.292	.318	.284	.309	.335
10.95	.279	.300	.327	.294	.320	.346
11.07	.290	.315	.341	.306	.331	.357
11.19	.300	.326	.352	.316	.342	.368
			MEANED VALUES OVER THE TIME SPAN			
10.95	.281	.307	.333	.295	.322	.348

TM	Z	AM	WM	WA	WS	RS	AT	ST	DB
11.75	.436	1.102	.860	.926	.967	.891	.926	.879	1037.77
11.86	.433	1.101	.859	.926	.967	.891	.926	.879	1037.91
11.97	.432	1.100	.859	.926	.967	.891	.926	.879	1037.97
12.08	.433	1.101	.859	.926	.967	.891	.926	.879	1037.95
12.21	.435	1.102	.860	.926	.967	.891	.926	.879	1037.83
				MEANED VALUES OVER THE TIME SPAN					
11.97	.434	1.101	.859	.926	.967	.891	.926	.879	1037.89

EVALUATION OF RANGES OF DIRECT BEAM RADIATION BY ACTINOMETER AND RESIDUAL

TM	MIN	MEAS	MAX	MIN	MEAS	MAX
11.75	680.53	700.95	721.37	674.30	694.54	714.77
11.86	669.14	689.22	709.30	665.42	685.39	705.36
11.97	667.94	687.98	708.03	647.69	667.12	686.56
12.08	661.94	681.81	701.67	651.26	670.80	690.35
12.21	682.63	682.51	702.40	682.36	682.24	702.11
		MEANED VALUES OVER THE TIME SPAN				
11.97	665.44	686.49	708.55	660.21	680.02	699.83

LINKE TURBIDITY CALCULATED FOR ACTINOMETER AND RESIDUAL MEASUREMENTS

TM	MIN	CALC	MAX	MIN	CALC	MAX
11.75	2.229	2.326	2.426	2.260	2.357	2.457
11.86	2.267	2.364	2.464	2.306	2.403	2.503
11.97	2.293	2.390	2.490	2.397	2.495	2.594
12.08	2.324	2.421	2.521	2.379	2.476	2.576
12.21	2.319	2.416	2.516	2.321	2.418	2.518
			MEANED VALUES OVER THE TIME SPAN			
11.97	2.290	2.387	2.487	2.332	2.429	2.529

UNSWORTH AND MONTEITH TURBIDITY FACTOR CALCULATED FOR ACTINOMETER AND RESIDUAL MEASUREMENTS

TM	MIN	CALC	MAX	MIN	CALC	MAX
11.75	.330	.356	.383	.338	.364	.391
11.86	.346	.372	.399	.351	.377	.404
11.97	.348	.374	.401	.375	.402	.429
12.08	.356	.382	.409	.371	.397	.423
12.21	.354	.380	.407	.355	.381	.408
			MEANED VALUES OVER THE TIME SPAN			
11.97	.347	.373	.400	.358	.384	.411

TM	Z	AM	WM	WA	WS	RS	AT	ST	DB
12.75	.463	1.117	.871	.925	.986	.890	.926	.878	1035.08
12.86	.472	1.122	.875	.925	.986	.889	.925	.877	1035.47
12.97	.482	1.126	.880	.926	.986	.889	.925	.877	1034.78
13.08	.494	1.135	.885	.926	.985	.889	.926	.876	1034.00
				MEANED VALUES OVER THE TIME SPAN					
12.92	.478	1.125	.878	.926	.986	.889	.925	.877	1035.06

EVALUATION OF RANGES OF DIRECT BEAM RADIATION BY ACTINOMETER AND RESIDUAL

TM	MIN	MEAS	MAX	MIN	MEAS	MAX
12.75	653.03	672.62	692.22	657.28	677.00	696.72
12.86	665.72	685.70	705.67	653.25	672.85	692.45
12.97	651.70	670.23	689.75	634.12	653.15	672.18
13.08	650.10	669.61	689.11	643.90	663.23	682.55
		MEANED VALUES OVER THE TIME SPAN				
12.92	654.89	674.54	694.19	647.14	666.56	685.97

LINKE TURBIDITY CALCULATED FOR ACTINOMETER AND RESIDUAL MEASUREMENTS

TM	MIN	CALC	MAX	MIN	CALC	MAX
12.75	2.355	2.452	2.551	2.333	2.430	2.529
12.86	2.256	2.382	2.481	2.349	2.446	2.545
12.97	2.357	2.453	2.552	2.444	2.540	2.639
13.08	2.354	2.450	2.549	2.386	2.482	2.581
			MEANED VALUES OVER THE TIME SPAN			
12.92	2.338	2.434	2.533	2.378	2.474	2.573

UNSWORTH AND MONTEITH TURBIDITY FACTOR CALCULATED FOR ACTINOMETER AND RESIDUAL MEASUREMENTS

TM	MIN	CALC	MAX	MIN	CALC	MAX
12.75	.361	.387	.413	.355	.381	.408
12.86	.342	.367	.391	.359	.384	.411
12.97	.360	.385	.411	.383	.406	.434
13.08	.356	.383	.409	.366	.391	.417
			MEANED VALUES OVER THE TIME SPAN			
12.92	.355	.381	.407	.366	.391	.417

TM	Z	AM	WM	WA	WS	RS	AT	ST	DB
13.75	.579	1.194	.932	.925	.985	.885	.925	.871	1027.20
13.86	.596	1.207	.942	.924	.985	.884	.924	.870	1025.72
13.97	.613	1.221	.953	.924	.985	.883	.924	.869	1024.14
14.08	.630	1.236	.965	.924	.984	.882	.924	.868	1022.43
14.20	.649	1.254	.978	.924	.984	.881	.924	.867	1020.43
				MEANED VALUES OVER THE TIME SPAN					
13.97	.613	1.222	.954	.924	.984	.883	.924	.869	1023.98

EVALUATION OF RANGES OF DIRECT BEAM RADIATION BY ACTINOMETER AND RESIDUAL

TM	MIN	MEAS	MAX	MIN	MEAS	MAX
13.75	612.85	631.24	649.63	599.52	617.51	635.50
13.86	602.63	620.72	638.80	593.34	611.15	628.95
13.97	605.04	623.19	641.35	583.53	601.04	618.55
14.08	597.83	615.77	633.70	576.45	593.74	611.04
14.20	589.43	607.11	624.80	568.91	585.99	603.06
			MEANED VALUES OVER THE TIME SPAN			
13.97	601.55	619.60	637.66	584.35	601.89	619.42

LINKE TURBIDITY CALCULATED FOR ACTINOMETER AND RESIDUAL MEASUREMENTS

TM	MIN	CALC	MAX	MIN	CALC	MAX
13.75	2.496	2.590	2.687	2.568	2.662	2.758
13.86	2.539	2.633	2.729	2.590	2.683	2.779
13.97	2.514	2.607	2.702	2.631	2.724	2.819
14.08	2.539	2.631	2.726	2.656	2.748	2.843
14.20	2.568	2.660	2.754	2.681	2.773	2.868
			MEANED VALUES OVER THE TIME SPAN			
13.97	2.531	2.624	2.720	2.625	2.718	2.814

UNSWORTH AND MONTEITH TURBIDITY FACTOR CALCULATED FOR ACTINOMETER AND RESIDUAL MEASUREMENTS

TM	MIN	CALC	MAX	MIN	CALC	MAX
13.75	.384	.408	.433	.402	.426	.451
13.86	.392	.416	.441	.405	.429	.454
13.97	.383	.407	.431	.413	.437	.461
14.08	.387	.410	.434	.416	.440	.464
14.20	.391	.414	.438	.419	.442	.466
			MEANED VALUES OVER THE TIME SPAN			
13.97	.388	.411	.435	.411	.435	.459

TM	Z	AM	WM	WA	WS	RS	AT	ST	DB
14.73	.739	1.351	1.054	.922	.982	.875	.922	.859	1009.69
14.84	.759	1.376	1.074	.921	.982	.873	.921	.857	1007.03
14.94	.777	1.400	1.092	.921	.981	.872	.921	.856	1004.46
15.07	.800	1.433	1.116	.920	.981	.870	.920	.853	1000.90
				MEANED VALUES OVER THE TIME SPAN					
14.90	.769	1.390	1.085	.921	.982	.872	.921	.856	1005.52

EVALUATION OF RANGES OF DIRECT BEAM RADIATION BY ACTINOMETER AND RESIDUAL

TM	MIN	MEAS	MAX	MIN	MEAS	MAX
14.73	567.77	584.81	601.85	551.93	568.49	585.05
14.84	549.10	565.57	582.05	528.60	544.47	560.33
14.94	532.46	546.40	562.32	509.73	525.02	540.32
15.07	526.87	542.68	558.49	506.29	523.54	538.80
			MEANED VALUES OVER THE TIME SPAN			
14.90	543.56	559.87	576.18	524.64	540.38	556.12

LINKE TURBIDITY CALCULATED FOR ACTINOMETER AND RESIDUAL MEASUREMENTS

TM	MIN	CALC	MAX	MIN	CALC	MAX
14.73	2.609	2.659	2.780	2.587	2.776	2.856
14.84	2.681	2.759	2.860	2.798	2.886	2.977
14.94	2.765	2.853	2.943	2.887	2.974	3.054
15.07	2.756	2.843	2.932	2.865	2.951	3.040
			MEANED VALUES OVER THE TIME SPAN			
14.90	2.701	2.788	2.879	2.809	2.897	2.987

UNSWORTH AND MONTEITH TURBIDITY FACTOR CALCULATED FOR ACTINOMETER AND RESIDUAL MEASUREMENTS

TM	MIN	CALC	MAX	MIN	CALC	MAX
14.73	.383	.404	.426	.404	.425	.447
14.84	.398	.419	.441	.426	.447	.468
14.94	.414	.435	.456	.443	.464	.485
15.07	.407	.427	.448	.432	.452	.473
			MEANED VALUES OVER THE TIME SPAN			
14.90	.401	.421	.443	.425	.447	.468

TM	Z	AM	WM	WA	WS	RS	AT	ST	DB
15.75	.926	1.669	1.295	.917	.977	.856	.917	.836	977.44
15.86	.947	1.707	1.332	.916	.976	.853	.916	.833	972.73
15.97	.968	1.756	1.372	.915	.975	.850	.915	.829	967.70
16.08	.988	1.813	1.414	.915	.974	.847	.915	.825	962.34
16.20	1.011	1.878	1.465	.914	.973	.844	.914	.821	955.08
			MEANED VALUES OVER THE TIME SPAN						
15.97	.968	1.763	1.376	.915	.975	.850	.915	.829	967.26

EVALUATION OF RANGES OF DIRECT BEAM RADIATION BY ACTINOMETER AND RESIDUAL

TM	MIN	MEAS	MAX	MIN	MEAS	MAX
15.75	481.97	496.43	510.89	462.91	476.60	490.69
15.86	476.97	493.34	507.71	458.10	471.65	485.59
15.97	469.96	480.97	494.99	452.11	459.37	468.64
16.08	453.10	466.76	480.35	429.18	442.06	454.93
16.20	428.55	441.41	454.27	402.99	415.06	427.18
			MEANED VALUES OVER THE TIME SPAN			
15.97	461.92	475.78	489.64	439.06	452.23	465.41

LINKE TURBIDITY CALCULATED FOR ACTINOMETER AND RESIDUAL MEASUREMENTS

TM	MIN	CALC	MAX	MIN	CALC	MAX
15.75	2.823	2.904	2.987	2.936	3.017	3.100
15.86	2.803	2.882	2.964	2.926	3.006	3.088
15.97	2.832	2.911	2.992	2.982	3.060	3.141
16.08	2.871	2.948	3.028	3.017	3.094	3.174
16.20	2.969	3.045	3.123	3.132	3.208	3.286
			MEANED VALUES OVER THE TIME SPAN			
15.97	2.860	2.938	3.019	2.999	3.077	3.158

UNSWORTH AND MONTEITH TURBIDITY FACTOR CALCULATED FOR ACTINOMETER AND RESIDUAL MEASUREMENTS

TM	MIN	CALC	MAX	MIN	CALC	MAX
15.75	.391	.408	.426	.415	.432	.450
15.86	.381	.398	.415	.407	.424	.441
15.97	.381	.398	.415	.413	.429	.446
16.08	.383	.399	.415	.413	.429	.445
16.20	.396	.412	.427	.429	.444	.460
			MEANED VALUES OVER THE TIME SPAN			
15.97	.387	.403	.420	.415	.432	.449

Appendix 3

Figures of the Sivkov T for comparison to the Unsworth and Monteith τ_a. All days that are represented in the synoptic analysis have corresponding graphs in Appendix 2.

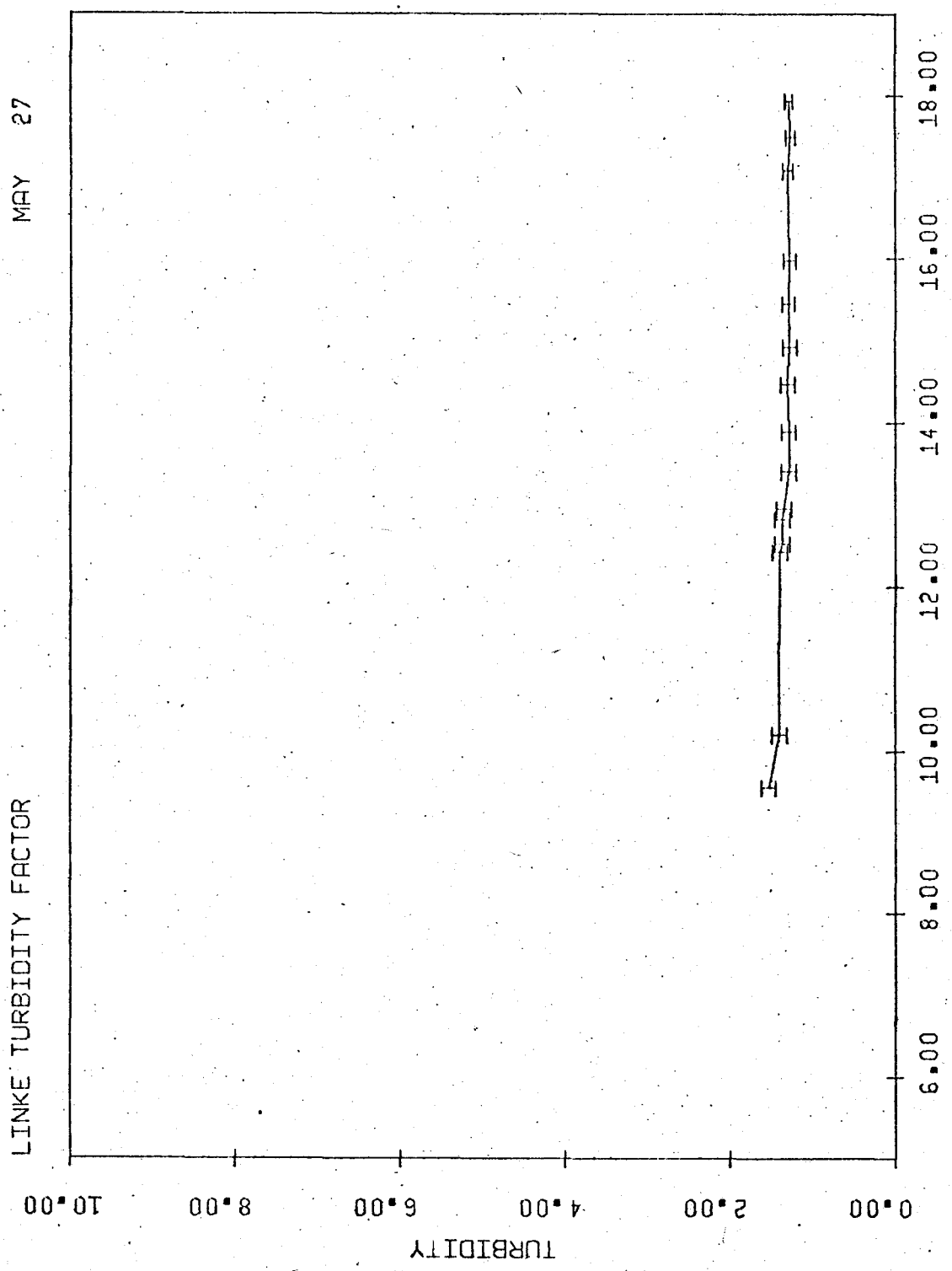
LINKE TURBIDITY FACTOR
MAY 27
TURBIDITY
0.00
2.00
4.00
6.00
8.00
10.00
6.00
8.00
10.00
12.00
14.00
16.00
18.00
LOCAL APPARENT TIME (DECIMAL HOURS)

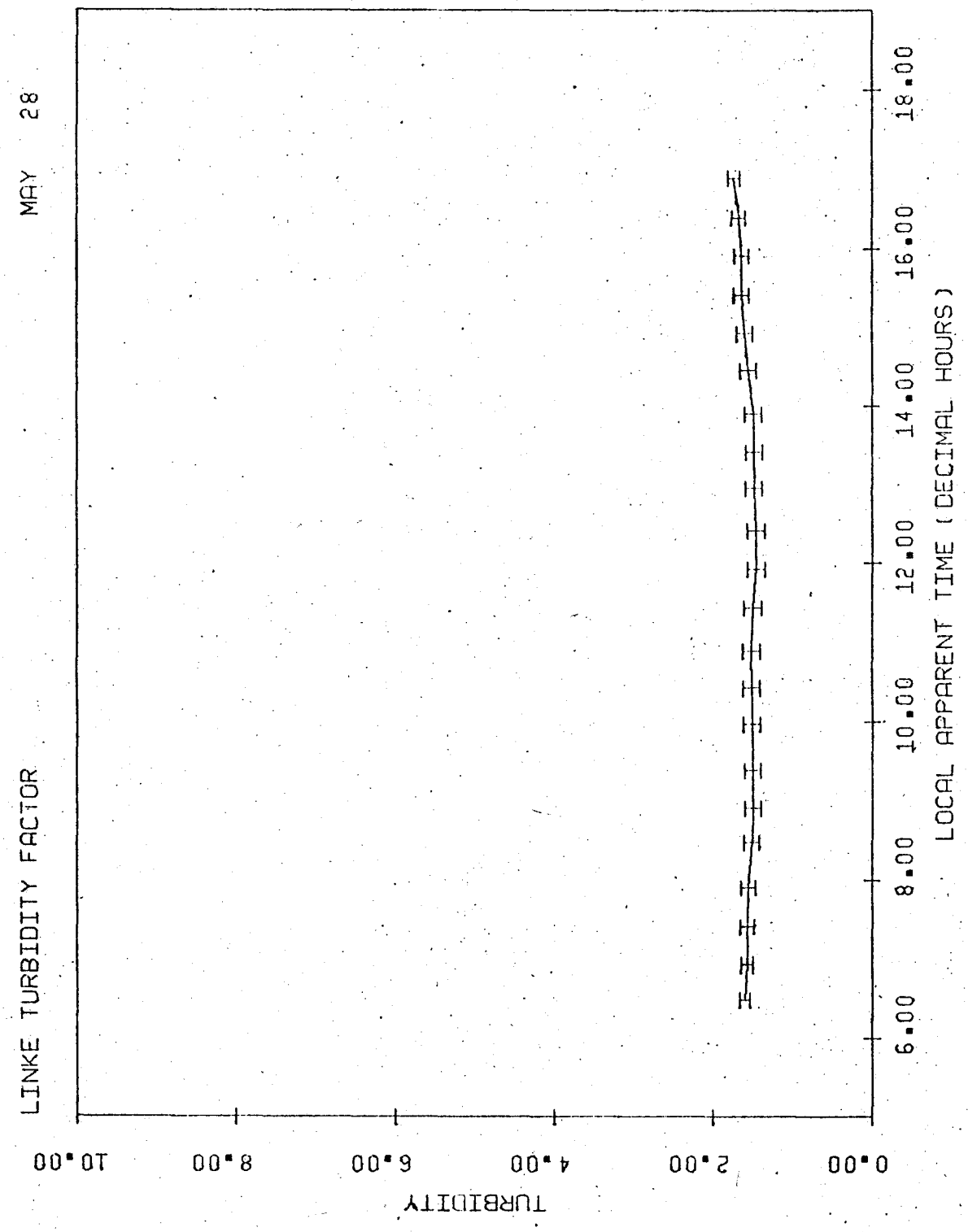
LINKE TURBIDITY FACTOR
MAY 28
TURBIDITY
0.00
2.00
4.00
6.00
8.00
10.00
6.00
8.00
10.00
12.00
14.00
16.00
18.00
LOCAL APPARENT TIME (DECIMAL HOURS)

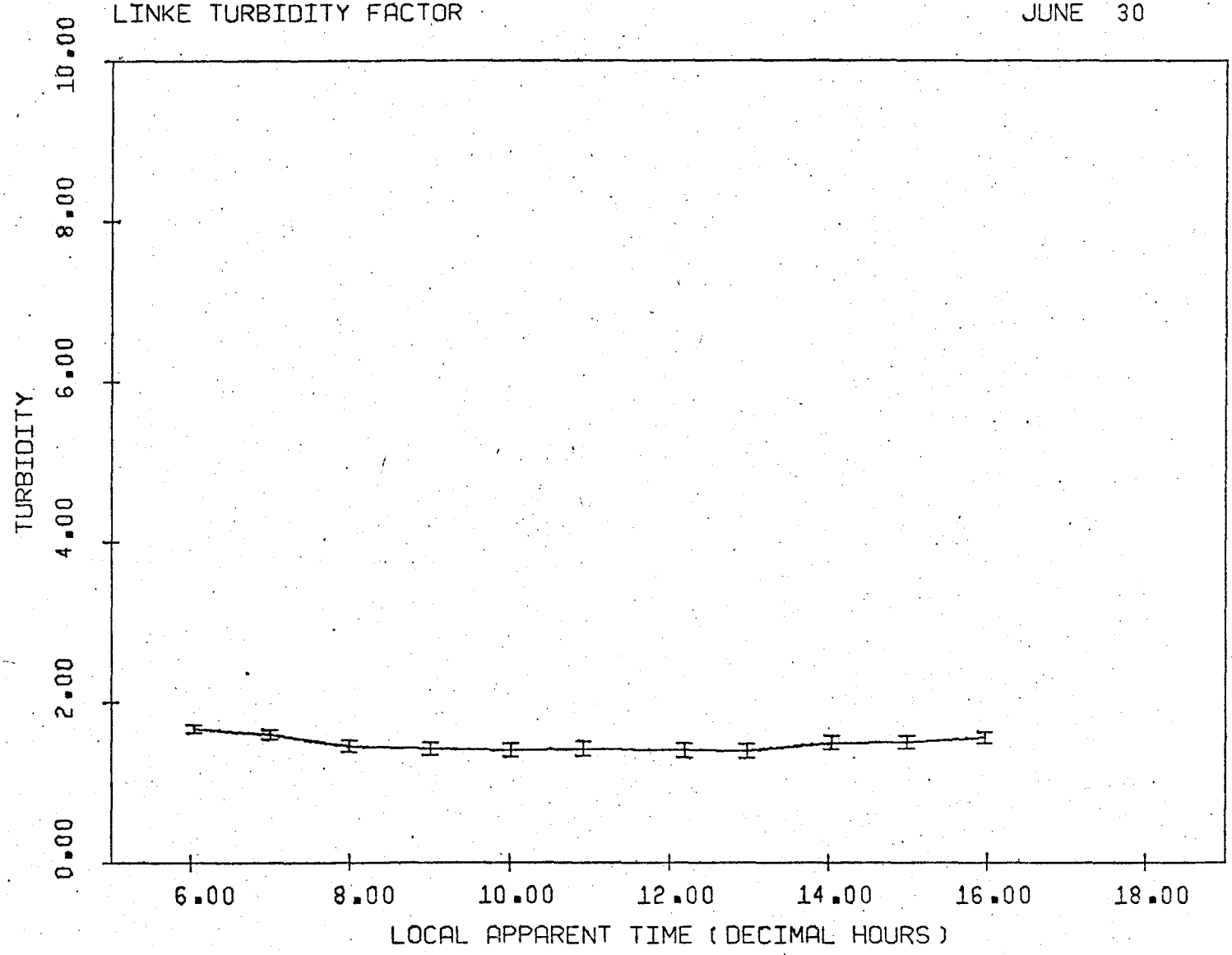
LINKE TURBIDITY FACTOR
JUNE 30
TURBIDITY
0.00
2.00
4.00
6.00
8.00
10.00
6.00
8.00
10.00
12.00
14.00
16.00
18.00
LOCAL APPARENT TIME (DECIMAL HOURS)

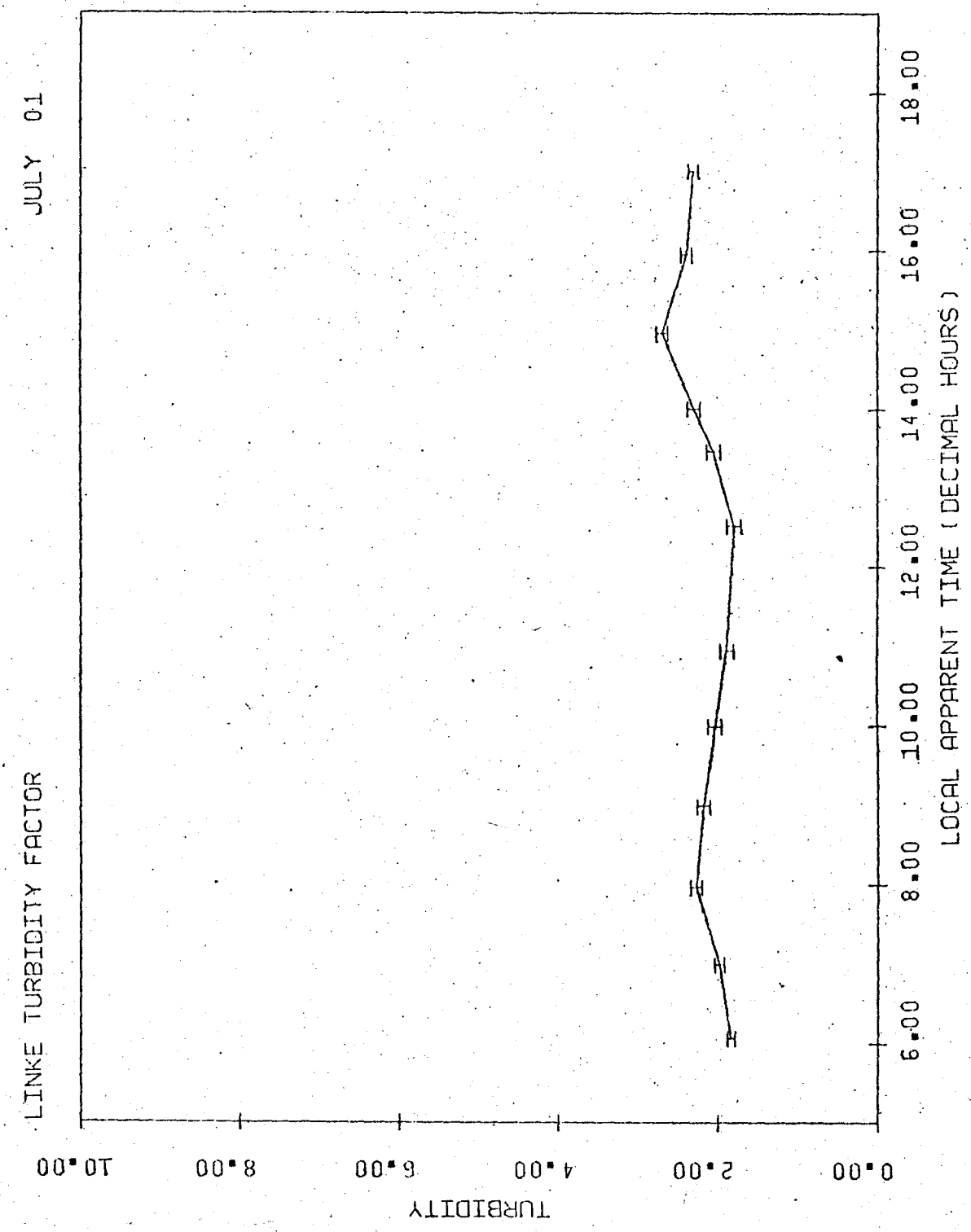
JULY 01
LINKE TURBIDITY FACTOR
TURBIDITY
0.00
2.00
4.00
6.00
8.00
10.00
6.00
8.00
10.00
12.00
14.00
16.00
18.00
LOCAL APPARENT TIME (DECIMAL HOURS)

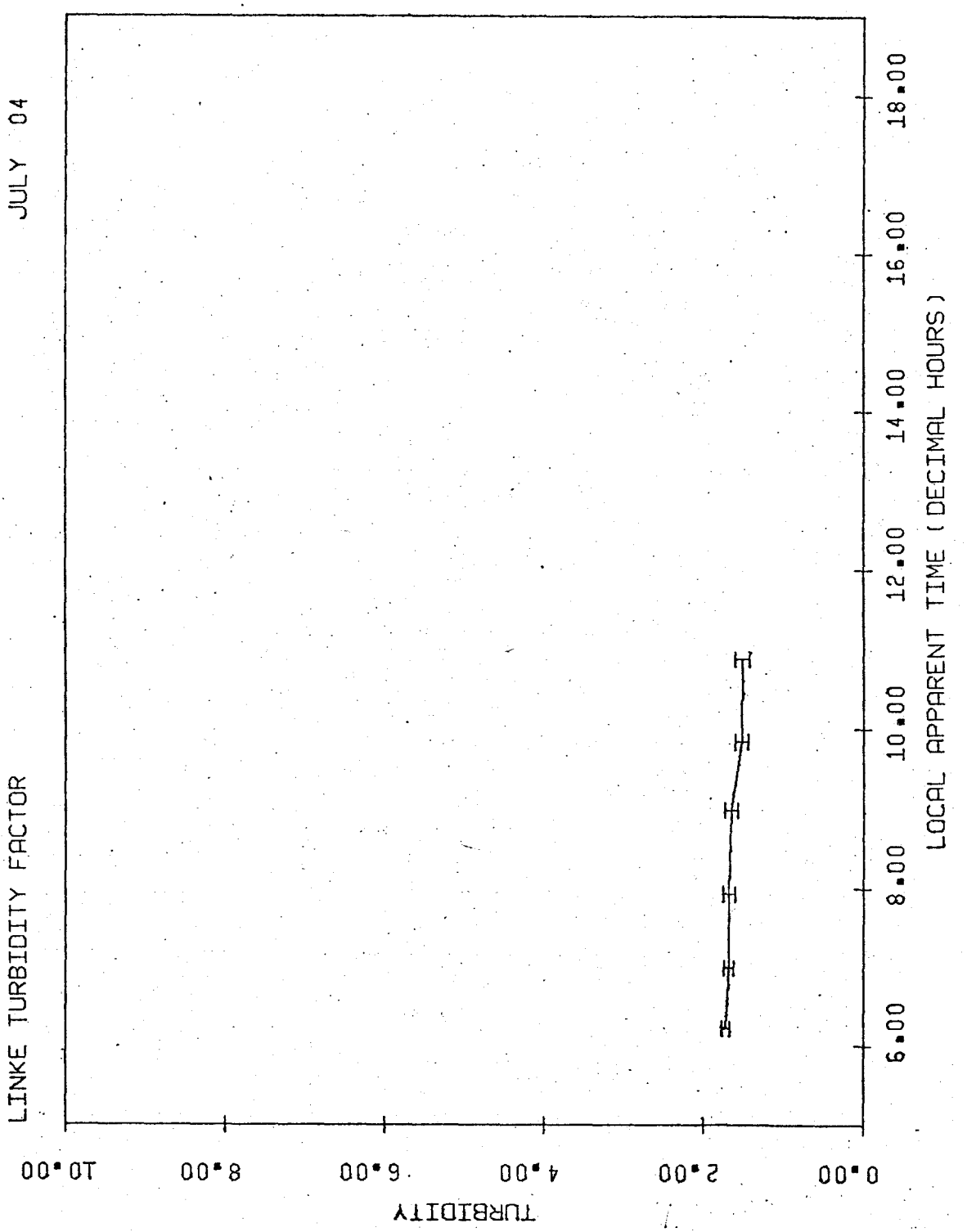
LINKE TURBIDITY FACTOR
JULY 04
TURBIDITY
0.00
2.00
4.00
6.00
8.00
10.00
6.00
8.00
10.00
12.00
14.00
16.00
18.00
LOCAL APPARENT TIME (DECIMAL HOURS)

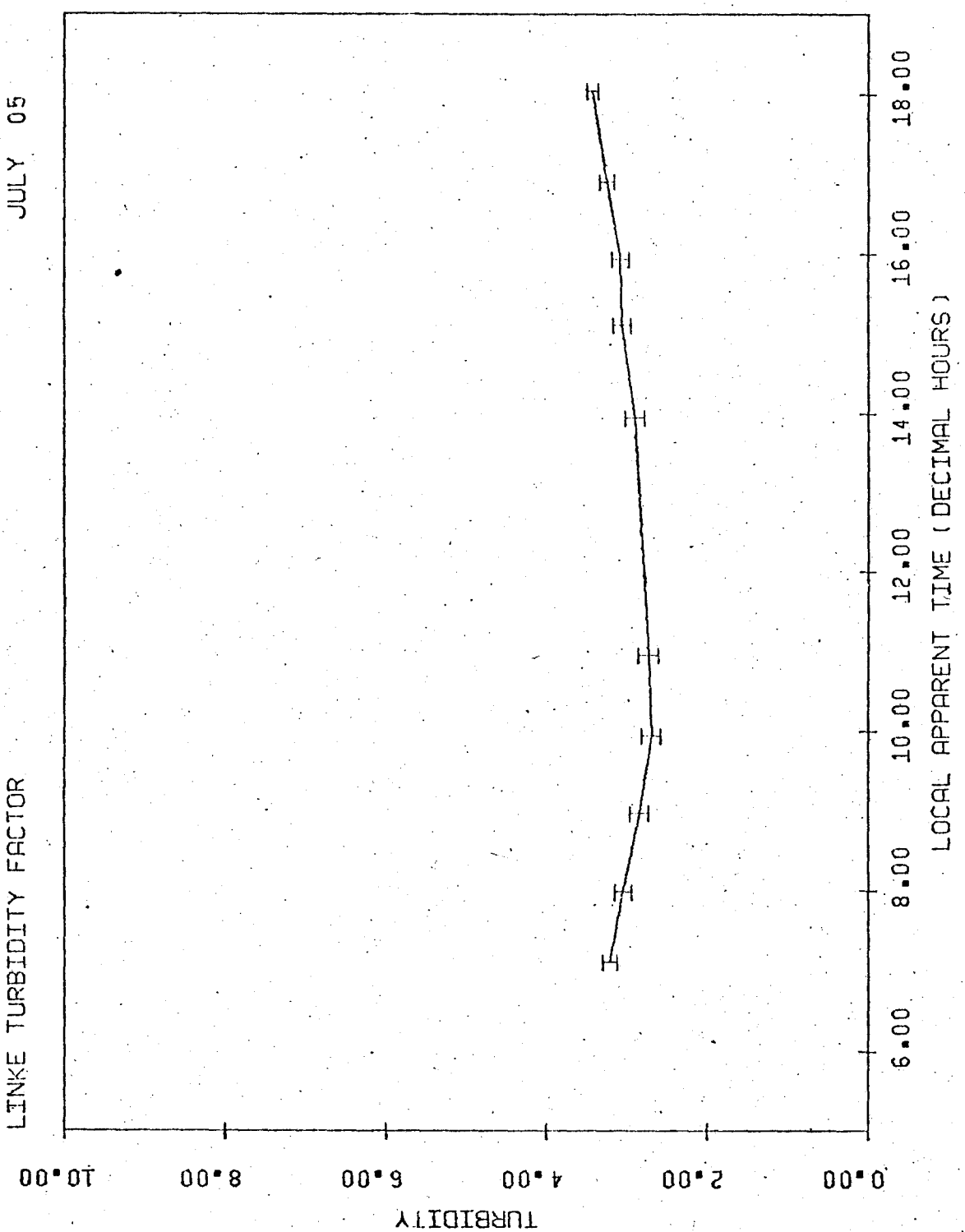
LINKE TURBIDITY FACTOR
JULY 05
TURBIDITY
0.00
2.00
4.00
6.00
8.00
10.00
6.00
8.00
10.00
12.00
14.00
16.00
18.00
LOCAL APPARENT TIME (DECIMAL HOURS)

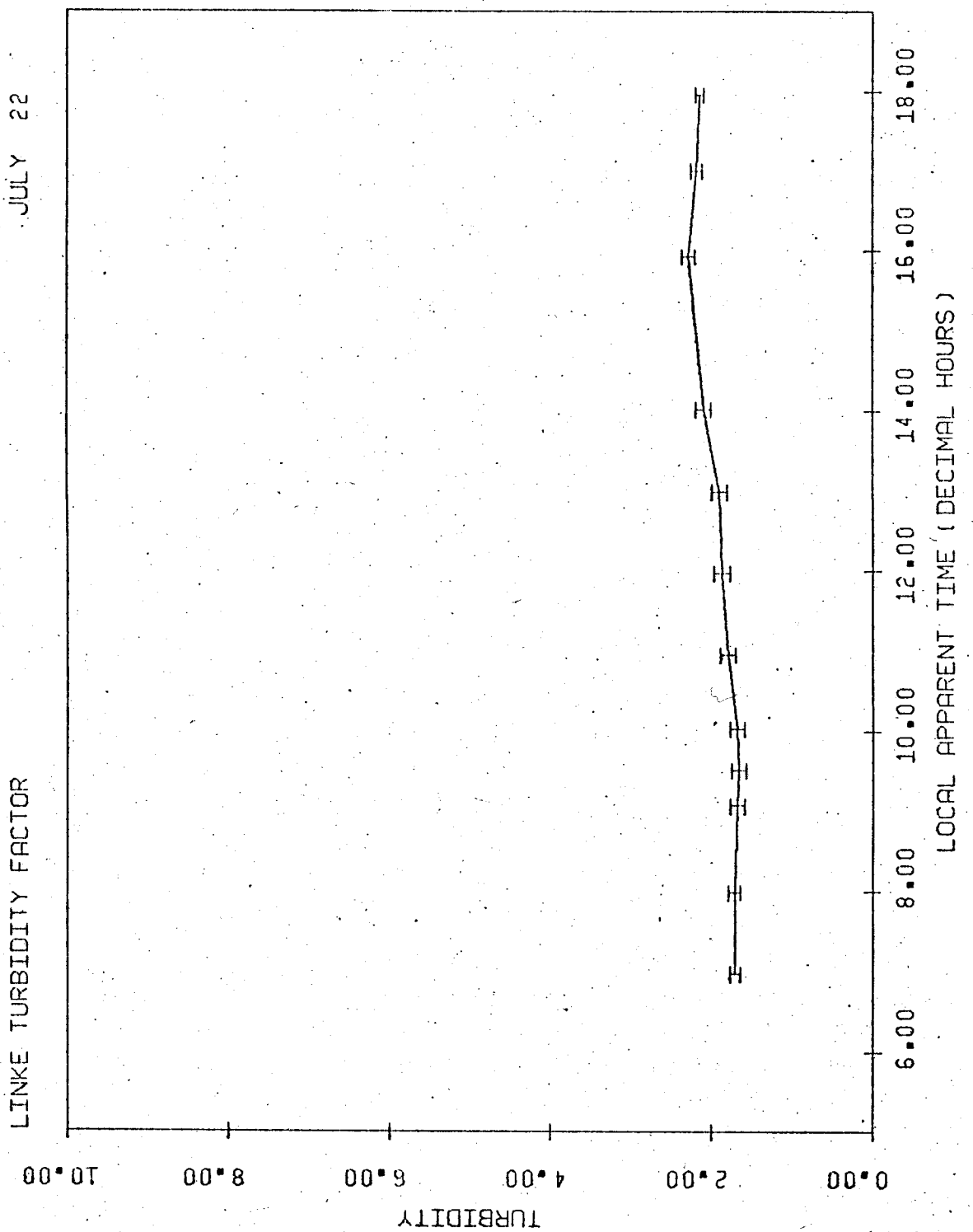
LINKE TURBIDITY FACTOR
JULY 22
TURBIDITY
0.00
2.00
4.00
6.00
8.00
10.00
6.00
8.00
10.00
12.00
14.00
16.00
18.00
LOCAL APPARENT TIME (DECIMAL HOURS)

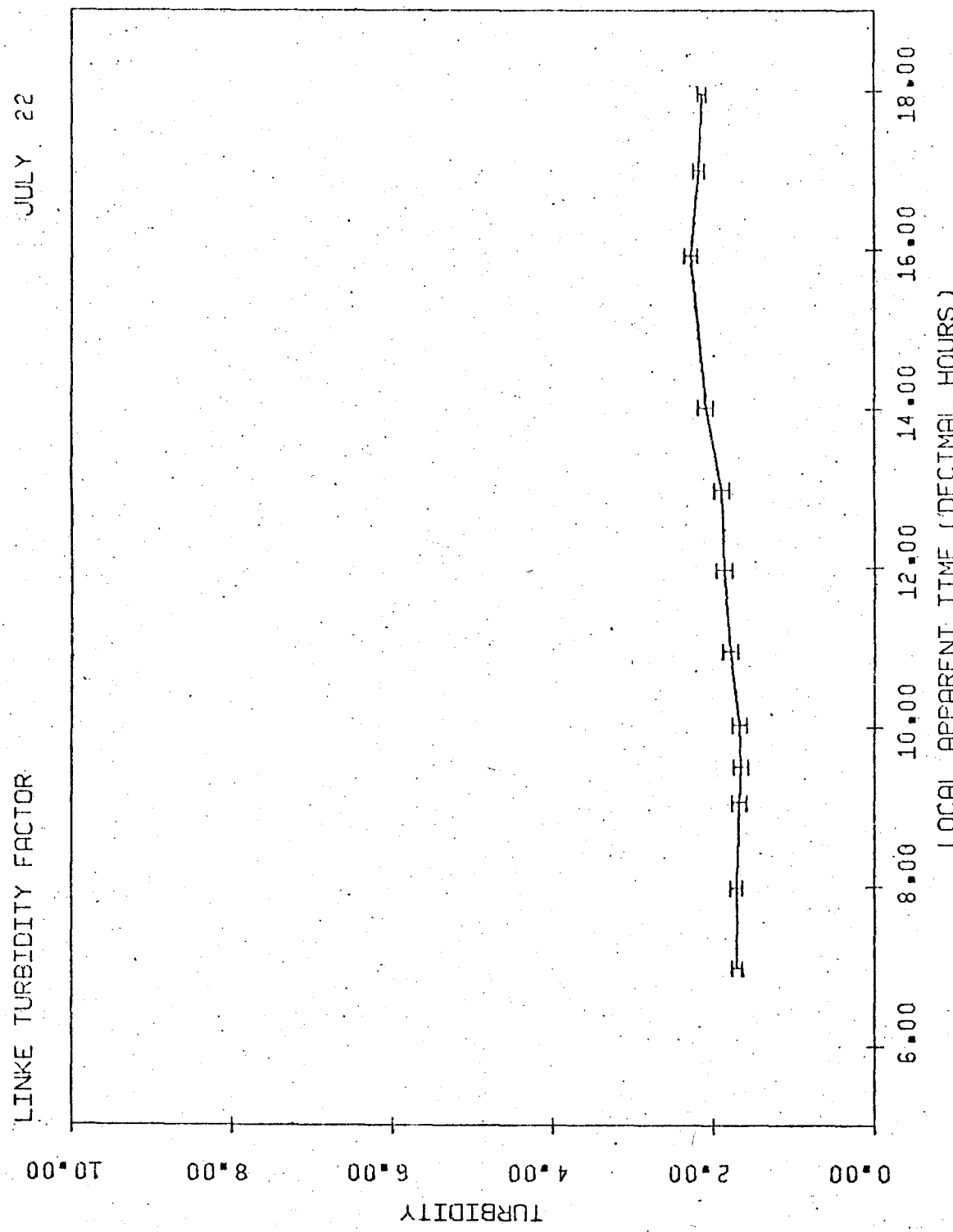
LINKE TURBIDITY FACTOR
JULY 22
TURBIDITY
0.00
2.00
4.00
6.00
8.00
10.00
6.00
8.00
10.00
12.00
14.00
16.00
18.00
LOCAL APPARENT TIME (DECIMAL HOURS)

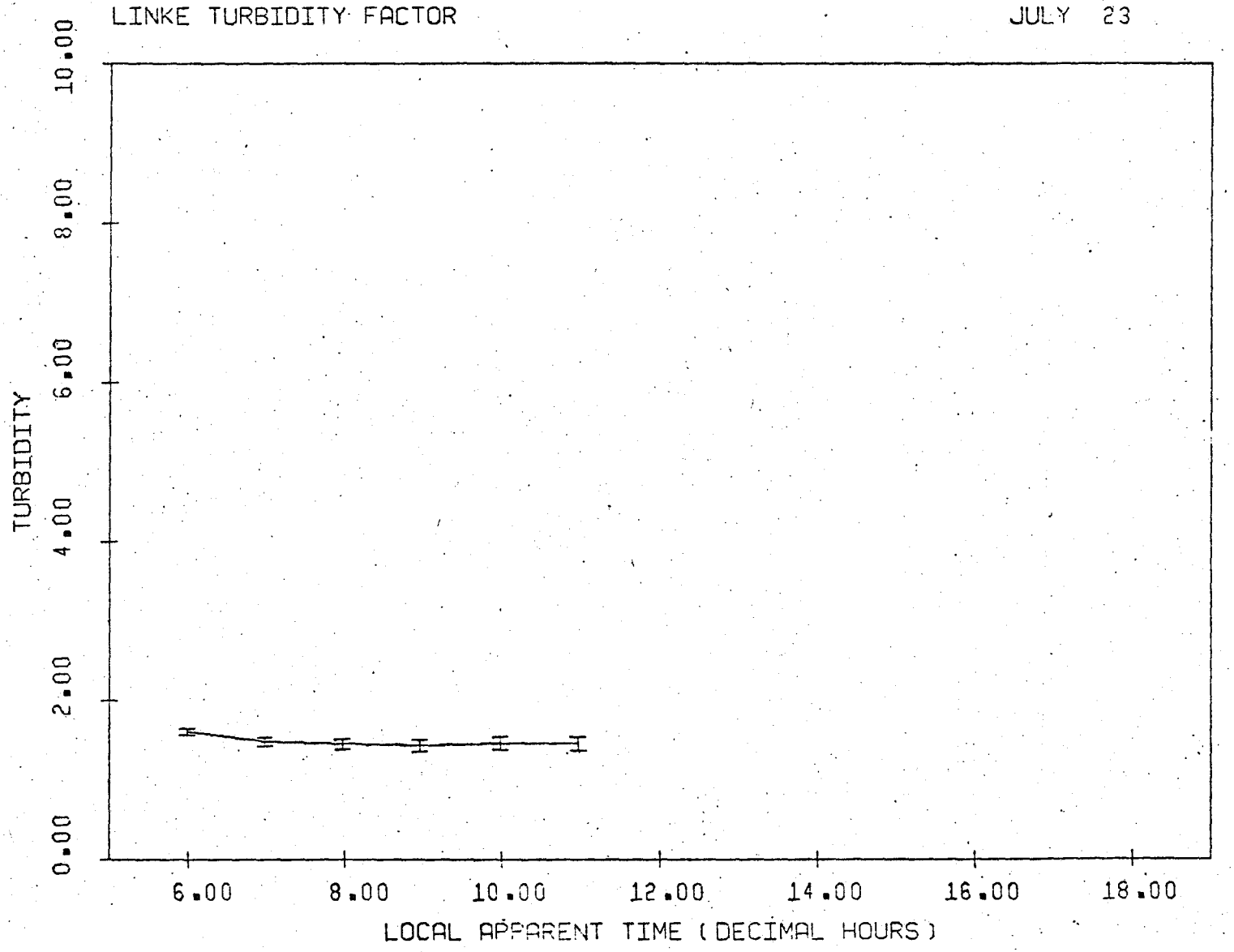
LINKE TURBIDITY FACTOR
JULY 23
TURBIDITY
0.00
2.00
4.00
6.00
8.00
10.00
6.00
8.00
10.00
12.00
14.00
16.00
18.00
LOCAL APPARENT TIME (DECIMAL HOURS)

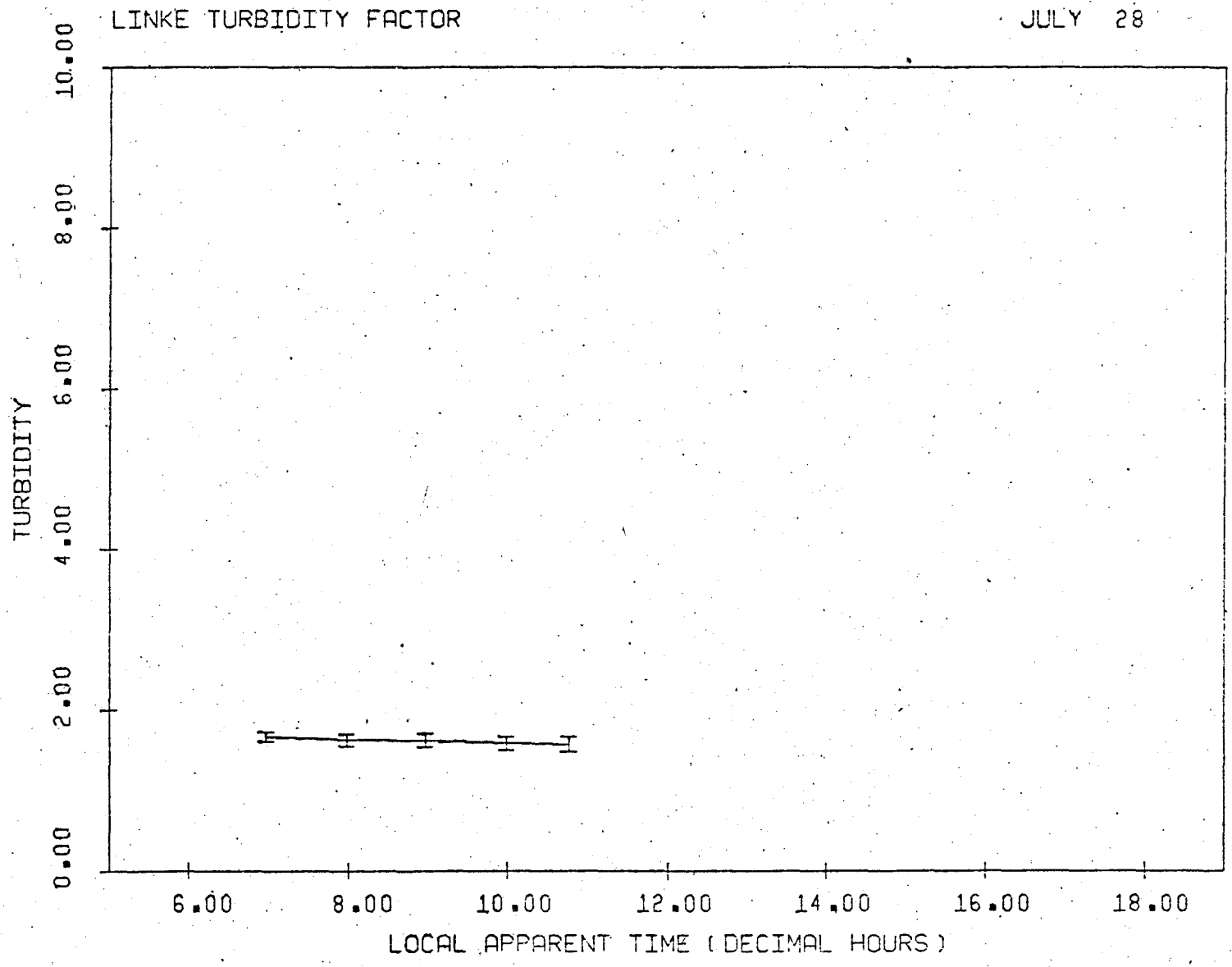
LINKE TURBIDITY FACTOR
JULY 28
TURBIDITY
10.00
8.00
6.00
4.00
2.00
0.00
6.00
8.00
10.00
12.00
14.00
16.00
18.00
LOCAL APPARENT TIME (DECIMAL HOURS)

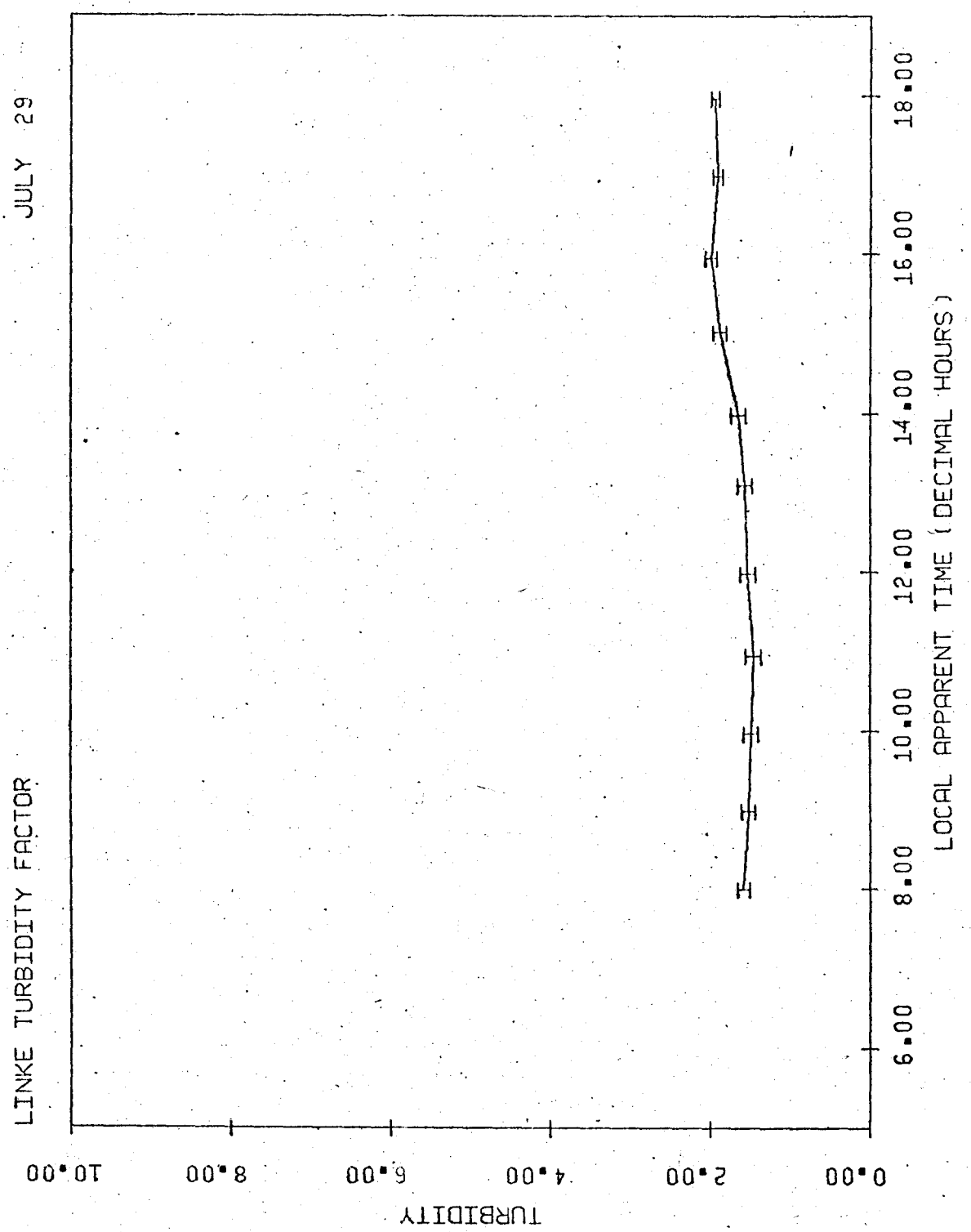
LINKE TURBIDITY FACTOR
JULY 29
TURBIDITY
0.00
2.00
4.00
6.00
8.00
10.00
6.00
8.00
10.00
12.00
14.00
16.00
18.00
LOCAL APPARENT TIME (DECIMAL HOURS)

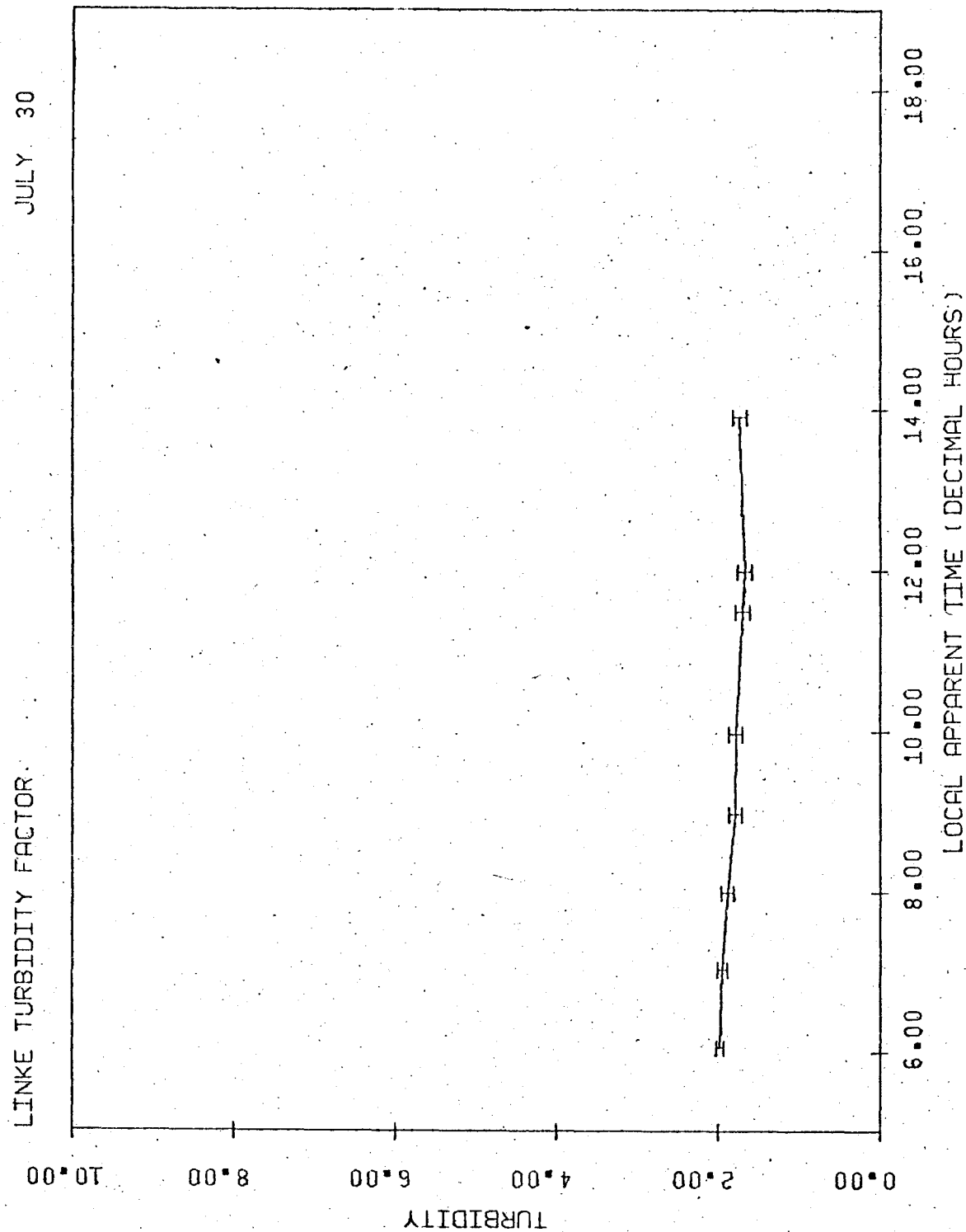
LINKE TURBIDITY FACTOR
JULY 30
TURBIDITY
0.00
2.00
4.00
6.00
8.00
10.00
6.00
8.00
10.00
12.00
14.00
16.00
18.00
LOCAL APPARENT TIME (DECIMAL HOURS)

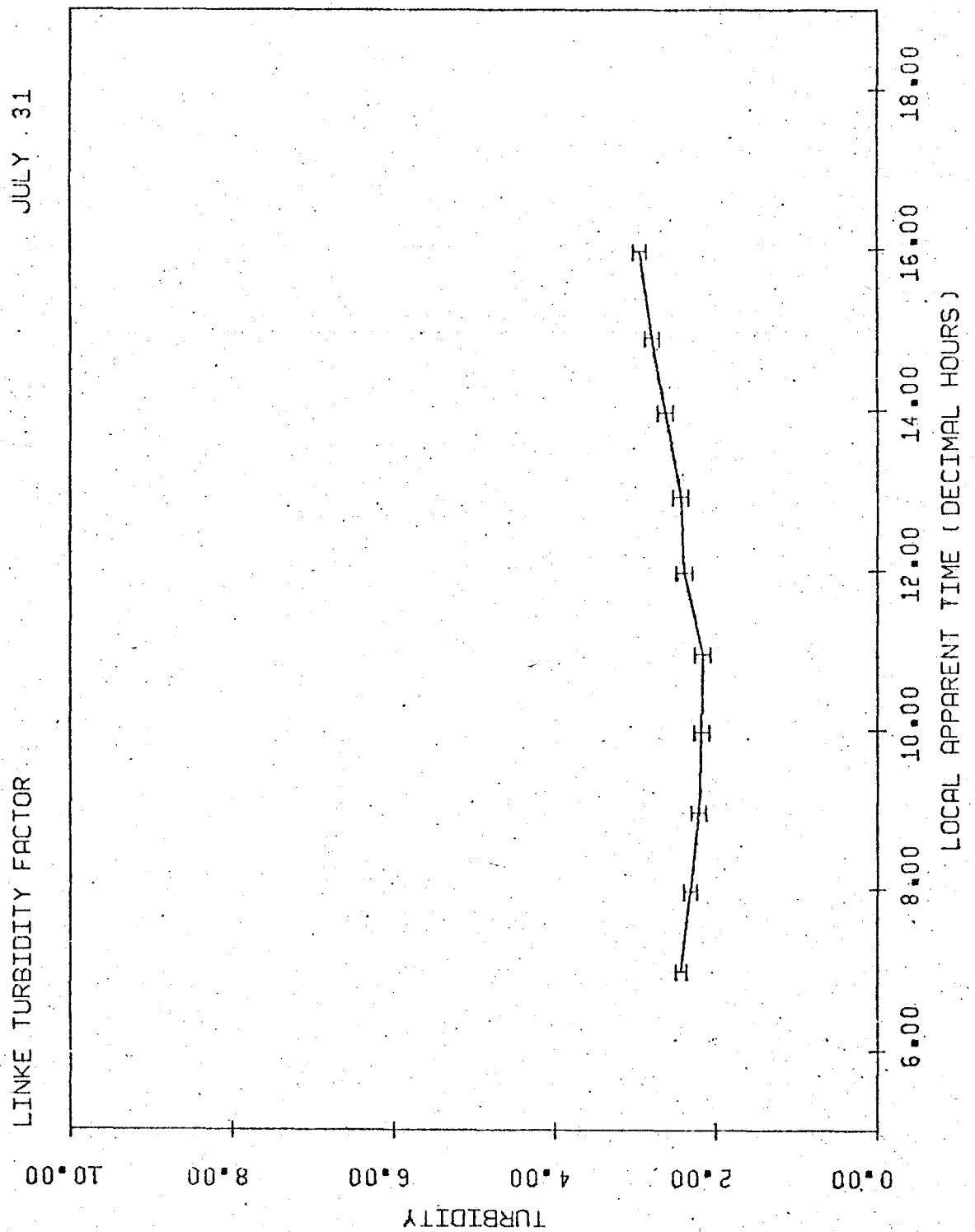
LINKE TURBIDITY FACTOR
JULY . 31
TURBIDITY
0.00
2.00
4.00
6.00
8.00
10.00
LOCAL APPARENT TIME (DECIMAL HOURS)
6.00
8.00
10.00
12.00
14.00
16.00
18.00

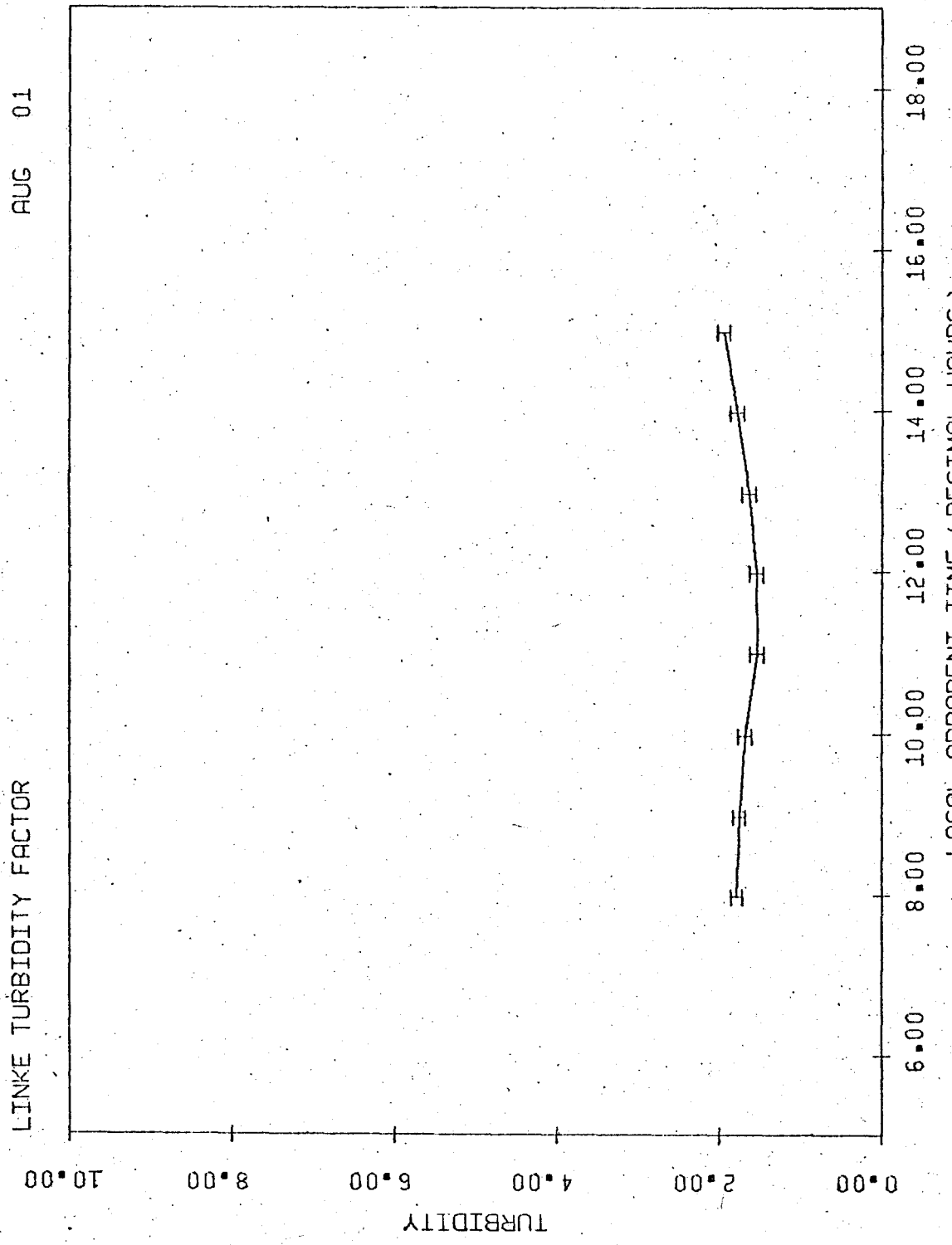
LINKE TURBIDITY FACTOR
AUG 01
TURBIDITY
0.00
2.00
4.00
6.00
8.00
10.00
6.00
8.00
10.00
12.00
14.00
16.00
18.00
LOCAL APPARENT TIME (DECIMAL HOURS)

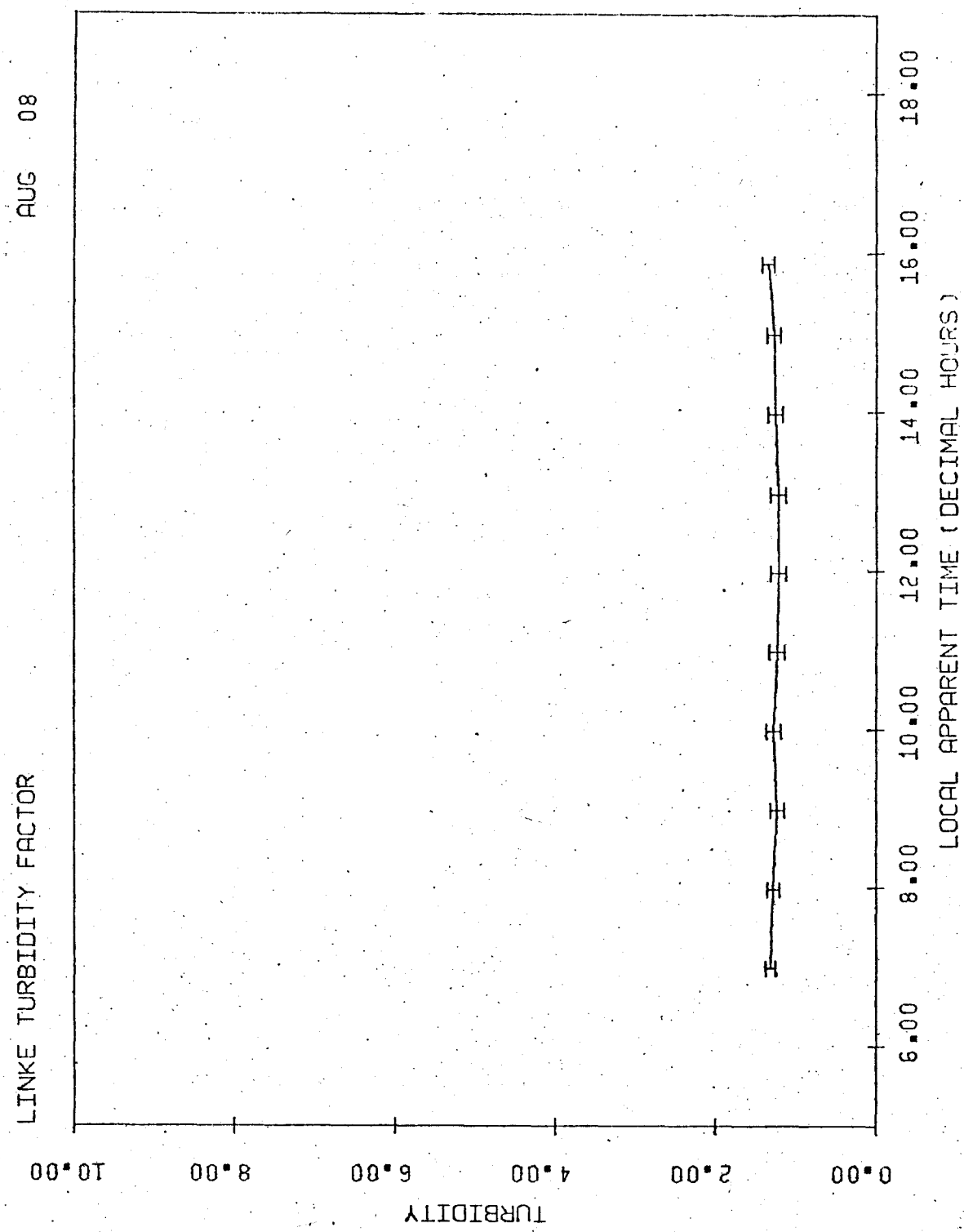
LINKE TURBIDITY FACTOR
AUG 08
TURBIDITY
0.00
2.00
4.00
6.00
8.00
10.00
6.00
8.00
10.00
12.00
14.00
16.00
18.00
LOCAL APPARENT TIME (DECIMAL HOURS)

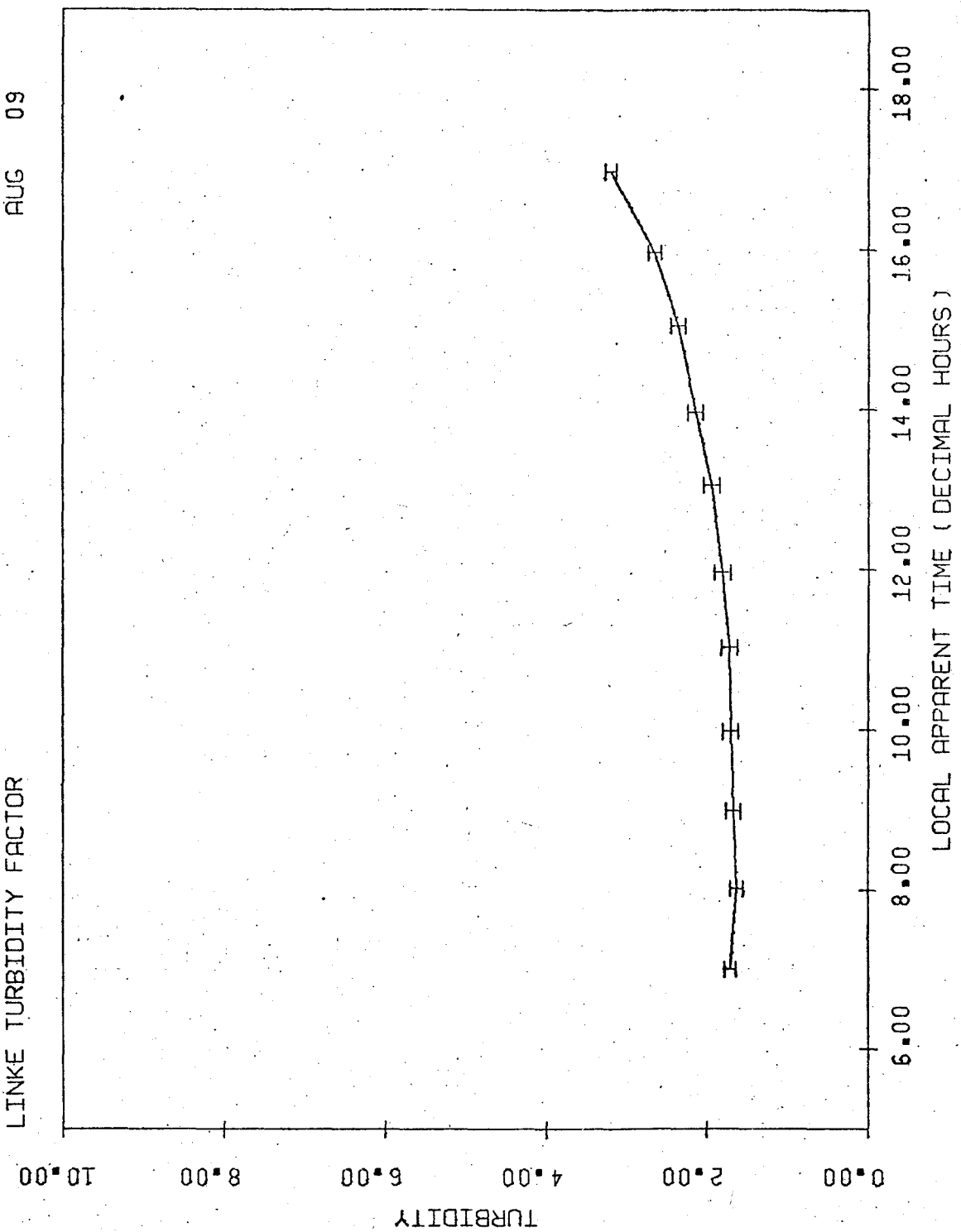
LINKE TURBIDITY FACTOR
AUG 09
TURBIDITY
0.00
2.00
4.00
6.00
8.00
10.00
6.00
8.00
10.00
12.00
14.00
16.00
18.00
LOCAL APPARENT TIME (DECIMAL HOURS)